

SOLAR RADIO BURSTS WITH DRIFTING STRIPES IN EMISSION AND ABSORPTION

G. P. CHERNOV

IZMIRAN, Troitsk, Moscow Region, 142190, Russia

(Received 14 December 2006; Accepted in final form 15 December 2006)

Abstract. This review covers fairly comprehensively experimental and theoretical research on the fine structure of types zebra pattern (ZP) and fiber bursts (FB) in solar type II+IV radio bursts. The basic attention is given to the latest experimental data. A comparative analysis of several recent solar type IV radio outbursts with these fine structure in dynamical radio spectra is carried out using available ground-based and satellite data (Yohkoh, SOHO, TRACE, RHESSI). New data on microwave zebra structures and fiber bursts testifies that they are analogous to similar structures observed at meter wavelengths. The discovery of the superfine structure, in the form of millisecond spikes is the most significant new effect in the cm range. All basic theoretical models of the zebra pattern and fiber bursts are discussed critically. Two main models are studied for their interpretation: (i) interactions between electrostatic plasma waves and whistlers, (ii) radio emission at double plasma resonance (DPR). The relative significance of several possible mechanisms remains uncertain.

Keywords: solar flare, radio emission, zebra pattern

1. Introduction

Solar radio astronomy has grown into an extensive scientific branch since its birth in the forties of 19-th century, initiated by the subsequent discovery of the main basic components of solar radio emission: the quiet Sun, the slowly varying component and various types of radio bursts including noise storms (Krüger, 1979). It was quickly revealed, that radio bursts are observed during chromospheric flares.

The radio bursts were classified in five distinctive types at the dynamical spectrum (Wild *et al.*, 1963) and the noise storms in the meter wave range proved to be the most widespread manifestation of solar activity, when against the background of the prolonged increased continuous emission numerous narrow-band short-term bursts of type I appear at different frequencies.

Type III bursts are too fairly frequent bursts received from the solar corona. They are characterized by their brief duration and rapid drift from high to low frequencies in decimeter and meter wave range. It is assumed, that the radio emission is generated by beams of fast electrons at levels of the local plasma frequency or its second harmonic (*'plasma hypothesis'*).

Slow-drift type II bursts are outstanding events associated with large flares. They occur much more rarely. The frequency drift to low frequencies is found to

correspond to a velocity of order of 10^3 km s^{-1} and the moving agency is identified with a collisionless MHD shock wave set up as a result of an explosion at the time of flare flash phase (Wild and Smerd, 1972).

Type IV bursts are continuum radiation following type II bursts, or they are superimposed on the time, and then such events are called as the type II+IV. Their radio sources can be stationary or moving, and the continuum can be extended from meter into decimeter and microwave ranges almost simultaneously (Zheleznyakov, 1964; Kundu, 1965; Wild and Smerd, 1972).

The type V burst is a broad-band continuum radiation following a type III burst, as a diffuse prolongation (usually below 150 MHz). It is assumed, that this is emission of a part of the electrons, producing the type III burst, trapped in a magnetic loop.

Already the first spectral observations of the large type IV (and II+IV) bursts revealed the rich variety of the fine structure of the radio emission in the form of wide-band pulsations in emission and absorption with the different periods, rapid bursts (spikes), narrow-band patches. Modulation of the continuum emission in the form of narrow stripes in the emission and the absorption appeared by the most intriguing elements of the fine structure (Krüger, 1979).

The study of the fine structure of the solar radio emission is a key to understanding of plasma processes in the solar corona. It remains a reliable means for both diagnosing the solar corona and verifying the results of laboratory plasma experiments on the wave-wave and wave-particle interactions. High time and frequency resolution data have improved our studies of similar fine structures in star flares. So, the continuum radio emission of the type IV was associated for long time with the synchrotron emission of electrons trapped into a magnetic cloud (after the work of Boischoat, 1957), but the analysis of fine structure testified, that the plasma mechanism is predominant in the meter and decimeter wave band.

Stripes in emission and absorption against the continuum background of solar type IV radio bursts in the meter and decimeter wave ranges are traditionally subdivided into two kinds: zebra pattern (ZP) and fiber bursts (FB) (or intermediate drift bursts (IDB)). (Kuijpers, 1975a; Slottje, 1981). Since the end of the seventies, microwave observations of solar emission with high temporal and spectral resolution have also shown fine structures: millisecond spikes (with the duration of single spikes of a few tens of milliseconds), and fast pulsations, usually superimposed on a smooth continuum emission (Benz, 1993). We could also find some indications of a probable zebra pattern in the microwave range in Isliker and Benz (1994).

The new solar broadband radio spectrometers of NAO (China, Huairou station) with higher resolution (10 MHz and 5–8 ms) can observe detailed zebra patterns and fiber bursts at high frequencies, 2.6–7.6 GHz (Chernov *et al.*, 2001b). In the microwave range the same variety of fine structure is observed. Thus the relative frequency parameters of zebra structures in microwave and meter wave bands appear

identical. This testifies to the identical nature of the formation of fine structure in different frequency ranges.

Some recent observations with a time resolution of 0.1 s, using Ondřejov radiospectrographs in the range 0.8–4 GHz, have allowed us to find new properties of zebra structures and to verify theoretical models (Ledenev *et al.*, 2001; Karlicky *et al.*, 2001; Sawant *et al.*, 2002). We are obligated to examine the historical interval of studies of ZP and FB for four solar cycles, since the previous surveys were or very brief (Fomichv and Chertok, 1977), or they were limited only to the description of the observant properties of fine structure in the meter range (Slotjje, 1981), or to short theoretical description of the generation mechanisms (Kuijpers, 1980).

It is important to allocate the most important moments of all past studies without repeating all details, being contained in the known reviews. In recent years, observations of fine structures have been considerably expanded and new properties of ZP and FB have been revealed. At present, an analysis of new events usually implies a more thorough study of flare processes in the X-ray emission (Yohkoh, RHESSI) and the ultraviolet lines (SOHO, TRACE). It is therefore important at this stage to identify new properties of the fine structure observed at various frequencies and analyze them in the context of various theoretical models; this is the goal of the current review.

2. Observations

ZP and FB were recorded at the end of the fifties by observations with the first spectrographs. The first narrow stripes in emission and absorption were observed in the event on 4 November 1957 (Boischoot *et al.*, 1960). The short description of this event entered in the monographs on 1964 (Zheleznyakov, 1970; Kundu, 1964), where a special attention was turned to the very characteristic property of stripes – close mutual arrangement of the stripes in emission and absorption. The name ‘zebra pattern’ was introduced by Slotjje (1972) as most adequate to observations, after the detailed measurements of the frequency separation between stripes by Elgarøy (1972), testifying about, that they are not always parallel between themselves. But the first front-pager about the observations of zebra structure was made by Elgarøy (1959, 1961) in the event August 18, 1959 (Figure 1).

The basic properties of ZP were already visible based on this example: preferred drift to the high frequencies, at times the non-parallelism of stripes, the frequency separation between stripes increases with frequency, abrupt changes in frequency drift (hooks and jumps) and even a transition into the braided zebra pattern with drifting spikes as elements of such patterns. Then the set of the descriptions of separate events appeared, and between others *parallel drifting bursts* (PDB) in Tarnstrom and Philips (1971), PDB- events, similar to ZP. Slotjje (1972) opened new stage in study of non-stationary ZP in the event March 2, 1970.

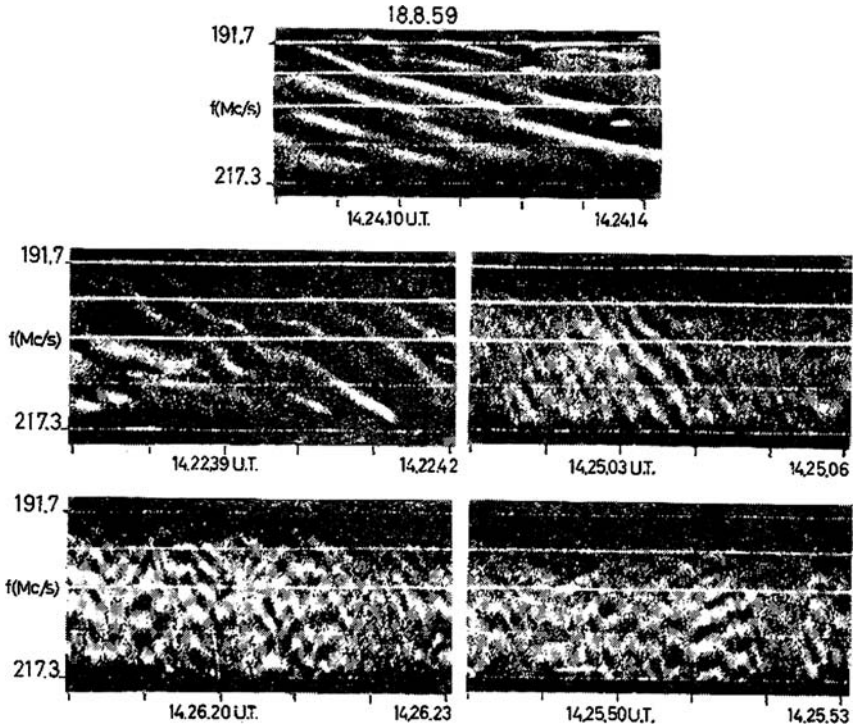


Figure 1. An example of zebra structure in the event August 18, 1959 (from Elgarøy, 1961).

The first short survey about ZP and FB was included in the review of Fomichev and Chertok (1977), devoted to the fine structure. But the most complete description of properties of the ZP and FB in the meter wave band was represented in atlas of Slottje (1981).

Young *et al.* (1961) the first reported observations of 'intermediate drift bursts' in the range 500–950 MHz in five events of 1959 (Figure 2). The authors noticed almost all basic properties of IDB: the presence of absorption ('shadow'), moreover as from the high-frequency edge, so from the low-frequency one; the wide spread of frequency drift to low frequencies and even the reverse drift; the bursts occur usually in regular groups with almost constant frequency spacing, but on some occasions as isolated bursts.

With the development of observations it became obvious, that this name 'intermediate drift bursts' (intermediate between the drift of types II and III bursts) did not always prove to be accurate, since the fibers were frequently observed with different frequency drift, also even of opposite sign. And gradually all authors began to call them simply 'fiber bursts', (finally after Slottje (1972)). The basic properties of FB are successfully represented by Kuijpers (1975a) (Figure 3), from the event March 6, 1972.

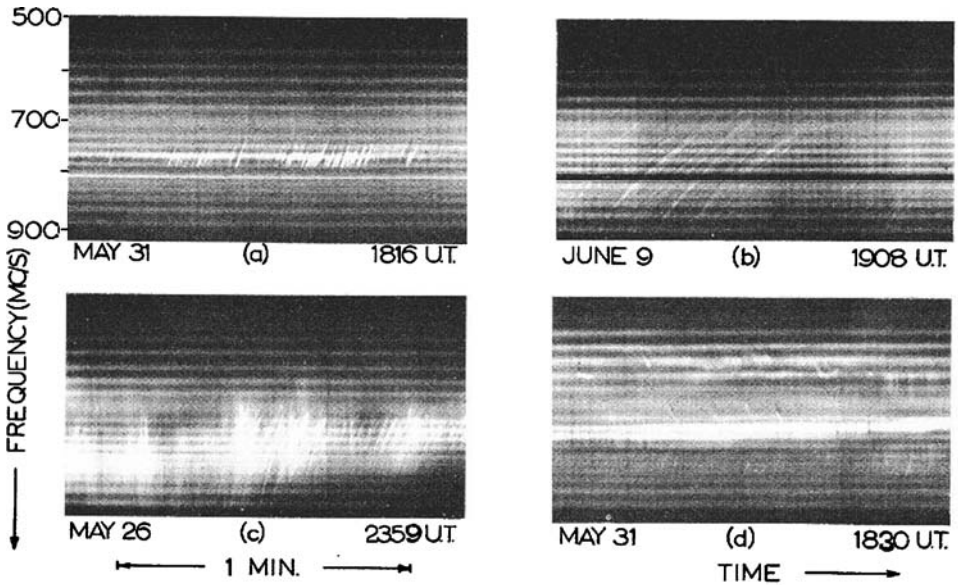


Figure 2. Intermediate drift bursts in three events of 1959 (from Young *et al.*, 1961).

Kuijpers (1980) summarized basic observed properties of ZP and FB in the following Table I.

If we do not turn attention to the different frequency drift of stripes, then all other parameters of ZP and FB have close values. Let us note, that in the section of Table I for the ZP there are no two lines (Duration and Single frequency duration), although for ZP approximately the same values are characteristic. Furthermore, generally there is no parameter of the frequency separation between emission and absorption (characteristic to both types of the structures).

The large contribution to the statistics of observations of FB in the broad frequency range 150–1000 MHz was made by Elgarøy (1982) (Table II). He has found a linear dependence between frequency drift velocity and observed bandwidth, the duration at one frequency t_f is determined by the length of exciter rather, but not by electron collision time. He proposed to define the magnetic field strength B in different ways: the values obtained with frequency separation between emission and absorption $\Delta f_{ea} \approx b_t = f_w \approx 0.25 f_B$, (where f_w – whistler frequency, f_B – electron cyclotron frequency) are compared with values defined using df/dt in the form:

$$B = 6.4(\ln f - 1.3)^{-2} |df/dt|, \tag{1}$$

if to identify the exciter velocity, defined by df/dt in the double Newkirk model with the group velocity of whistlers. He got a magnetic field of 1.4–1.8 G at 150 MHz, and about 13.5 G at 1000 MHz. These values give the plasma $\beta = nk_B T / (B^2 / 8\pi)$

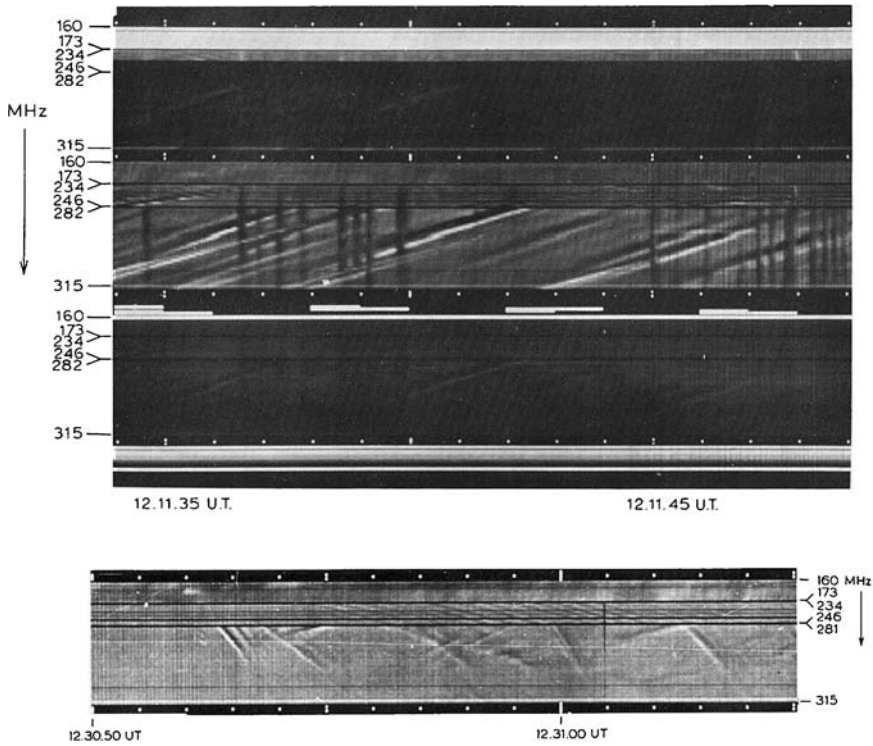


Figure 3. Two examples of intermediate drift bursts observed with 60-channel Utrecht spectrograph on March 6, 1972. Each channel has a width of 0.9 MHz. In the top panel fibers are clearly visible on the sensitive channels in the middle. Lower part – normal channel, upper part – circular polarization (from Kuijpers, 1975).

nearest to 1 ($n = n_e + n_i$, $T = 1.5 \cdot 10^6 K$, k_B – Boltzman's constant, e,i- designate electrons and ions).

Sometimes the regularity of the ZP is not particularly strong and individual stripes show a FB profile. In this connection let us note, that for their more detailed comparison it is convenient to use the following parameters: the instantaneous frequency separation between the stripes (or spacing) Δf_s ; the frequency separation between adjacent intensity peaks in emission and absorption Δf_{ea} ; the instantaneous frequency bandwidth of a single emission stripe Δf_e ; the full frequency bandwidth of all stripes in the spectrum Δf ; the total number of stripes and their frequency drift df/dt .

Slottje (1981) and Elgarøy (1982) discuss the absorption mainly in FB. Elgarøy (1982) obtained the frequency profiles, using the microphotometer, and he found a nice symmetry between absorption and emission. The absorption was observed usually at the low frequency side in about 30% of all cases. Slottje (1981) noted that the absorption-emission character is also true for ZP. He measured the frequency

TABLE I
Observed characteristics of ZP and FB (from Kuijpers, 1980)

Zebra patterns	
Frequency extent	≥ 40 MHz
Number of consecutive stripes	5–20 (up to 70)
Stripe spacing at 160–200 MHz	2–3 MHz
at 800–900 MHz	20 MHz
Fiber bursts	
Frequency extent	30 MHz (up to 120 MHz)
Duration	5–10 s
Single frequency duration	0.2–0.4 s
Instantaneous bandwidth	≤ 1 MHz
Drift rate, $-df/dt$	$10^{-2} f + 6 \cdot 10^{-5} f^2$ (Elgarøy, 1982)
Number in one group	10–30 (up to 300)
Flux	
At 160–320 MHz	200 sfu
At 50–600 MHz	500 sfu

TABLE II
Summary of observed parameters for FB (From Elgarøy, 1982)

Parameters	Frequency			
	150	300	500	1000
$ df/dt $ (MHz/s)	3.1	7.5	23	66.5
t_f (s)	0.37	0.29	0.18	0.08
b_t (MHz)	1.1	2.1	3.6	> 5
t_i (s)	0.2	0.2	0.1	(0.05)
b_i (MHz)	0.5	1.0	2.0	> 2

$|df/dt|$ - frequency drift velocity; t_f -duration at one frequency;
 b_t - instantaneous bandwidth; t_i - intrinsic (or exciter) duration;
 b_i - intrinsic bandwidth: $b_t = b_i + t_i |df/dt|$; $t_f = t_i + b_i |df/dt|$.

separation between emission and absorption for FB and the frequency spacing between emission stripes for ZP. Two such distributions are shown in Figure 4.

The regularity of the instantaneous frequency spacing (Δf_s) is the most striking aspect of ZP. A closer look reveals that generally Δf_s increases with frequency (Chernov, 1976a). But sometimes, in one event the spacing changes with time up to a factor of two (Slottje, 1981).

The distribution shown in Figure 4a was constructed by Slottje (1981) using 79 events with ZP near 300 MHz. The histograms are cut off below 2 MHz due to the resolution limit of the spectrograph (the frequency spacing between channels).

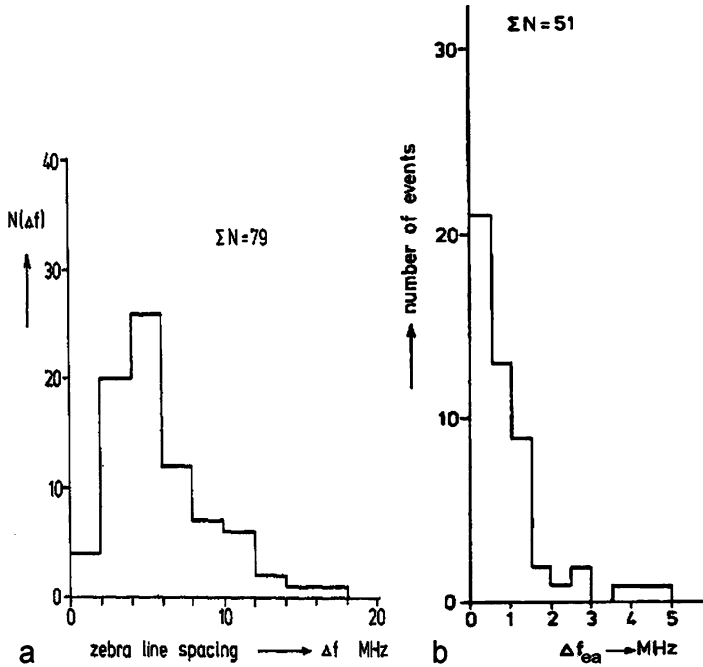


Figure 4. The distribution of frequency spacing in zebra patterns in 79 events where a value was found (a); and the distribution of the apparent frequency separation of emission and absorption of fiber bursts in 51 events where a value was found (b) (from Slotje, 1981).

The distribution of Δf_{ea} for FB (Figure 4b) continues up to zero values, but the values less than 2 MHz were obtained in frames of an assumption that $\Delta f_{ea} \approx \Delta f_e$, then the value of Δf_e can be calculated more precisely using the drifting time between the channels. Slotje (1981) found, that about 56% of FB have the separation $\Delta f_{ea} < 1$ MHz.

Slotje (1981) denotes, that ZP often demonstrates some particularities. For example, discontinuous stripes within patterns (an intriguing phenomenon, crucial for the interpretation of ZP), appearance and disappearance of stripes amidst a continuous pattern. Hooks and jumps of stripes or wave-like frequency drift put also some additional questions for the interpretation.

Without repeating all properties of ZP, described in Slotje (1981), let us note the basic parameters of ZP and FB, which with the development of observations proved to be very important.

The full frequency bandwidth of ZP and the total number of stripes are difficult to determine, because of the narrow frequency bandwidth of spectrographs. ZP and FB are usually observed as a modulation of the strong circularly polarized continuum emission, and zebra stripes as FB are also strong polarized in the same sign as continuum emission (Chernov *et al.*, 1975; Chernov, 1976). Let us note the

first important property: ZP and FB are usually observed against the background of type IV continuum emission with wide-band pulsations of radio emission. Among the latter (Slottje 1981) has alluded, first of all, to pulsation in the absorption BSA (broad-band short-lived absorption pulses or ‘sudden reductions’ of background continuum intensity) and BEP (broad-band emission pulses), though far less abundantly than BSA. This property must be considered as very important condition during the construction of a model of the formation of the stripes in emission and absorption.

The survey of the first observations showed already, that the frequency separation Δf_s smoothly increases with the frequency from 1–1.5 MHz at 150 MHz up to 10 MHz at 700 MHz (see figure 9 in Chernov (1976)). Slottje encountered the difficulty of determining this dependence since the multichannel spectrograph (NERA station and Dwingeloo station after 1972, respectively with 60 channels between 160–320 MHz with the bandwidth of one channel of ≈ 0.9 MHz) did not make possible to accurately determine this parameter.

Slottje showed, that the instantaneous frequency bandwidth of a single emission stripe Δf_e is equal about to one half of the frequency spacing $\Delta f_s \approx 2\text{--}4$ MHz at a frequency range 160–320 MHz.

For fiber bursts Slottje (1981) draws conclusion, that $\Delta f_e \approx \Delta f_{ea} \approx 1\text{--}2$ MHz. This is rather true also for ZP, taking into account the conclusion of Slottje (1981), that the emission-absorption character of zebra stripes and FB is about the same. This was shown in figures 5, 6 and 7 in Chernov *et al.* (1975).

ZP and FB differ in the frequency drift: the zebra stripes drift usually synchronously (sometimes detecting very rapid oscillations), and FB have usually the constant (more often negative) drift velocity. However, in the atlas of Slottje (1981) it is shown already, that it is sometimes difficult to distinguish zebra stripes and FB, when they are almost continuously transforming into each other (e.g. see spectrum August 18 1970, 16:43 UT). Therefore Chernov *et al.* (1975) and Slottje (1981) draw conclusion, that the origin of both types of strips can be determined by the same mechanism.

The large spread of the values of all parameters indicates not a wide spectrum of the observed frequencies, but more likely the big variety of values in the different events. Therefore it is more important to compare the relative values of those parameters (relative to the observing frequency). Such a comparison of the ZP parameters in five events, observed in the recent time is given in Table III.

In the Table III for 4 events (besides 1994 10 25) ZP and FB were observed practically simultaneously and their parameters were coincided on the value. The parameters $\Delta f_s/f$ and $\Delta f_{ea}/f$ grow with frequency, clearly in connection with the faster growth of the magnetic field than the density with decrease of the height. The parameter $\Delta f/f$ decreases with frequency, which corresponds to a decrease in the size of the radio sources in the lower corona. Only the quantity $\Delta f_e/f$ remains more stable. In four events, the radio fine structure corresponded to the ordinary mode.

TABLE III
Parameters of the zebra pattern in five events (from Chernov, 2004).

Date	f(MHz)	Flare					Magnetic	Sign of
Time UT	Frequency range	coordinates	$\Delta f_s/f$	$\Delta f_{ea}/f$	$\Delta f/f$	$\Delta f_e/f$	polarity	polarization Wave mode
1998 05 02 14:41	35 20–70	3B X1.1 S15W15	0.0036	0.0024	0.88	0.0035	S(N)	L R ?
1994 10 25 10:08	175 100–500	1N C4.7 S09W12	0.015	0.006	0.4	0.0049	S	R O
1999 07 28 08:15	360 45–520	1B M2.3 S15E03	0.014	0.006	0.22	0.0054	N	L O
1998 09 23 08:00	360 100–700	3B M7.1 N18E09	0.064	0.032	0.3	0.014	N	L O
2000 10 29 02:20	3000 1000–3800	2B M4.4 S25E35	0.033	0.015	0.16	0.0059	S	R O

Since the statistical evidence is inconclusive, in the following presentation the primary attention we will give to several individual events.

2.1. POLARIZATION

A question about the polarization of ZP and FB is one of the most crucial items for the construction of theoretical models. Let us pause at it in more detail, since in the old reviews the polarization was barely discussed (in the absence of authentic observations). Generally the ZP appears merely as positive and negative modulation of the strong polarized continuum emission. Quite often polarization outputs of the Utrecht spectrograph were saturated, and some quantitative values for the polarization degree were obtained by Chernov *et al.* (1975) for the event May 3, 1973, shown in the Figure 5.

Above north magnetic polarity of the leading spot in AR McMath 12336 (S14E51) the fully left polarized emission in this event corresponds to the ordinary mode.

The detailed polarization profiles in the decimeter range have been subsequently presented by Bernold (1983). In Figure 6 an example of very interesting profiles in right and left circular polarization is shown. These data have not been included in Bernold and Treumann (1983), and Bernold (1983) does not discuss behavior of polarization in time, though evolution of polarization from almost zero in the

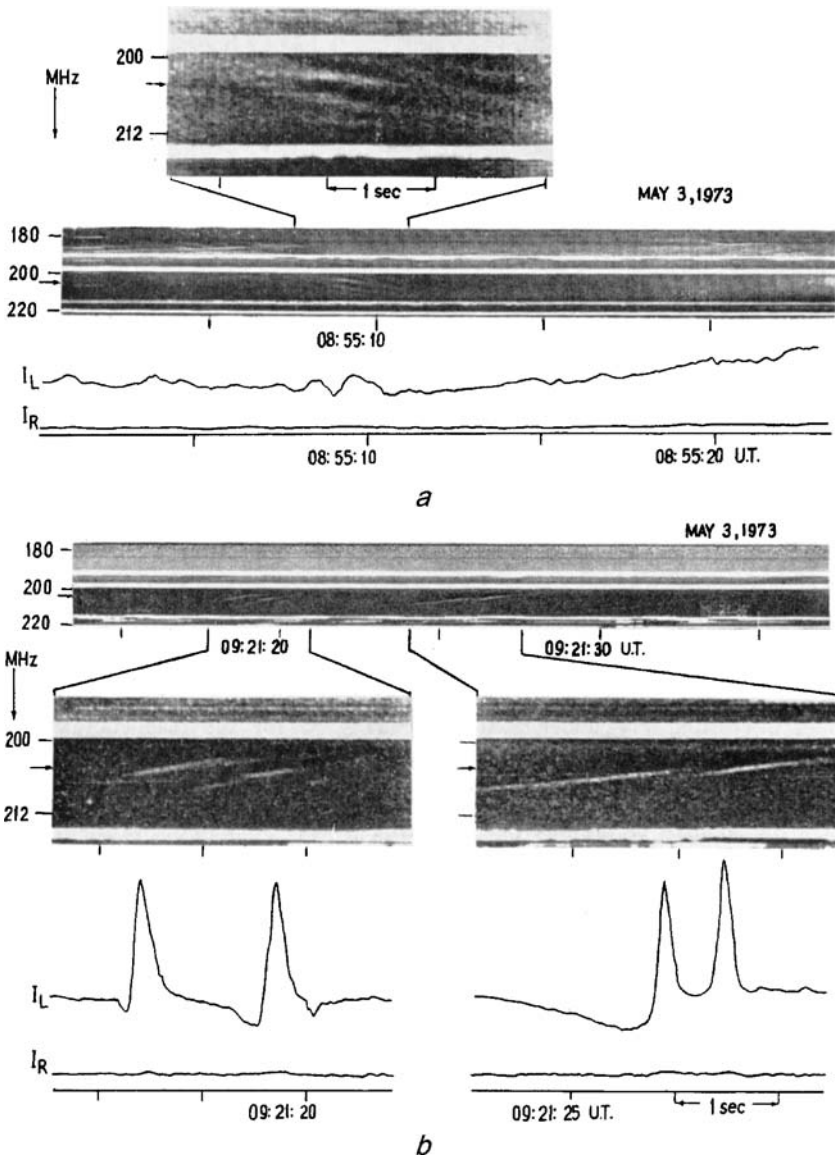


Figure 5. Spectra and polarization profiles of ZP (a) and FB (b) with time resolution 0.02 s (IZMIRAN data) in the event May 3, 1970. The emission is fully left circularly polarized as for continuum as for fine structure. The frequency bandwidth of low-frequency absorptions is varying during different time moments (from Chernov *et al.*, 1975).

beginning up to strong in the middle and again weak in the end of a fiber represents a difficulty at the interpretation in any theoretical model. The main conclusion there: in two events the polarization indicates the ordinary mode for the radiation (on the criterion of the leading spot magnetic polarity).

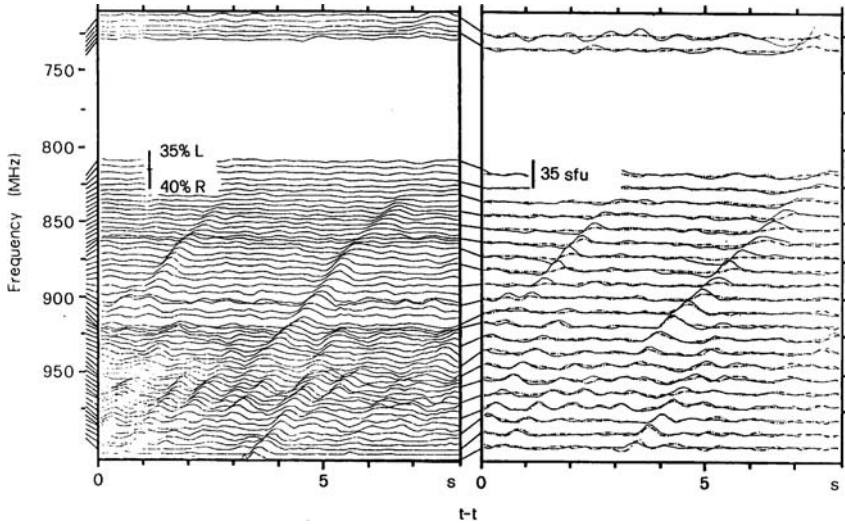


Figure 6. Time profiles of the intensity (left profiles) and right (dotted lines) and left (full lines) circular polarization (right profiles) after subtraction of the continuum in the event November 22, 1981 (from Bernold, 1983).

The more detailed analysis of polarization of ZP and FB is realized by Chernov and Zlobez (1995), owing to comparison of the dynamic spectra (IZMIRAN) and polarization recordings at the fixed frequency (Trieste AO). In Figure 7 an unusual fiber is shown. The position of the absorption changed from high frequency edge in the beginning to low frequency edge in the end of the fiber in emission. Note an undulation in the polarization plot during the absorption and a time delay of the L-component relative to R-component on approximately 0.02 s. This particularity means that the noted undulation is not due to a real change in polarization but to a small delay of the signal of the weaker polarimetric channel, the L-handed one, in respect to the stronger one, R-handed, because the radiation was R-handed polarized on about 80%.

Even the more complex behavior of the polarization in ZP was observed in the event of April of 24, 1985, shown in Figure 8. In the left time interval the more pronounced delay of R-polarization channel was recorded ($\approx 0.03s$). But in the right interval we can see in the same series of ZP very complicated behavior of polarization due to the different (noisy) delays between L- and R-channels. The polarization was R-handed and very variable between 20–80%, but the noted delay of R-channel is the most important detail here, that is the delay of the more intense channel. The similar delay of the strongest component (of $\approx 0.8s$) was also registered in the short complex event April 26, 1984 during a transformation of second pulsations into zebra pattern (shown below in Figure 20).

In both events (May 18 and April 24) the radiation was rather in the ordinary mode (on the criterion of the leading spot magnetic polarity), and if in the May 18

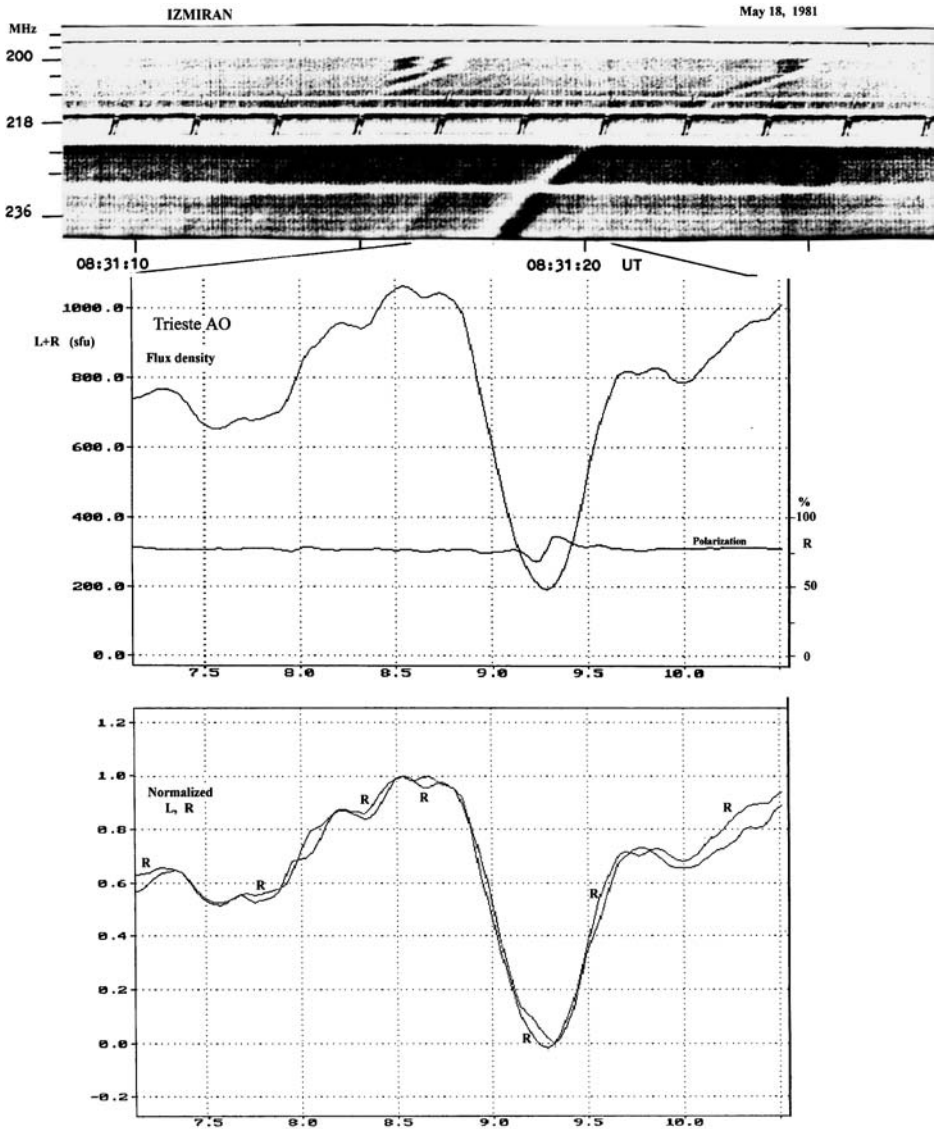


Figure 7. The dynamical spectrum in the range 190–240 MHz (IZMIRAN) and flux density, polarization profiles and normalized (separately L and R components at 237 MHz, Trieste AO) for an unusual isolated fiber during the short impulsive type IV burst May 18, 1981 (from Chernov and Zlobec, 1995).

event it is possible to recognize the delay as expected one, the weak polarization component was delayed, i.e. the extraordinary (X) wave, in the event of April 24 the strong component was delayed, O-mode. The emission in the ordinary mode looks to be the most probable one not only on the criterion of the polarity of leading

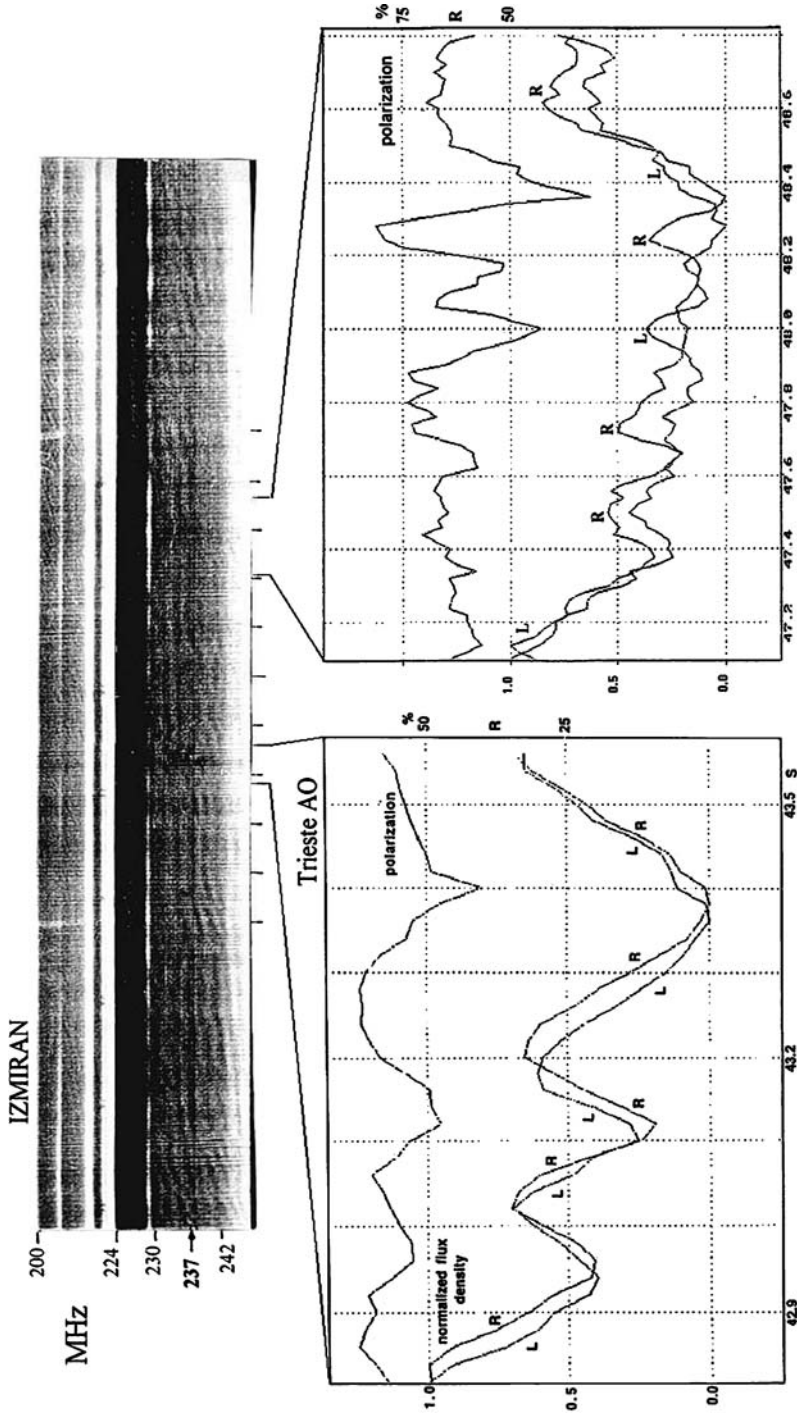


Figure 8. Under the dynamic spectrum of the zebra normalized L and R components are presented. In the same box the polarization trend is also given (after the accurate subtraction of the continuum radiation) (from Chernov and Zlobez, 1995).

spot, as this was done for the event of May 3, 1973 and for many other events with fine structure (Zlobec *et al.*, 1987), but also with the information of the position observations with the Nançay radio-heliograph (NRH) (Chernov *et al.*, 1994; 2001c).

The study of the moderate polarization is of significant interest, in order to be disentangled, whether actually in the source only one mode is emitted, and polarization depends on propagation conditions. However, the moderate polarization of fine structure was observed very rarely, 4 events are only analyzed in Chernov and Zlobec (1995). More than in 90% of cases the completely polarized radiation is usually recorded.

Chernov and Zlobec (1995) conclude that the moderate polarization is result in the course of propagation in the corona. When waves cross a quasi-transverse (or zero magnetic field) this should affect the propagation time of the O- and X-waves in a different way, in particular the weakest X-mode should be more delayed. The change of the polarization degree is very critical on the dependence of the angle to the magnetic field very near 90° : the polarization sign can change in the angle interval $89.4\text{--}89.8^\circ$ (see Table III in Chernov and Zlobec (1995)). Meanwhile for the delay of O-mode (in the events April 26, 1984 and April 24, 1985 (Figure 8)) the probable explanation is related to the reflection of waves from density inhomogeneities. The reflections and delays of O-mode were described by Hayes (1985).

In Chernov *et al.* (1994) an attempt is undertaken to analyze polarization time profiles together with the positions of the radio sources of the separate zebra stripes by means of Nançay Radio Heliograph (NRH) at 164 and 236.6 MHz. In the IZMIRAN's dynamic spectrum of Figure 9, zebra stripes with opposite frequency drift are seen in the event of June 5, 1990 (09:35–11:50 UT). This long lasting type IV event is related possibly with a filament activation and eventual eruption, but is not initiated by a conspicuous flare. In such a case it was very simply to show that the radio source positions were connected to a region of southern magnetic polarity near the active region (AR) 6086. The radio emission was fully R-handed polarized and is thus likely to be in the ordinary mode.

In this case ZP was more pronounced in absorption (see in Figure 9 below spectra the flux density time profiles in left-hand and right-hand polarization of Trieste AO at 237 MHz), and the stripes with the negative frequency drift are similar to fiber bursts with low-frequency absorption. When an emission stripe from one set intersects an absorption stripe from another set, the emission stripe is strongly reduced. The process by which the continuum is extinguished therefore also reduces the emission stripe. This can only occur if the emission and absorption stripes are generated in the same volume.

The absorption may be very pronounced: at 10:45:21 UT the modulation depth m_d at 237 MHz is about 90%. It is defined as $m_d = (I_{\max} - I_{\min}) / (I_{\max} + I_{\min})$, where I , denoting the whole Sun flux density. It varies with time, e.g. after 6 s m_d decreases gradually from 66 to 27%. However near the end of the event a series of zebra stripes only in emission is observed.

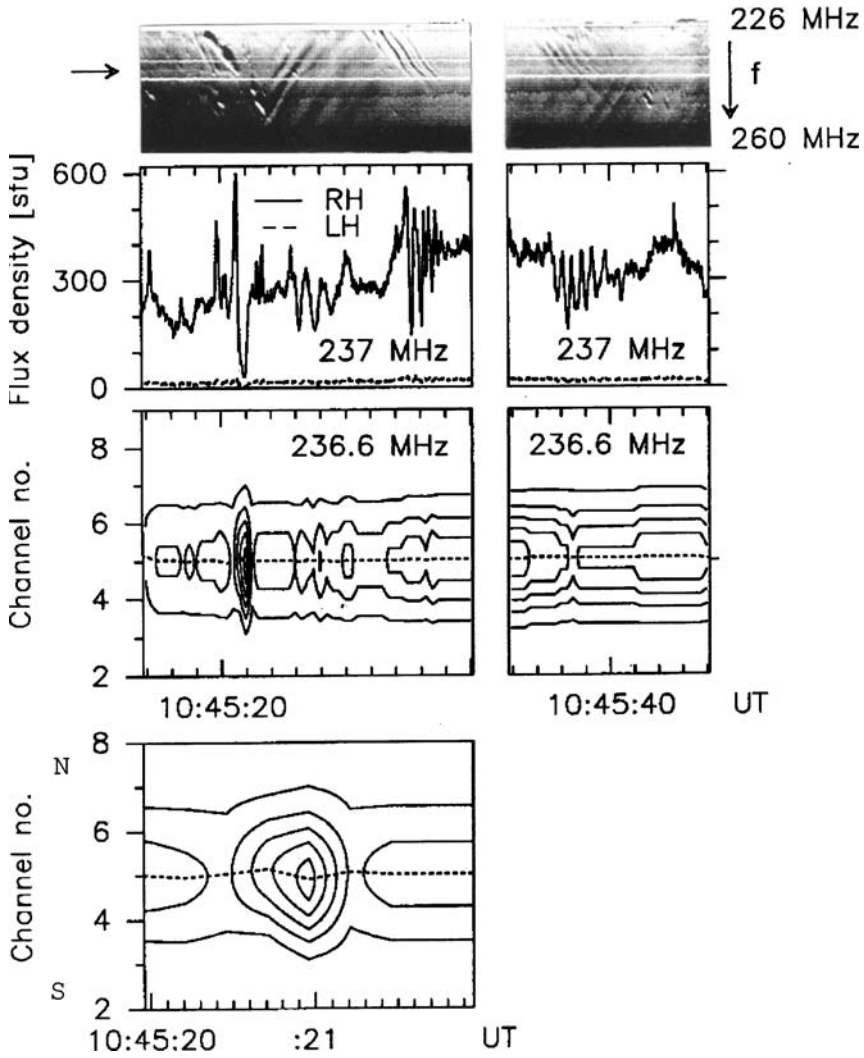


Figure 9. Oppositely drifting zebra stripes in the event June 5, 1990. The *two top panels* give the dynamic spectrum (IZMIRAN, the arrow points to 237 MHz) and the 237 MHz records of the flux density in RH and LH polarization (Trieste AO). The abscissa is graded in steps of 1 s. The *third panels* from the top give the evolution of radio brightness and source position at 236.6 MHz (Nançay Radio Heliograph (NRH)), north-south array) with contours from 9 to 89% of the biggest intensity, in steps of 20%. The *dashed line* through the centre of highest contour gives the position of peak brightness. The vertical axis is graded in $1.4'$, channel numbers of NRH from terrestrial south to north. The projected position of the centre of the solar disk is in channel 0. The *fourth panel* shows a zoom of the zebra source around 10:45:21 UT (from Chernov *et al.*, 1994).

Position data in Figure 8 will be discussed in the following section.

Some conclusions from polarization data

- The zebra patterns are usually strong polarized, in about of 90% cases.
- The radio emission corresponds to ordinary wave mode.
- In several events a moderate polarization was observed, and complex behavior of polarization is defined by propagation effect and depends of a delay of the extraordinary wave relative to the ordinary one.
- The polarizations parameters of zebra stripes and fiber bursts are usually identical.

2.2. SPATIAL SIZE AND POSITIONS SHIFTS OF ZEBRA PATTERN (ZP) RADIO SOURCES

2.2.1. *The June 5, 1990 Event*

In Chernov *et al.* (1994) the first detailed position measurements are executed, therefore it is worthwhile to extract the meaningful results of this work. The spatial properties of the ZP radio sources are approximately identical, in spite of different kinds of the zebra stripes in the investigated event of June 5, 1990: stripes with their degeneration in the course of drift into the almost dot elements in emission and absorption shown in Figure 9, or more regular ones, but accompanying by several wiggles, almost simultaneous in entire occupied frequency range (Figure 10).

The sources of zebra stripes are not point-like. Sizes up to 1.9' are observed. During the absorption stripes, slightly larger sources are seen ($\approx 2.1'$). These sizes are close to those of the unperturbed continuum.

Apparent displacements of radio sources are observed during many zebra stripes. Due to the limited time resolution of the NRH north-south array (the integration time of 0.25 s) we cannot describe the time history of displacements of all rapid variations seen e.g. in Figure 9 in the spectra and Trieste polarization profiles with the integration time of 0.02 s. The centroid of the continuum source, plotted by the dashed line through the center of the strongest contour (3rd row in Figure 9) was stable during the 13-s interval. However, during the zebra stripe the centroid undergoes an oscillating drift (the bottom panel): northward at the onset of the stripe, then southward near the brightest emission. The monotonic southward displacements were also observed in other series of zebra stripes in emission with the positive frequency drift (see Figure 6 in Chernov *et al.*(1994)). The maximum shift covered 0.56 channels (about 47'') that corresponds to the velocity component along the terrestrial north-south baseline of about $7 \times 10^4 \text{ km s}^{-1}$. The measured r.m.s. variation around the mean value was of 0.025 channels (2''), therefore the position changes detected during zebra stripes are significant.

Similar shifts of emission throughout isolated zebra stripes are also visible at 164 MHz with the east-west array (50 ms resolution). For example, during the interval of zebra stripes shown in Figure 10 the centroid of the source starts at a position east of the preceding continuum and drifts westward throughout the maximum brightness of the three emission stripes between 10:36:55–57 UT with the negative frequency

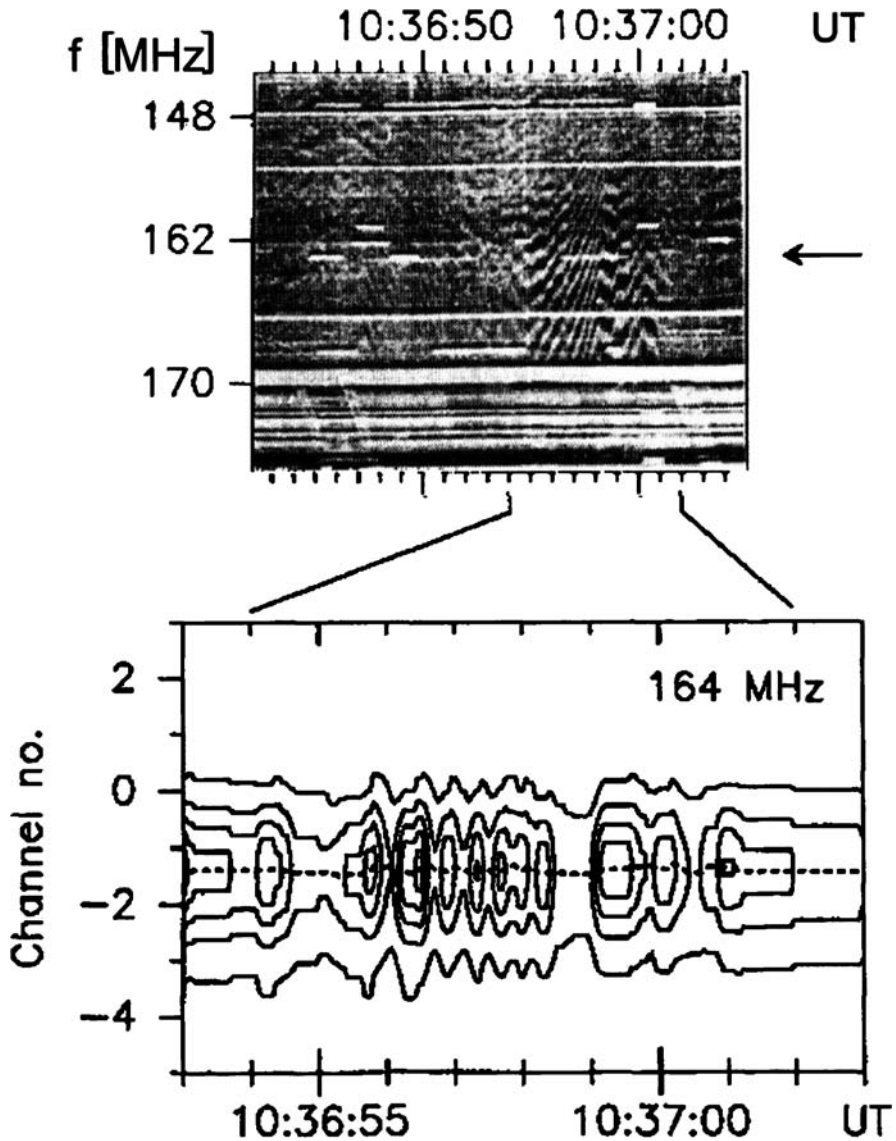


Figure 10. Temporal evolution of the dynamic spectrum (IZMIRAN) and source position (NRH) during an interval of zebra pattern in the event June 5, 1990 near 164 MHz (the horizontal arrow on the right indicates 164 MHz). Below – the one-dimensional map at 164 MHz with east-west array; the position of maximum brightness is noted by the dotted line; 1 channel $\approx 1.0'$, time resolution 0.05 s (from Chernov *et al.*, 1994).

drift. The total distance covered by the space drift is of the order of 2×10^4 km and the projected velocity $\approx 10^5$ km s $^{-1}$.

The zebra stripes undergo several wiggles with a spasmodic (saw-tooth) sign change of the frequency drift. We can note two such moments, 10:36:58 and

10:37:01 UT, and in both cases the space drift changes direction, to eastward. Furthermore, during one second into 10:36:59–10:37:00 UT the frequency drift was almost zero, and the spatial drift in this source was also retarded. Thus, we observe specific relation between the directions of the frequency drift on the spectrum and the spatial drift of sources.

Figure 11 represents source structure and dimensions during zebra pattern (shown in Figure 10). One-dimensional scans are displayed in Figure 11(a) for three features: the unperturbed continuum before zebra stripes (10:36:53.5 UT, long dashes), an emission stripe (10:36:56.45 UT, short dashes, and the subsequent absorption stripe (10:36:56.7 UT, solid line). The sources are structureless, and no qualitative difference is apparent between them. The main remarkable feature is the brightness, which is reduced in the whole source of unperturbed continuum emission during the absorption stripe and enhanced during the emission stripe. Figure 11(b) shows the time history of the peak brightness (top) and of the size (bottom) of the emitting source. Near the brightest phase of the zebra stripes, the source width is 1.5–1.6 times the beam of the NRH. The measured half width is $1.9'$, and gives a brightness temperature of roughly 10^{10} K (for a circular source) during the brightest peak at 10:36:56.45 UT. During the phase of absorption and of the unperturbed continuum emission the source appears slightly broader, typically $2.1'$ and $2.0'$, respectively.

Thus, in absorption stripes we see the whole continuum source. For this reason we always notice the shift of the center of source upon transfer from the emission stripe into the absorption stripe, (see Figures 9 and 10) since the position of the maximum brightness of continuum, as a rule, is considerably displaced from the maximum in the emission stripe. The similar behavior of radio sources we observe upon the comparison of type I bursts in the noise storm which preceded the type IV event (Figure 11(c)). The diameter of type I sources is also less than the diameter of the continuum. The source of type I bursts is also not point-like (~ 1.3 times the beam). The source sizes of the zebra emission stripe and the type I bursts are therefore comparable.

In these measurements the great significance has the mutual arrangement of the sources of continuum and fine structure. They rarely coincide. It is shown in Figure 12 two-dimensional positions of radio sources in the event June 5, 1990: sources of the continuum (marked by c), zebra stripes in emission (z) and fast pulsations (p) are spread in the projection on the disk along the active filament.

2.2.2. *The March 12, 1989 Event*

In the event March 12, 1989 zebra patterns were observed during almost three hours (09:00–11:40 UT) and were also related with an active filament. Without the determination of the positions of radio sources we could not understand at all polarization data in this event, since the zebra pattern was observed against the background of weak continuum in the RH polarimeter channel, and a strong continuum with pulsations only in LH channel. Spectral features and position data of radio sources of the

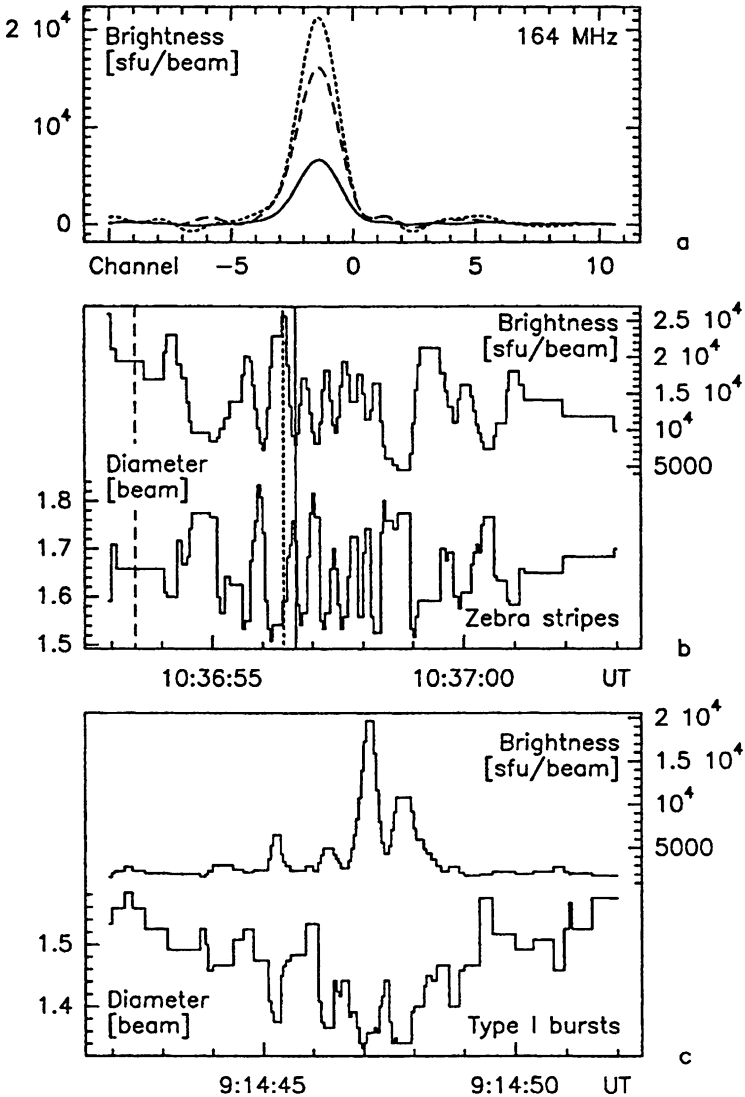


Figure 11. Temporal evolution of zebra pattern shown in Figure 10 at 164 MHz. (a) One-dimensional brightness distributions with 50 ms integration time during unperturbed continuum (10:36:53.5 UT, *long dashes*), an emission stripe (10:36:56.45 UT, *short dashes*) and the subsequent extinction stripe (10:36:56.70 UT, *solid line*). (b) Time history of the brightness (*top*) and half-power diameter (*bottom*) during the zebra-pattern. (c) Time history of brightness and diameter of type I bursts during the noise storm preceding the type IV event. The brightness and diameter in (b) and (c) are those of a Gaussian fit to the observed source profiles (from Chernov *et al.*, 1994).

zebra pattern during one minute, 11:18–11:19 UT are shown in Figure 13. The upper panel represents gray-scale plots of one-dimensional (North-South) brightness distribution in polarization (Stokes V) measured by NRH at 236.6 MHz. The emission sources of the zebra stripes are visible in white (RH-polarized) at about the

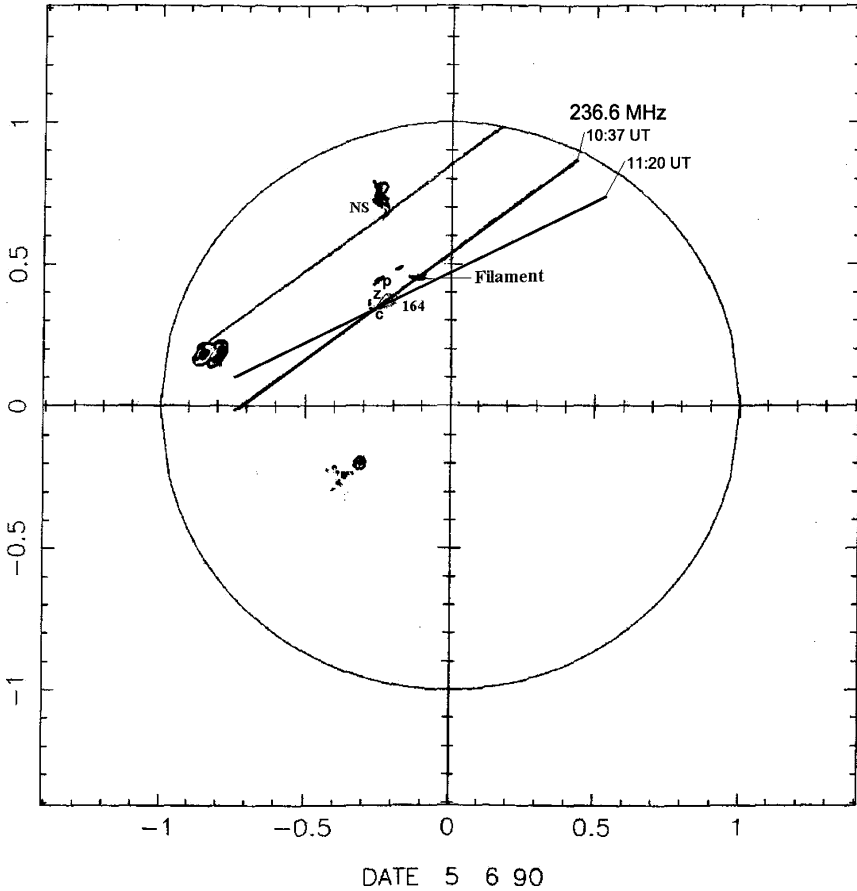


Figure 12. Two-dimensional positions of radio sources at different moments of the event June 5, 1990 with NRH, of zebra patterns (marked by z) and fast pulsations (p). All radio sources were tightly related with an active filament. Positions of the burst continuum at 164 MHz is marked by c, and at 236.6 MHz by an intersection of two one-dimensional scans at 10:37 and 11:20 UT. Sources of ZP at 164 MHz were located under the filament (marked by a cloud) (from Chernov *et al.*, 2001c).

position of the NRH channel number +1, the strong continuum source was located in the channel number +4. It appears in black (LH-polarized) with numerous pulsating sources, chaotically shifted from the center of the continuum source, predominantly directed towards the position of the zebra sources. Chernov *et al.* (1999) note the explicit shifts of the centers of sources of absorption stripes (weak remnant continuum emission, clear-gray) in respect to the white sources of the emission stripes, predominantly directed towards North, the position of the strong continuum. According to a more precise profile evaluation of source positions the displacement at Figure 13 was about 0.4 channel (38×10^8 cm). This property remained distinctive during the whole event, i.e. for about 3 hours, and sometimes of a more value, $50\text{--}70 \times 10^8$ cm.

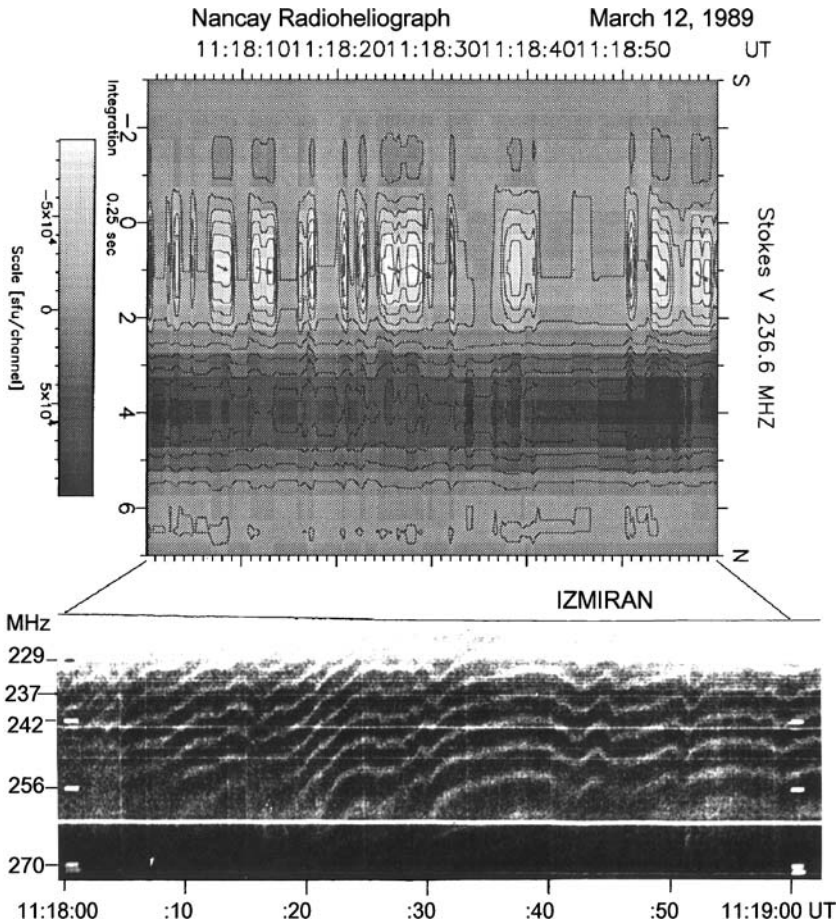


Figure 13. Radio source positions and dynamic spectrum of zebra pattern in the event March 12, 1989 during one minute 11:18–11:19 UT. The *upper panel* represents gray-scale plots of one-dimensional (North-South) brightness distribution in polarization (Stokes V, white – RH- and black – LH polarization) measured by NRH at frequency 236.6 MHz. The vertical axis gives the coordinate along the terrestrial N–S direction in units of channel numbers of NRH with one channel $\approx 2.2'$ (0 indicates the center of the solar disk). *Short arrows* in some white source centers show direction of spatial drift of maximum brightness during some wiggles of zebra stripes at the dynamic spectrum (*lower panel*) obtained with the IZMIRAN spectrograph in the range 220–270 MHz (from Chernov *et al.*, 1999).

We can also note the specific correlation between the frequency drift of zebra stripes in emission on the spectrum and the spatial drift of their sources, that it was already noted above, in the event on 5 June 1990. The frequency of 236.6 MHz in essence came to the stripes with the negative drift with its gradual flattening to the zero value. At these moments the sources detected displacement towards the North. Such displacements are marked at the position plot in Figure 13 by short arrows. Only in 11:18:16–17 UT along the frequency of 236.6 MHz the zebra stripe experienced the jump of drift to the reverse side (with the positive drift), and then

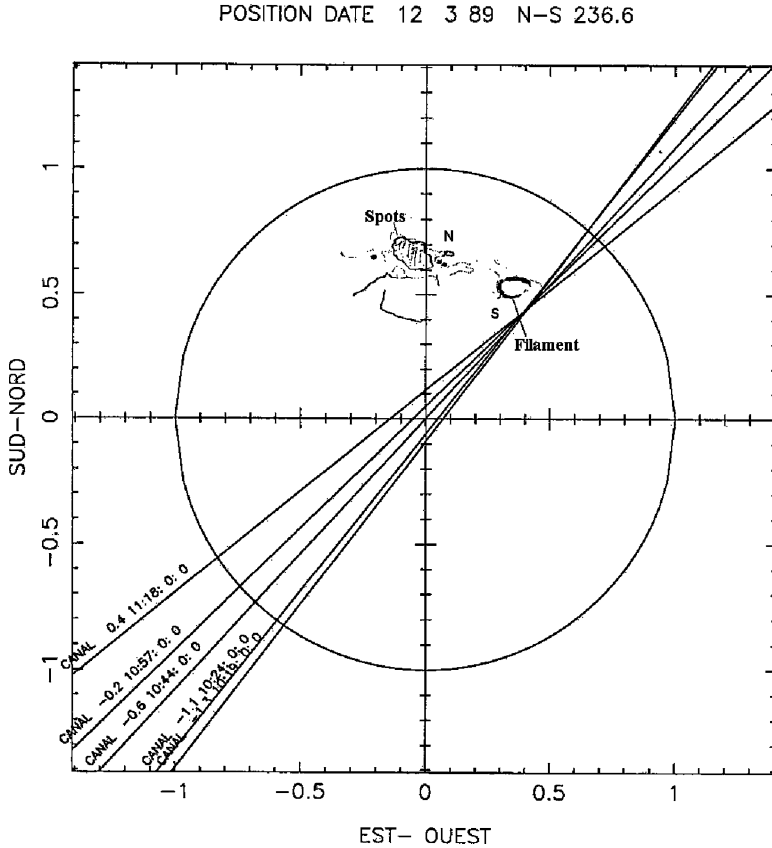


Figure 14. Two-dimensional positions of radio sources of zebra patterns (LH polarized) in the event March 12, 1989 at 236.6 MHz obtained by intersections of one-dimensional S-N scans of NRH in different moments. The radio source positions were tightly related with an active filament in the south magnetic polarity (S). The strong burst continuum source (RH polarized) was located near AR NOAA 5395 with the predominant north magnetic polarity (marked by N) (from Chernov *et al.*, 1999).

the source was displaced towards the South. Such displacements were even more pronounced in other zebra pattern series during the event.

One should note, that the source of the zebra against the background of weak continuum (30–60 s.f.u., 1 solar flux unit = $10^{-22} \text{ W m}^{-2} \text{ Hz}^{-1}$) in the course of the event, was also slowly displaced towards the north. So, in one hour 10:20–11:20 UT it was displaced from channel -1 to $+1$, i.e. up to distance of $190 \times 10^8 \text{ cm}$, with an average speed of about 50 km s^{-1} . The source of strong continuum (200–600 s.f.u.) was also displaced towards the North, but up to the noticeably smaller distances. We constructed a two-dimensional position of the zebra source in Figure 14, using the crossing of one dimensional scans of NRH at 236.6 MHz during the event. The strong continuum source was located near the AR 5395 (Spots), meanwhile the zebra sources was located (in projection) near a dark (in the line H_α) filament.

According to Stanford magnetogram in SGD 537, part 1 (1989) the predominant magnetic polarity near Spots was North (N), and near the filament it was South (S). Hence we assume that the radio emission of both sources corresponded to the ordinary wave. The radio event started after the end of the 2B H_{α} flare (N28E05) in AR 5395 and after a small maximum (08:28 UT), of importance M6.7 of SXR (GOES-7). The zebra patterns had been observed during the three hours lasting interval between two CMEs. Taking into account that the maximum energy release taken place in the meter radio range and a source merging of zebra absorption stripes and pulsations (in the strong continuum) we assume that the radio event was caused by a global magnetic reconnection high in the corona, and the radio sources of the zebra patterns were related with magnetic islands during a long-lasting restoration of the magnetic structure after the CME.

2.2.3. The February 17, 1992 Event

In the event February 17, 1992 the zebra patterns were observed in a complex type IV event during about four hours in the time interval 08–12 UT, and the radio source was also connected with an active dark filament without a big H_{α} flare and microwave activity (Chernov *et al.*, 1998). For the first time we can see an entire frequency range occupied by ZP in a oscillating regime in the interval 180–350 MHz (Figure 15). The polarization changed the sign during the event from LH into

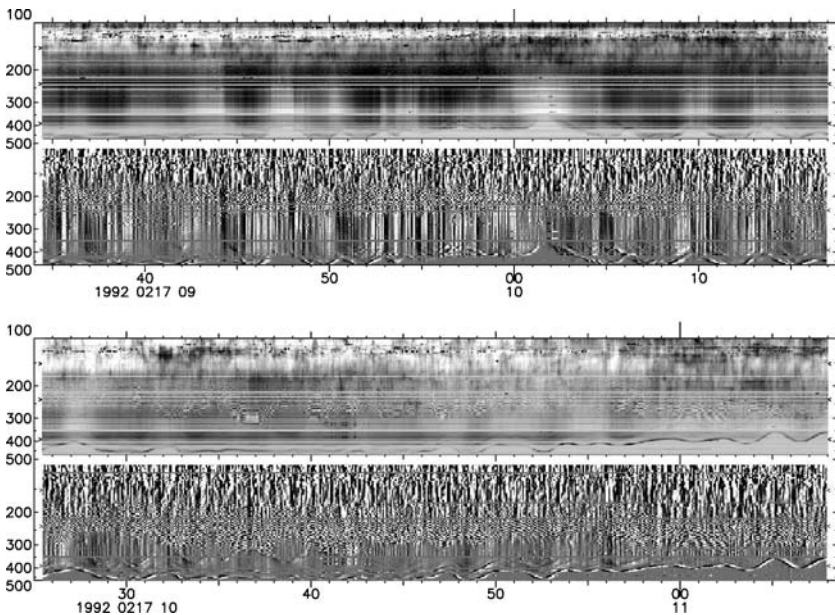


Figure 15. ARTEMIS dynamic spectrum over a 1 h 45 min period (flux density/time derivative). Besides the 3 min pulsations (in phase with the EEL around 400 MHz), additional pulsations with periods of ≈ 20 s can be seen, as well as zebra patterns between 190 and 350 MHz, and noise storm at frequencies < 190 MHz (from Chernov *et al.*, 1998).

RH beginning from 236.6 MHz (10:00 UT) then at 327 MHz (10:52 UT) and 407 MHz (10:58 UT), i.e. beginning from the upper corona layers to the lower ones.

The change of the polarization sign was accompanied by a smooth decrease in the emission, as continuum so zebra patterns (in the time interval 10:00–10:02 UT the zebra pattern almost disappeared). Figure 16 gives representation about the change the nature of zebra pattern before the change of the polarization sign (with the sharp jumps of drift) and after the change of sign (with a slow drift, when the stripes are almost parallel to time axis). The frequency range of the zebra patterns began gradually to become narrow. It is possible to explain this by a capture of the zebra radio source into a magnetic cloud.

It is remarkable, that the radio emission of the oscillating fiber limiting all the emission from the high frequency edge, discussed in Chernov *et al.* (1998) as *Evolving Emission Line* (EEL), retained the sign of polarization even during several minutes to 11:06.5 UT, although the continuum at 407 MHz changed the sign of polarization rapidly at 10:58.5 UT. Probably, its source was located in the corona in the old configuration of the magnetic field lower than the new magnetic cloud. Thus, in the February 17, 1992 event it was difficult to define the wave mode, because the polarization changes were probably caused due to the magnetic reconnection high in the corona.

However we could compare the frequency drift with the spatial source shifts during one of unusual frequency splitting of zebra stripes. For the larger persuasiveness we added to Figure 16 the one-dimensional SN distribution of zebra-stripe sources. We had time resolution of NRH only 1 s, but the zebra stripes changed the sign of frequency drift at 10:58:22 UT from positive into negative with enough low frequency drift (remaining almost parallel to the time axis). Therefore this time resolution make it possible to recognize the spatial drift of sources as significant. So, we see the spatial drift at 236.6 MHz in the beginning of this interval (about 10:58:08 UT) towards South and in the end (about 10:58:35 UT) towards North. In Figure 16 the direction of the spatial drift are marked by arrows in the centers of sources at the corresponding moments of SN distribution. Looking at Figure 3 in Chernov *et al.* (1998) and being based on several Yohkoh/SXT images, it is tempting to locate the radio source of zebra patterns in this event within a large trans-equatorial closed loop connecting AR 7056 and 7058. The source displacements in the direction S–N are quite anticipated therefore.

Some main conclusions from positional observations.

- The zebra pattern radio sources are not point-like, they occupy the noticeable part of the background continuum source or even of entire active region (AR). The measured half width is $1.9'$, and gives a brightness temperature of roughly 10^{10}K .
- Different positions (or displacements) of the sources of stripes in emission and absorption are almost always observed, they prove to be maximum in cases when the sources of zebra patterns and continuum are strongly spread. In the

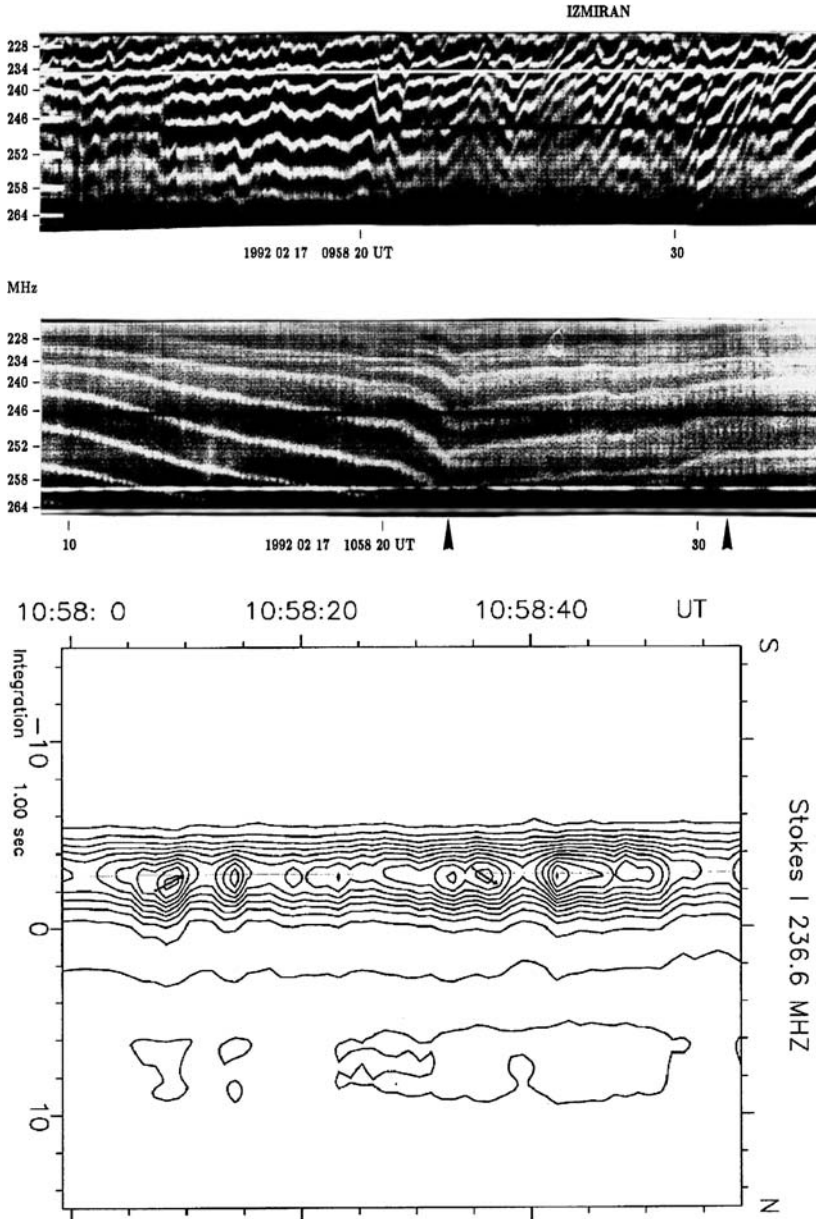


Figure 16. Top: Two fragments of zebra patterns recorded with the IZMIRAN spectrograph, (before and after the change of polarization sign) illustrating two kinds of sub-structures discovered. The top spectrum shows numerous sudden frequency shifts of zebra stripes. The bottom spectrum shows a case of stripe splitting (first arrow is the beginning) and dot-like structure of the upper frequency component (second arrow). Bottom: Contour plots of the one-dimensional SN brightness distribution measured by NRH at 236.6 MHz in intensity. The 0 channel gives the center of the solar disk. The arrows in the centers of sources at 10:58:07–10 UT and 10:58:34–37 UT show the direction of the spatial drift of sources (from Chernov *et al.*, 1998).

absorption stripes we see actually not real motions, but rapid switchings towards the center of the continuum source.

- A correlation is noticed between the directions of frequency drift of stripes on the spectrum and the spatial drift of sources at the fixed frequency. The speeds of motion in the projection on the solar disk prove to be very large, $\geq 10^{10}$ cm s⁻¹.

Below, in the section 4.4.1 a more detailed description of source displacements of zebra stripes in the event October 25, 1994 is presented.

2.3. SUB-STRUCTURE OF ZEBRA STRIPES

Two new kinds of sub-structures are visible in the zebra patterns recorded by IZMI-RAN spectrograph on February 17, 1992. The first new feature is a rapid frequency shift of the whole zebra pattern, like at 09:58:21 UT (Figure 16, upper panel). All zebra stripes jump by an amount comparable to the zebra stripe separation. They do not do it simultaneously, but with a frequency drift rate $df/dt \approx 50$ MHz s⁻¹, comparable to type III burst drift rates. The zebra pattern seems to be broken along a slanted “fault”. These frequency shifts occur frequently and randomly during the whole event, without any characteristic time period, sometimes within a second, sometimes episodically during one minute.

The second new feature consists in sub-splitting of a zebra stripe into two separate stripes, like at 10:58:21–22 UT (Figure 16, middle panel, after the hook). The split stripes have different characteristics: the low-frequency stripe is continuous, while the high-frequency stripe consists of regular dots with a characteristic period ≈ 0.25 s. These frequency splittings last for minutes. Occasionally two continuous stripes exhibit chaotic frequency drifts, or cross each other.

The oscillating fiber in the event February 17, 1992 had the frequency bandwidth in emission 10–15 MHz (Figure 15). It oscillates almost sinusoidally and in phase with flux density of broadband pulsations. One or two weaker additional stripes (15–20 MHz wide) appear episodically on the low frequency side of the EEL, at 20 to 100 MHz from it. The EEL is distinctly different from zebra stripes at lower frequencies. It mostly consists of one single emission stripe instead of many, with a larger relative bandwidth $\Delta f/f \approx 12/450 \approx 0.03$, instead of $\approx 1.3/250 \approx 0.005$ for zebra stripes. It is also continuous over two hours instead of being intermittent.

Very dilated plots using ARTEMIS high time resolution (Figure 17), reveal that the EEL is structured into a succession of dots every 0.25 s or so. Each dot consists of an emission (black) on its low-frequency side and an absorption (white) on its high-frequency side. The duration of each dot is about half their period, that is ≈ 0.12 s. The dots are synchronized with zebra stripe dots (after the splitting, Figure 16) and 0.25 s sudden reductions.

The source position of the EEL is also different: it is north of the continuum/zebra pattern common position.

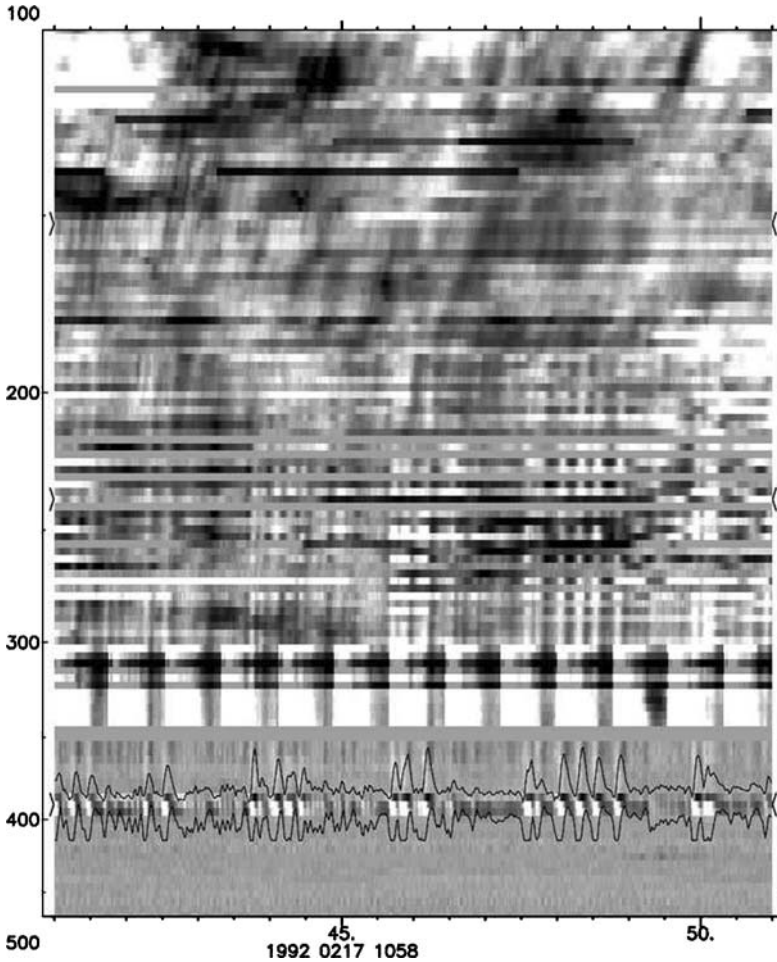


Figure 17. ARTEMIS spectrum at high time resolution, over a time interval when zebra patterns exhibited marked sub-structures. Zebra stripes are the horizontal black bands around 250 MHz; each one is visible in a given frequency channel for a few seconds only, because of its frequency drift. The EEL is visible on 2 channels around 400 MHz; we superimposed the 2 corresponding time profiles showing the 0.25 s period clearly. This set-up emphasizes the spectral structure of the EEL, made up of emission (black) and absorption (white) dots, synchronized with zebra stripe dots and 0.25 s sudden reductions. At frequencies <200 MHz, we notice fast structures drifting at type III rates (from Chernov *et al.*, 1998).

2.3.1. Braided Zebra Patterns

In some events the overlap of different fine structures may be just a chance. Slottje (1981) shown statistics of the simultaneous appearance of fast pulsations, spike bursts and fiber burst with the zebra patterns: the percentage of such event is low and their occurrence may be independent, e.g. because they arise in spatially different sources. A number of events were observed where zebra stripes are not continuous

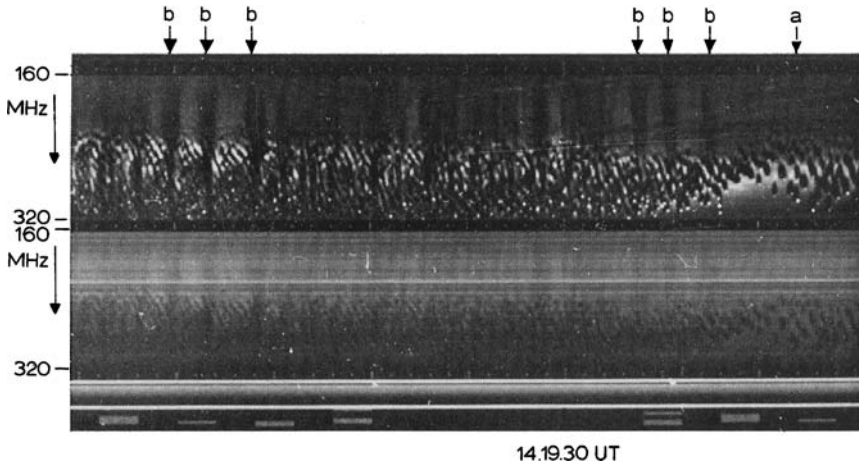


Figure 18. ZP ending in separate tadpoles in the event March 2, 1970 (from Slottje, 1972).

emissions, but the trajectories of a substructure of narrow-band short-lived elements (spike bursts), which themselves show different drift rates. Such a degeneracy of regular zebra stripes into different substructure elements can be seen already based on the first example, given by Elgarøy (1959) (see Figure 1, two bottom panels). Slottje (1981) consider drifting spikes, organized in zebra-like patterns as distinctive structure which was called ‘braided zebra pattern’.

After the conclusion of Slottje (1981) that the braided zebra patterns are events themselves, all consequent observations shown that in many events the regular zebra pattern sometimes degenerates into the braided one. Karlicky *et al.* (2001) named similar structures as *lace bursts*.

2.3.2. Tadpoles

In one event (March 2, 1970) Slottje (1972) observed a degeneracy of zebra stripes into so-called tadpoles. These burst got their name because of their aspect on the spectrum: an absorption “body” with a low frequency emission “tail” and a high frequency emission spike, the “eye” (Figure 18). Tadpoles were very developed, and Slottje isolated this element as a special structure. They were described in detail also in Slottje (1981). The 3-dimensional scheme of one tadpole is also described in monographs Krüger (1979) and Zheleznyakov (1995).

Although it is possible to find examples also in other events when the unsteady (irregular) zebra stripes produce on the spectrum whimsical forms, including the tadpoles. Such an example is shown in Figure 19. In the middle panel a small tadpole is marked by an arrow. In this event (July 3, 1974) the regular zebra stripes appeared only during very short time interval, as this is shown (by the arrows) in two other panels. The frequency profiles shown at the right of each spectrum present modulation depth typical for ZP.

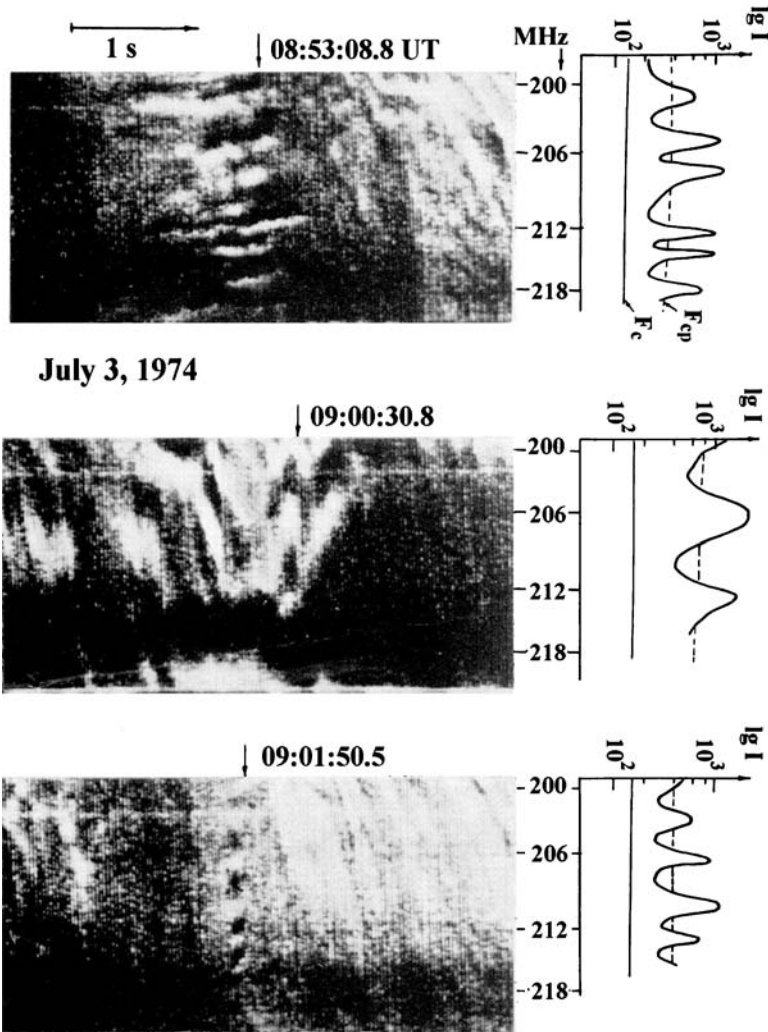


Figure 19. Three fragments of spectra with non stationary ZP on July 3, 1974, registered by IZMIRAN spectrograph (time resolution is 0.02 s, frequency resolution ≈ 0.15 MHz). Frequency profiles obtained by microphotometry of the spectra in relative logarithmic units at the time marked by arrows above the spectra are presented in the same frequency scale as the spectra (from Chernov, 1976a).

These examples already show, what a wide variety the irregular ZP presents in each event. However, this in no way indicates, that each new element is excited by new mechanism. Most likely, entire diversity of stripes on the spectrum is determined by the parameters of plasma in the radio source and by the form of the distribution function of fast particles, which, naturally, cannot be strictly identical in the different events.

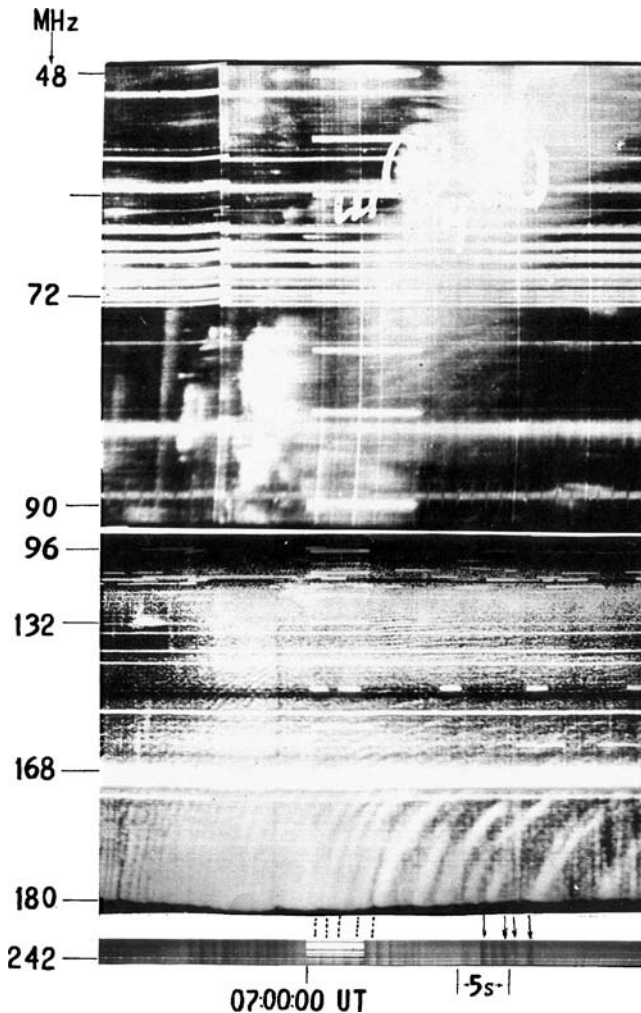


Figure 20. Dynamic spectrum of type V on April 26, 1984 showing a transformation of pulsations in HF part (220–240 MHz) into ZP between 120–180 MHz (spectrograph of IZMIRAN) (from Chernov *et al.*, 1984).

2.3.3. Unusual Behavior of ZP

2.3.3.1. *The April 26, 1984 event.* An intriguing conversion of the second pulsations into ZP was observed on April 26, 1984, shown in Figure 20. The continuum burst began after a group of type III+V burst (and after the small 1B flare). In the high frequency part of the spectrum (200–242 MHz) the burst has the form of instantaneous pulsations in emission and absorption (sudden reductions) with the time scale of seconds. At lower frequencies the frequency drift of pulsations becomes measurable, and it decreases gradually from $\approx -180 \text{ MHz s}^{-1}$ to $\approx -0.5 \text{ MHz s}^{-1}$

and pulsations turn into arch stripes similar to the ZP (or fiber bursts, shown by dashed lines in Figure 20). The stripes are not continued below 130 MHz, but in the frequencies 84–72 MHz some drifting fibers (or striae) are also present in the continuum of type V burst .

At the end of the event it is clearly visible that the stripes are superimposed to spike-like pulsations with a strict period of 0.8–1.0 s. All the emission consists of the second pulsations and drift stripes. Sudden reductions in the range 242–220 MHz correspond to the spaces between the pulsations in the emission at the lower frequencies (shown by arrows in Figure 20).

Thus, in this event a continuous conversion of second pulsations at HF part of the spectrum into zebra stripes with gradually decreasing frequency drift at lower frequencies was observed. This testifies on a close connection of the nature of sudden reductions and stripes of ZP.

2.3.3.2. The July 28, 1999 event. The analysis of the zebra-patterns is based on the dynamic spectra of IZMIRAN and Phoenix-2 (Messmer *et al.*, 1999), single frequency polarization data of the Trieste AO and spatial positions of the Nancay Radioheliograph (NRH). This event included long-lasting zebra-patterns between 08:15 and 10:30 UT related to a small flare (1B M2.3) in AR 8649 localized at S15 E03 with maximum at 08:14. The event was accompanied by a CME of HALO type at 09:06. The peak radio flux in the decimetric range was 42000 s.f.u. at 606 MHz at about 08:48.

Concerning fine structures, three main phases can be selected: the impulsive (08:15–08:30), followed by the peak (08:50–09:25) and the decay (10:15–10:30). During the first two phases narrow banded zebra-patterns with 50–150 MHz bandwidth appeared in the frequency range from 200 up to 1500 MHz (Ondrejov spectra). The interval between different bursts was lasting about one minute. During the decay phase zebra-patterns appeared mainly at frequencies between 300 and 400 MHz.

The two top panels of Figure 21 show examples of the zebra-patterns during the impulsive phase (left, IZMIRAN) and the decay phase (right, Phoenix-2). In the left panel zebra stripes drift towards higher frequencies. In the later decay phase the zebra lines show different frequency drifts with tendency towards lower frequencies. With this frequency drift behavior zebra stripes resemble fiber bursts. A common property of both zebra and fiber burst was the absorption of the continuum emission at the low frequency edge of each stripe. The middle panels in Figure 21 show evident absorption in the L- and R-plots of the Trieste AO at 237 MHz (left) and 327 MHz (right). The circular polarization was weak at the beginning of the event (weakly R-handed at 327 and 408 MHz during the impulsive phase at 08:15) and moderately L-polarized (about 30–40%) after 08:25. At the maximum the L-polarization increased to about 60–80% and then towards the end became once more moderate.

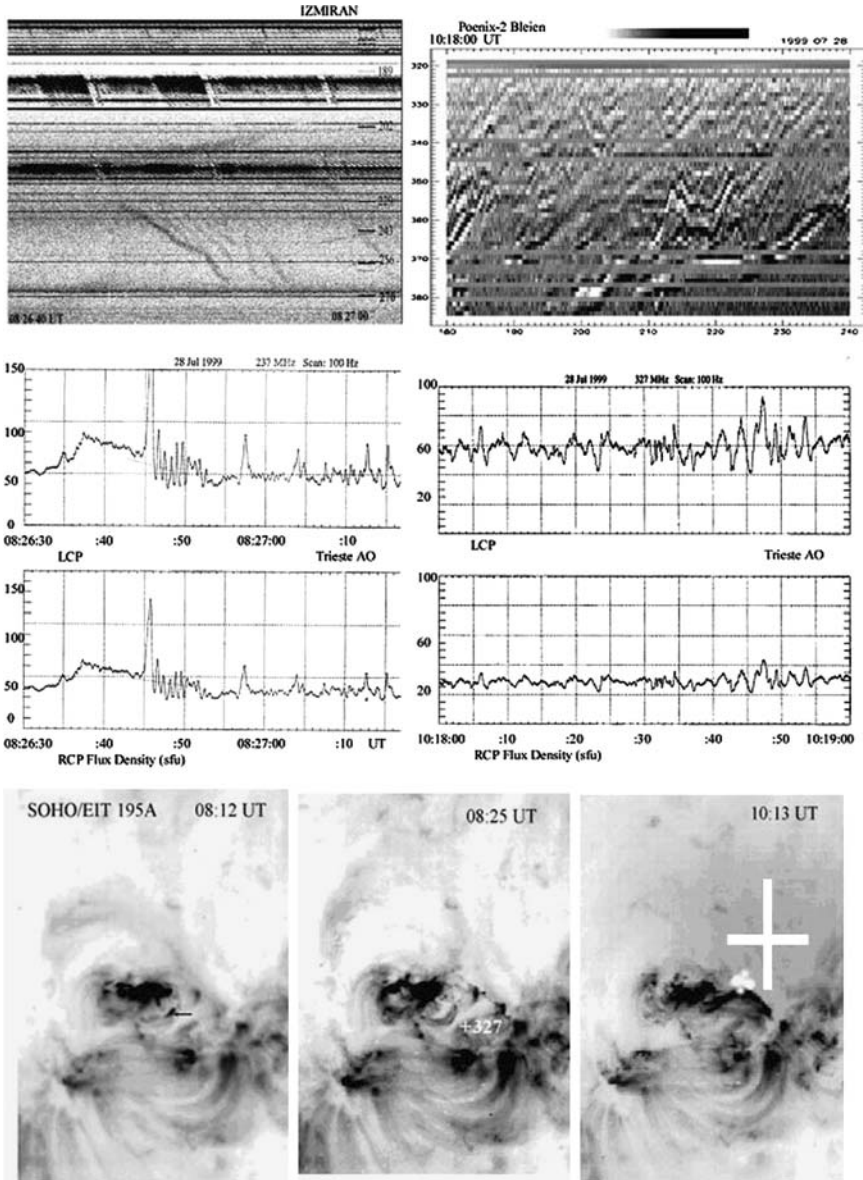


Figure 21. Top panel: Two spectra showing zebra-patterns at about 08:26 between 189 and 270 MHz recorded by IZMIRAN (left) and at about 10:18 between 320 and 385 MHz by Phoenix-2 (right). Middle panel: time profiles of the Trieste AO polarimeter at 237 (left) and 327 MHz (right). Bottom panel: Flare evolution in EUV line 195 Å (SOHO/EIT). The arrow in the left panel indicates a new rising bright loop. The positions of the NRH radio source centers are shown by crosses (small cross –327, big cross –164 MHz) (from Chernov, 2004).

After the event maximum (08:55) some unusual fiber bursts appeared with absorption at both low and high frequency edges of the emission stripe (Figure 22). Additionally, some stripes were observed in absorption only. After 10:19 almost all zebra stripes and fiber bursts showed absorption at the high frequency edge (Figure 22, bottom). During that interval zebra-stripes formed some cascades with U-burst like change of the frequency drift (from negative to positive). In such cases fiber bursts were continuously converted into zebra-stripes.

SOHO/EIT data show two new bright loops that appeared earlier than the two intervals of zebra-pattern structures (bottom panels at the Figure 21). According to NRH data the radio sources were located above these loops. During the impulsive phase, the zebra-patterns between 450–550 MHz can be connected with the appearance of new bright kernels (arrow in Figure 21, left SOHO/EIT panel). According to SOHO/MDI magnetograms these evolving kernels appeared above the neutral magnetic line, that explains the change of polarization sign at that moment. Afterwards, flare kernels form the raising bright loop and the radio source at 327 MHz were localised just above this loop.

A common interpretation of the above observations is that the zebra-patterns occurred in the new formed coronal flare loops. The narrow bandwidth of the zebra-patterns is determined by the vertical dimensions of these emergent loops. The change in frequency drift can be interpreted as the change of the density gradient at the radio source and of the whistler group velocity direction due to the quasi-linear scattering of whistlers on fast particles. The partial L-polarization suggests ordinary emission mode.

The striking feature is the inverted position of the absorption stripe in the zebra-pattern during the decay phase, i.e. at the high-frequency side of the emission stripe. This has to be accounted for by any theory of the zebra-burst emission mechanisms. A similar behavior of fiber bursts was considered in Chernov (1990b) where it was shown that in such a case the observed emission is obtained by wave decay $l \rightarrow t + w$, with emission at the frequency difference between $l-$ and $w-$ waves. The continuous conversion of fiber bursts into zebra-lines with positive frequency drift, considering that the other parameters of both structures are identical, testifies an unique origin of both structures in frames of whistler model.

2.3.3.3. The September 23, 1998 event. According to Solar Geophysical Data (SGD), a 3B M7.1 flare began at 06:40 UT in the active region NOAA 8340 (N18E09), reaching its maximum at 07:13 UT. The radio event was observed from 06:52 to 11:00 UT, and included a type II outburst (06:52–07:02 UT) and a prolonged type IV outburst with several maxima. Zebra structure was observed in the interval 08:00–08:10 UT. In the spectrum in the upper panel of Figure 23, obtained with the new ARTEMIS IV spectrograph (Greece) at 250–450 MHz (Caroubalos *et al.*, 2001), we can see a fiber burst (08:03–08:04 UT), rib-like zebra structure (08:05–08:06 UT), and rapid pulsations in emission and absorption (08:08–08:09 UT). Below the spectrum, a rare property of the fine structure is visible in the

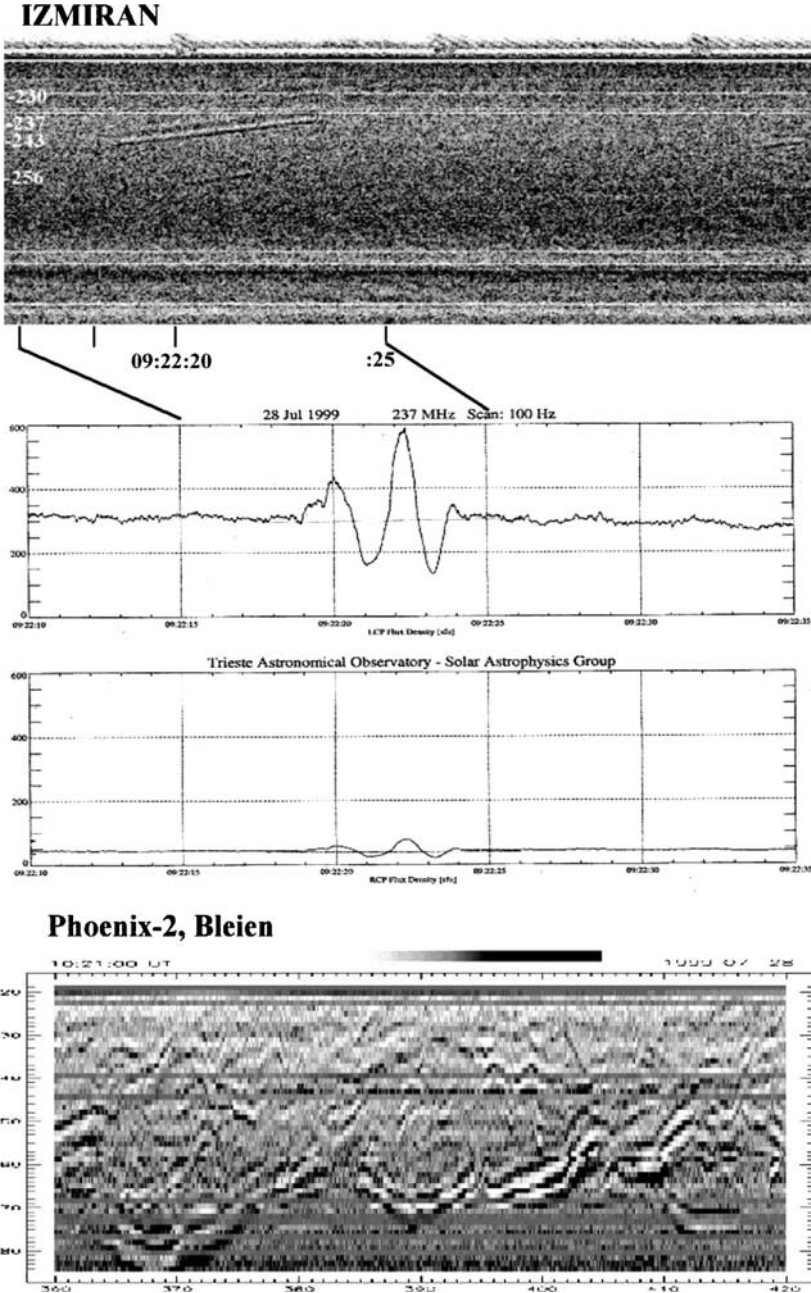


Figure 22. Top panel: IZMIRAN spectrogram showing the absorption at both low and high frequency edge of the emission in a fiber burst, confirmed by the Trieste AO polarization measurements (middle panel). Bottom panel: Phoenix-2 spectrum between 320 and 385 MHz displays an unusual zebra-pattern with absorptions at high frequency edge of the emission stripes (from Messmer *et al.*, 2002).

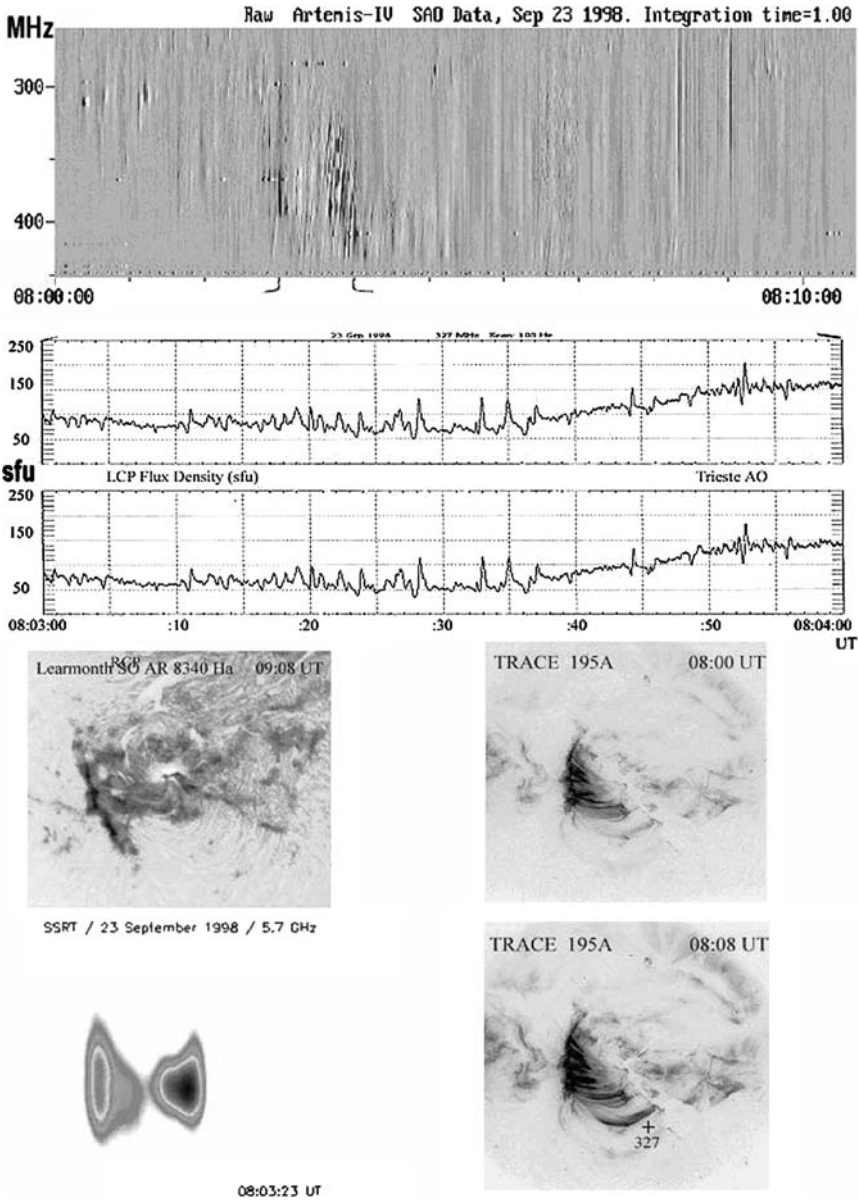


Figure 23. The event of September 23, 1998. *The upper panel shows the fine structure displayed between 08:00 and 08:10 UT at 250–450 MHz (the ARTEMIS-IV spectrograph, Greece). The next panel presents time profiles of the L and R channels of the Trieste Astronomical Observatory polarimeter at 327 MHz, which shows weak left-circular polarization. The lower set of panels presents the development of the H_{α} flare (upper left; Learmonth Solar Observatory), two EUV 195 Å frames, which show numerous hot loops between two parts of the neutral line (right, TRACE), and the radio brightness distribution at 5.7 GHz (lower left, SSRT). The position of the center of the radio source at 327 MHz (NRH) is indicated by the cross above the new loop at 08:08 UT (from Hillaris *et al.*, 2002).*

327-MHz polarization profiles obtained at the Trieste Astronomical Observatory: the radiation displayed very weak left-circular polarization. These profiles also show that the dips in intensity in the absorption stripes comprise about 20–30% of the mean continuum level. The zebra structure observed at 08:06–08:07 UT was most pronounced in absorption, and the rapid pulsations observed at 08:08–08:09 UT were also purely in absorption (i.e., they were of type sudden reductions).

The evolution of the flare is illustrated in four different panels in the lower part of Figure 23. A two-ribbon H_{α} flare was observed over three hours along the eastern and western parts of a neutral line of the magnetic field. The two TRACE 195 Å frames show numerous bright loops that appear (and disappear) between these two parts of the neutral line. A new bright loop appeared in the southern part of the flare region at 08:00 UT, and the center of the 327 MHz radio source observed at 08:08 UT (NRH) coincides with this new loop in the 195 Å TRACE frame.

Thus, the analysis of all the available observational data for these event show that fine structure was observed simultaneously with the appearance of new, hot magnetic loops, and that the frequency bandwidth occupied by the fine structure in the spectrum (280–450 MHz) could realistically be determined by the extent of these new loops in the corona. Again, the data demonstrate that the zebra structure consists not only of stripes of emission, but also of stripes with appreciable absorption, which are sometimes even dominant.

2.3.4. *Unusual Fibers*

2.3.4.1. Slow drifting fibers in the type II bursts. The term ‘unusual fibers’ we use only in connection with unusual frequency drift, characteristic for fiber bursts (IDB), (on classification of Slottje and Kuijpers), since in many events fibers as separate bursts have different speed of frequency drift (almost as zebra), which is already obvious based on the example of the first spectra of slow drifting fibers of Thompson and Maxwell (1962) (Figure 24). They showed such unusual fibers in type IV burst at frequencies 100–180 MHz and at frequencies 25–50 MHz in the end of type V burst in its low frequency part.

The subsequent observations showed, that the unusual fibers appear more frequently in the the type II bursts. Sometimes the II type emission degenerates simply into the narrow-band fibers. An example of such fibers is given by Chernov (1990a) in Figure 3. But more frequently slow drifting fibers appear in the flare continuum immediately after the type II burst. Specifically, such fibers at frequencies 72–140 MHz are analysed in detail by Bakunin *et al.* (1991) in the event February 3, 1983. The similar bursts are analyzed by Chernov (1997) at more high frequencies 186–236 MHz in a strong flare continuum in the event of October 12, 1981 (Figure 25). The unusual fibers were observed on the impulsive phase of flare, and the zebra patterns appeared just the same time and continued more than half hour. The microwave burst of the type gradual rise and fall (GRF) had the maximum (delayed relatively metric burst) and just the maximum phase of zebra pattern. The slow drifting fibers differ from the fiber bursts by many parameters: larger instantaneous

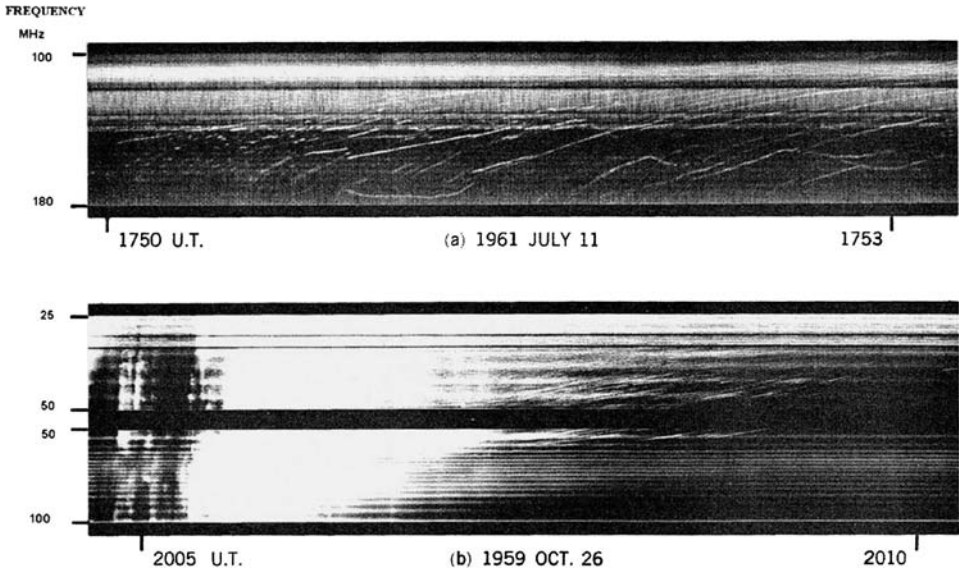


Figure 24. The first example of unusual fibers in the range 25–180 MHz (from Thompson and Maxwell, 1962).

frequency bandwidth (≈ 3 MHz at 115 MHz); slower frequency drift (about equal to drift of type II bursts); long duration (about one minute instead of some seconds). Nevertheless, sometimes they reveal low frequency absorption (Bakunin *et al.* 1991), typical for FB.

The first, natural suggestion that the emission from elongated density irregularities are observed (when a shock wave propagates through them), do not support by the registration some second after of the subsequent type II burst without similar fibers at the same frequencies in the same event. Since the formation and disruption of dense extended irregularities cannot occur in only a few second, we would suggest that in each case the fibers are created by an emission mechanism, rather than by the structure of the corona.

A number of data on interplanetary shocks indicate the presence of plasma wave and whistler in the upstream of fronts. It is, therefore, logical to consider the fiber structure of type II bursts to be the result of the propagation of whistlers through clumps of plasma waves ahead of a shock front. The absence of bounce motions of the fast particles ahead of the shock front explains the lack of strict periodicity of the fibers. Without diffusion of fast particles on whistlers the absorption at low-frequency edge cannot be created, as confirmed by the observations. Whistler wave packets can be almost standing before the front (when the whistler group velocity is about equal to the velocity of the shock) which explains the prolonged whistler propagation (without the cyclotron damping), i.e. longtime fibers.

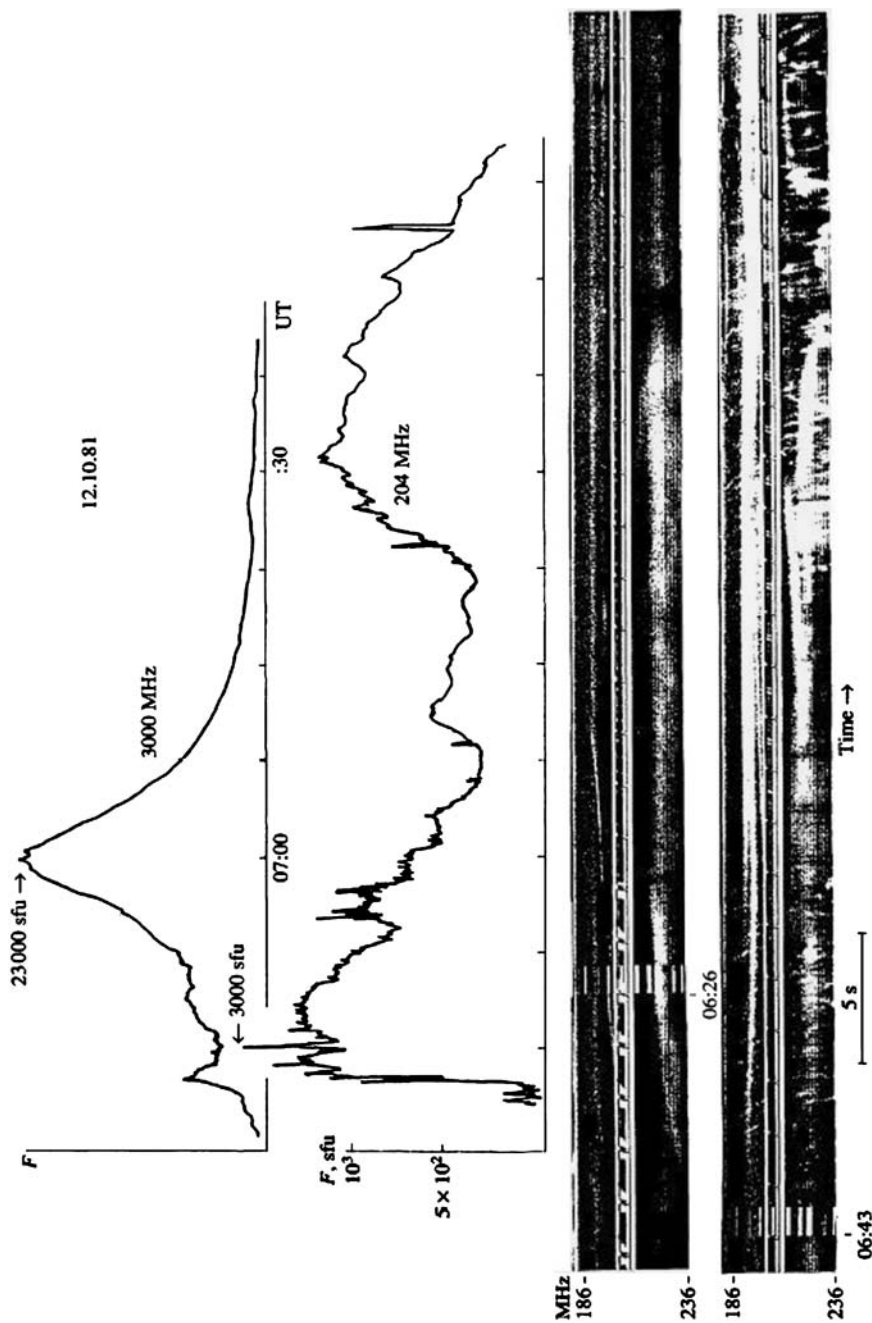


Figure 25. Two bottom panels: slow-drifting fibers recorded by IZMIRAN spectrograph in the strong flare continuum after the type II burst on 12 October 1981 (at 06:26 UT) and at the background of a braided zebra pattern (at 06:43 UT). Two top panels: time profiles at frequencies 3000 and 204 MHz; the maximum of microwave bursts (of type gradual rise and fall) delays noticeably relatively the burst maximum at 204 MHz (from Chernov, 1997).

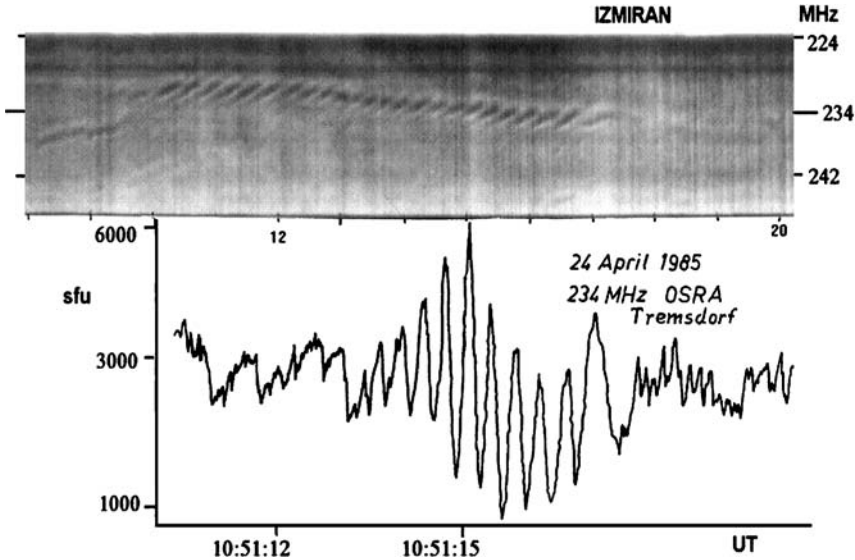


Figure 26. IZMIRAN spectrogram in the 224–247 MHz range of rope-like chains of fibers and corresponding radio flux registration at 234 MHz of the Tremtsdorf Observatory (from Aurass *et al.*, 1987).

The slowly drifting fibers in the flare continuum (after the type II burst) shown in Figure 25 (see also Figure 12 in Bakunin *et al.* (1991)) can be related with whistlers generated between two shock fronts or between shock front and CME propagating with almost equal velocities (see in more detail Chernov (1997)).

2.3.5. Rope-Like Fibers

For the first time, Aurass *et al.* (1987) reported on a new fine structure observed by IZMIRAN spectrograph during the type IV radio burst on April 24, 1985 (Figure 26). It was named as slowly drifting chains of narrowband fiber bursts, then as envelope of fibers (Mann *et al.* 1989) and as rope-like fibers (Chernov, 1997). This last name in the best way reflects their view of dynamic spectrum, and it will be used in the following presentation. The rope-like structures are characterized by a slowly positively or negatively drifting rope of narrowband, always negatively drifting fiber bursts. The fibers possess very pronounced absorptions at the low frequency side confirmed by a strong modulation depth presented by the radio flux profile at 234 MHz at the bottom of Figure 26.

In the same time the majority of ropes is accompanied by its own low frequency absorption, which sometimes proves to be more expressed, than emission, as this is shown in Figure 27: rope began from a black stripe only in the absorption. The instantaneous bandwidth of the ropes is roughly 2 MHz and of narrowband fibers is 0.5 MHz. The fibers have typical drift rates of -5 MHz s^{-1} and the ropes have

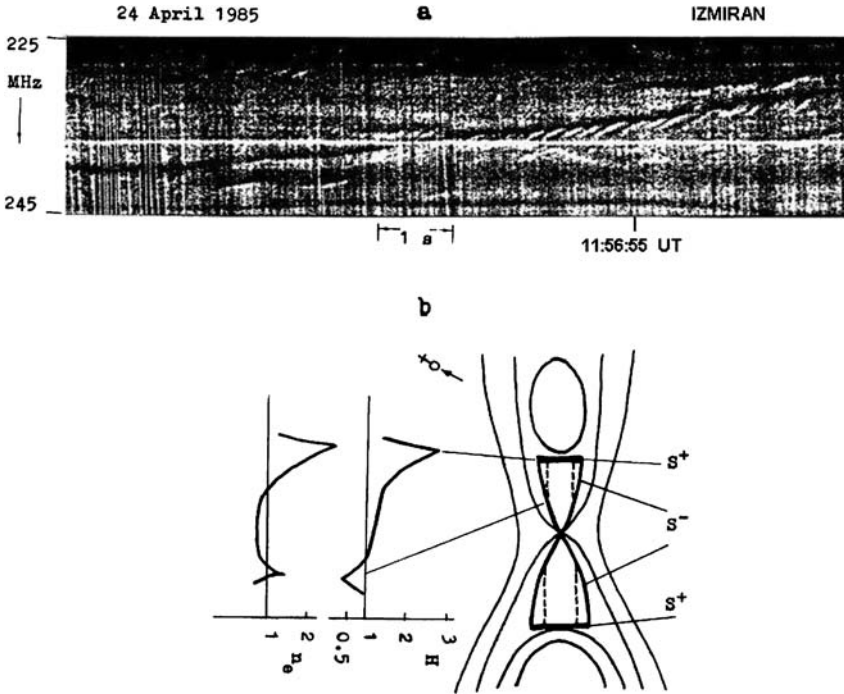


Figure 27. (a): the rope which has begun from pure absorption. (b): qualitative scheme of a possible radio source of the ropes in the form of a quasi-stationary magnetic reconnection with a type X neutral point (Forbes and Priest (1983) and the approximate variation of density and magnetic field strength in the reconnection region (Sidneva and Semenov, 1985); S⁻ – slow shock fronts, S⁺ – fast shock fronts, *dashed lines* denote whistler wave packet trajectories (from Chernov, 1990).

slow oscillating drift, not exceeding $\pm 1 \div 1.5 \text{ MHz s}^{-1}$. Thus, the fibers in a rope represent typical features of FB in the frequency range around 200 MHz, with exception of their small frequency extent of 2 MHz. The individual fibers in the rope have approximately the same characteristics. The time distance between the fibers in the rope is strictly constant, and on the average equal to 0.4 s, with the average duration at one frequency $\lesssim 0.1 \text{ s}$. Both these parameters are much less than for usual FB, according to Elgarøy (1982) and Kuijpers (1975a). So, we must stretch to explain the more rapid repetition of the fibers in the ropes.

In the section Polarization it was shown a weak polarization degree of 20÷30% in this event, which can be connected with depolarization effects during propagation.

The rope-like fibers were observed in the event April 24, 1985 during more than one hour. It is important to still note, that the ropes were observed against the background of broadband fast pulsations with the period \lesssim of 0.1 s.

2.3.5.1. *Rope-like fibers in other events.* It is not possible to say that a structure of such type is very rare. With small variations in the parameters they appear at

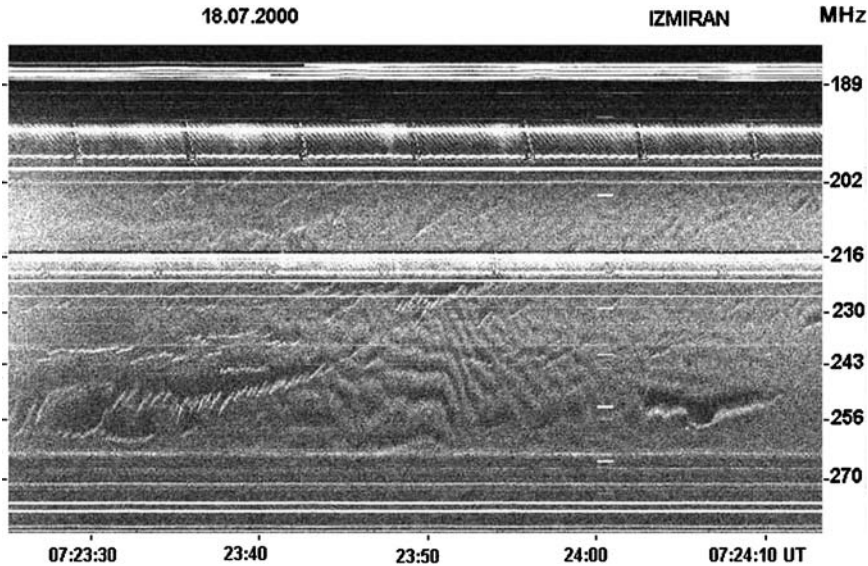


Figure 28. A set of ropes embedded in the developed ZP in the event July 18, 2000 (from archive data of digital IZMIRAN spectrograph).

different phases of the flare. A number of ropes similar to those of April 24, 1985 were observed in the event October 12, 1981 shown in Figure 25. They lasted more than an hour at the post maximum phase. Sometimes ropes appear simply in the composition of ZP. Specifically, such an example is shown in Figure 28. A set of ropes embedded in the developed ZP was observed during two minutes in a short event July 18, 2000. The fine structure appeared after strong group of type III+V bursts during a small, 1F C9.3 flare in AR 9087 (S13E16).

However, attempts are made to rename similar structures as a new type of bursts. A rope (named as sawtooth bursts) in the event November 3, 1997 are discussed in two versions of the work: Klassen *et al.* (2001) and Karlicky *et al.* (2002). For the comparison we show this event recorded by IZMIRAN spectrograph in Figure 29. Both papers are devoted to the analysis of fibers after 09:09 UT around 150 MHz, but one minute before two other chains of fibers are visible: one at about the same frequency range, and another at frequencies 210–215 MHz. And in both these chains the fibers overlap on the time. According to IZMIRAN spectrum the chain at 09:09 UT do not also completely satisfy condition, that the subsequent fiber begins only after the termination of the emission of previous one, although precisely this condition should justify the new name. It is undertaken by analogy with X-ray traces (obtained in TOKAMAK plasmas) generated by disruptive instability. Although, entire process more suits for explanation of simultaneous impulsive X-ray bursts and of type III bursts.

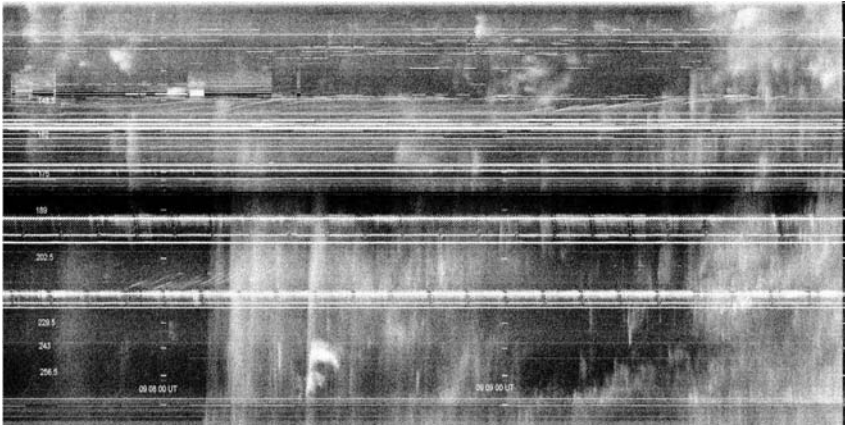


Figure 29. Three chains of fibers in the event November 3, 1997 at impulsive phase of flare during the strong type II burst (from archive data of the digital IZMIRAN spectrograph).

The new name stimulated the authors for the creation of new mechanism, moreover even without any references on their previous interpretations of similar bursts (Mann *et al.*, 1989). There is also no basis to use the interpretation of these fibers to Lace-bursts (or braided zebra), since as the regular fibers in the narrow frequency band are not similar to disorderly Lace-bursts on all parameters.

Besides, the mentioned authors do not discuss remarkable splitting of fibers before the termination, regular frequency drift of fibers and the entire chain (or rope). Comparing the chains (or ropes) of fibers in Figures 26–29, we can conclude, that these are identical phenomena. A certain variety of chains in the different events does not exceed variety of ZP, depending on the concrete plasma parameters in the source.

2.3.6. Rope-Like Fibers at Decametric Range; the May 2, 1998 Event

For the event May 2, 1998 ZP structures were first observed at frequencies between 22–46 MHz with Nançay DCM spectrometer-polarimeter (Figure 30). The radio event was simultaneous with a large 3B X1.1 flare at 13:30–13:42–15:13 UT in the active region NOAA 8210, with coordinates S15W15. The SOHO LASCO telescope detected a major halo-type coronal mass ejection (CME) extending to 26 R_{\odot} . The radio event included a large group of type III bursts, two type II bursts, and type IV continuum radiation. A global dynamical spectrum is presented by Leblanc *et al.* (2000). The maximum energy release in the corona occurred at the heights where the decimeter radiation was generated (22 000 s.f.u. at 606 MHz), but the event extended to lower frequencies and into interplanetary space, as type II and III radio bursts. Zebra pattern structures were first observed over approximately three minutes between 22–46 MHz (Nançay DCM spectrometer-polarimeter) against the flare continuum after the strong type II and type III bursts. The dynamical spectrum

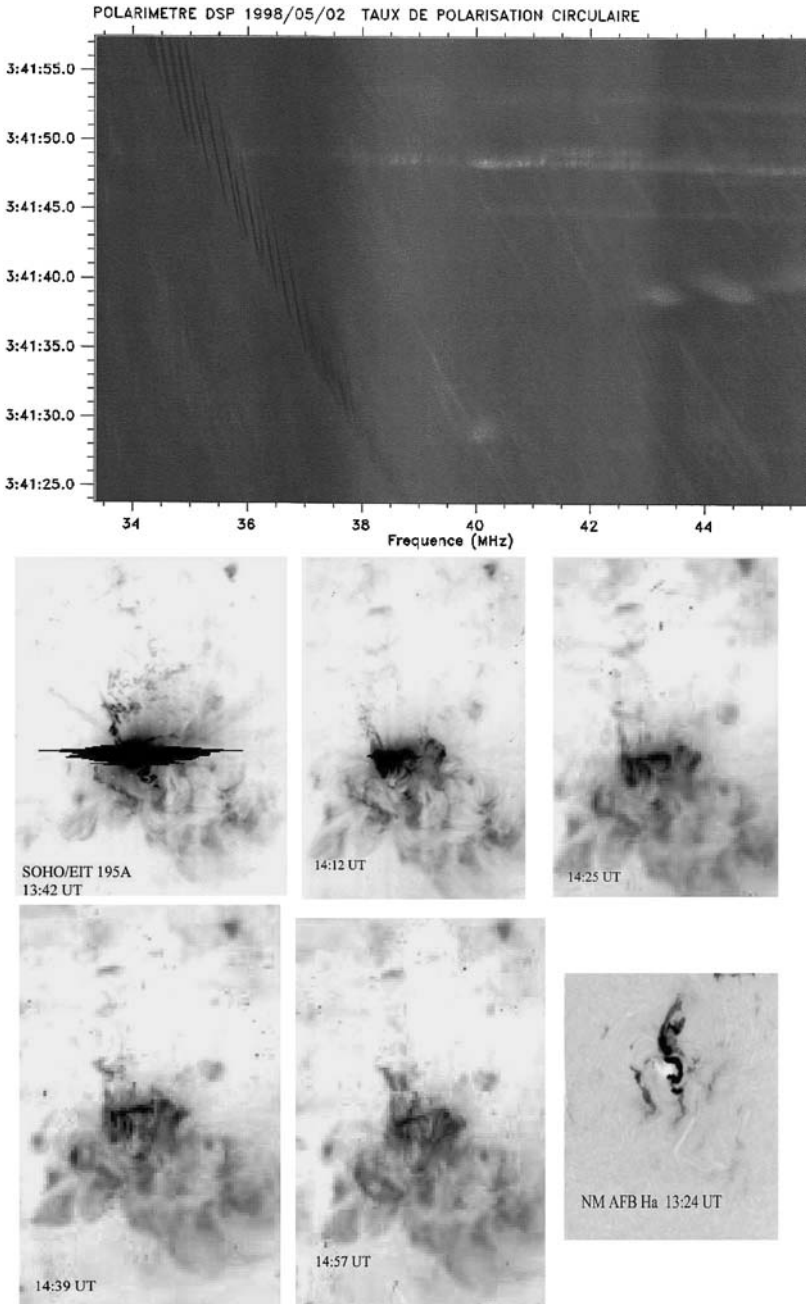


Figure 30. The event of May 2, 1998. The top panel shows the degree of circular polarization in the dynamical spectrum obtained using the decameter spectropolarimeter (DSP) of the Nançay Observatory (the time resolution is 0.05 s). The lower panels show the development of the outburst in the 195 Å EUV-line (SOHO/EIT) and the H_{α} emission in the Active Region 8210 (from Chernov *et al.*, 2006).

in the upper panel of Figure 30 shows that the zebra structure consists of numerous fragments of stripes with various frequency drift. The most evident long fragment resembles a narrow-band rope of fibers with a constant frequency drift. This main rope of fibers with the duration of about two minutes forms the low-frequency boundary of all the zebra-pattern fragments some of them also forming ropes of fibers at higher frequencies. The frequency drift of the main rope is approximately -0.13 MHz s^{-1} near 35 MHz. The frequency drift of separate fibers is much less, $\sim -0.04 \text{ MHz s}^{-1}$. We should note two more important properties of the main rope: its frequency width increased from 0.25 MHz at 43 MHz to 0.8 MHz at 22 MHz, accompanied by an appreciable decrease in the left-circular polarization.

The width of the frequency bands for individual stripes of emission was approximately the same for all the zebra-structure fragments, $\Delta f_e \approx 0.08 \text{ MHz}$, with the relative width of these bands being $\Delta f_e/f \approx 0.0024$. However, the frequency separations between the stripes of emission were appreciably different in different fragments ($\Delta f_s \approx 0.08 \div 0.17 \text{ MHz}$), and the short-time-scale fibers within the main rope are not strictly periodic in frequency. In some fragments, a low frequency absorption is observed, and frequency separation between an emission stripe and the neighboring absorption, Δf_{ea} is approximately equal to Δf_e .

The radio emission of all components of the type II and type III bursts was essentially unpolarized, while the main rope displayed strong left-circular polarization (black at the spectrum in Figure 30). Other fragments of the zebra structure displayed moderate right-circular polarization (white in Figure 30). Two-dimensional NRH radio source images of at 164 MHz show four radio sources above active region NOAA 8210. The complex behavior of the polarization of the fine structure may indicate that different radio sources are located in regions with different magnetic polarities.

The lower part of Figure 30 displays the evolution of the flare in the 195 \AA EUV line (five frames from SOHO/EIT sequence), while the sixth lower panel shows the onset of the H_α flare. We can see in this last panel that a helmet-like ejection has already formed above the sigmoid flare ribbon by 13:24 UT. The continuation of this ejection is clearly visible in the first 195 \AA frame, which corresponds to the maximum of the flare (13:42 UT). We can see also two ejections, northwards and southeastern. Taking into account the presence of the two type II bursts, it is probable, that the upper ejection caused the first type II burst, and the lower – the second one. Each subsequent frame contains new fragments of ejected material in projection onto the disk.

According to Nançay spectra the first type II burst began at 70 MHz on 13:40 UT and the second one on 13:48 UT. The frequency drift of the first burst was $\approx -0.143 \text{ MHz s}^{-1}$ which corresponded to the shock front velocity $\approx 960 \text{ km s}^{-1}$ (using the density model of Leblanc *et al.*, (1998), and the velocity of the second shock was much less, $\approx 380 \text{ km s}^{-1}$ (Leblanc *et al.*, 2000). This latter corresponds to the slower movement of the front in the southeast direction in the subsequent pictures in Figure 30. CME appeared at the height $1.0R_\odot$ on 14:06 UT. Taking into

account the CME velocity of 1040 km s^{-1} it is easy to show, that CME has arisen high in the corona, at any rate, near a plasma level of 80 MHz ($\approx 1 R_{\odot}$). Thus both shock fronts were blast, without any relation with CME.

The rope fiber structures were observed just at the flare maximum during the first type II burst. Behind this first shock front, the second slow shock front was located, and ahead of it was the CME with greater velocity, than the first shock front. Two type II bursts appeared at 14 MHz in *WIND* RAD2 spectrum approximately at 13:45 and 14:07 UT (the beginning of the first one hides behind the powerful type III bursts). The delay between them increased from 8 minutes on 70 MHz to 13 minutes at 14 MHz, which is related to the delay of the second slow shock front. It is obvious that, after the CME, the energy release proceeded in a vertical current sheet, which had structure with magnetic islands. Therefore the appearance of ZP in the decimeter range on 14:29 UT (shown in Jiricka *et al.* (2001) at the post-flare phase can be related with such magnetic islands. The appearance of a fiber structure in IP type II bursts it is probably connected with the passage of the shock front through a jet structure after CME. We exactly see such narrow streamers in the LASCO C2 image on 15:03 UT at the heights $\approx 3 R_{\odot}$, corresponding to plasma frequency of 4 MHz (according the model of Leblanc *et al.* (1998)). In the range 1–5 MHz the relative values of the parameters of fibers are greater approximately by an order of value, than in the metric range.

2.3.7. October 25, 1994 Event: Observations

Some features of this burst were previously analyzed in Manoharan *et al.* (1996), Aurass *et al.* (1999), Zaitsev and Zlotnik (2002), Aurass *et al.* (2003), Zlotnik *et al.* (2003); the main unusual properties of the ZP were not considered, however.

We used the data from simultaneous observations with several radio-spectrographs (ARTEMIS, 100–500 MHz (Nançay), IZMIRAN, 25–270 MHz, Trensdorf (Potsdam), 40–800 MHz), as well as the data from the radio-heliograph of Nançay (NRH) and the polarimeter in Trieste AO at frequencies 237, 327 and 408 MHz.

The radio event consisted of a type II burst drifting from frequencies below 90 MHz at 10:00 UT to 40 MHz at 10:06 UT, a short type IV burst (burst continuum) with a fine structure in the form of periodic type III bursts between 10:05:18 and 10:08:35 UT, and a ZP between 10:08:00 and 10:09:00 UT.

The dynamic spectrum observed with the ARTEMIS spectrograph is shown in Figure 31. The type III bursts drift very rapidly over frequency (perhaps, due to the elevated plasma density above the burst region). At lower frequencies, however, the drift is much slower. The energy release was mainly concentrated in the meter wavelength range. The maximal spectral intensity at a frequency of 204 MHz was 300–400 s.f.u. between 10:08 and 10:09 UT. A minor (49 s.f.u.) GRF type microwave burst was observed over about one hour. According to Solar Geophysical Data, No. 608 (II), 1994, a small H_{α} flare of 1N importance was observed from 09:40 to 12:36 UT (with a maximum at 10:04 UT) in the 7792 (S09, W12) AR.

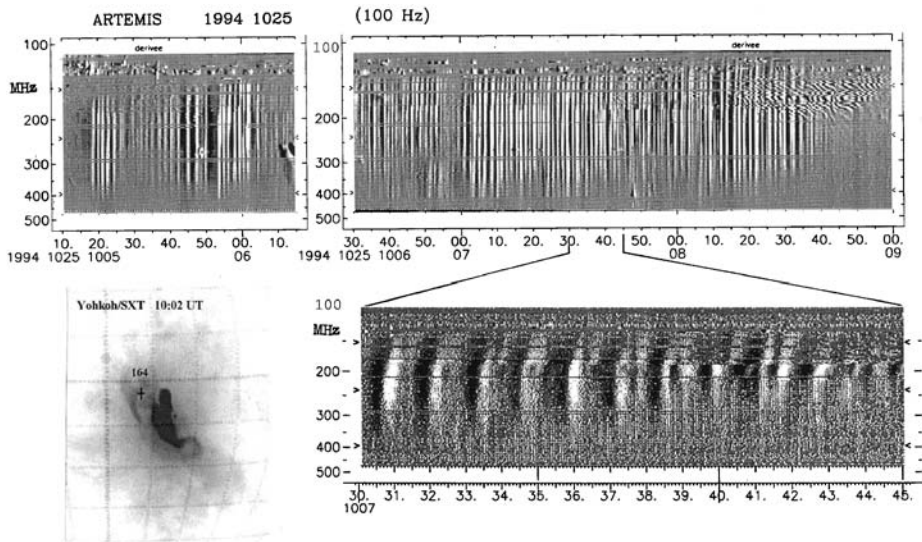


Figure 31. Dynamic spectrum of the periodic type III bursts (which are reminiscent of pulsations) in the event of October 25, 1994 over the entire range of the ARTEMIS spectrograph, 100–500 MHz (in the derivative of the signal). It can be seen *in the top panel* that a ZP appears in the frequency range of 135–210 MHz at the end of the event. *In the lower left panel*, a magnified fragment of the type III burst spectrum is shown, which demonstrates an abrupt stop of the frequency drift at a frequency of about 170 MHz just before the beginning of the ZP. It can be seen *in the lower left panel* that the center of the radio source at a frequency of 164 MHz (marked with a cross against a Yohkoh/SXT image with the thin A1.1 filter) is located beyond the bright flare region (from Chernov, 2005).

An active dark filament and a filament system over this AR were also observed. Some details of this type IV radio burst with different locations of the radio source beyond the AR were discussed in Aurass *et al.* (1999).

In Figure 31 (the lower left panel) it can be seen that the center of the radio source of the fine structure at 164 MHz (NRH) superimposed on the soft X-ray (SXR) burst image (Yohkoh/SXT) recorded using a thin A1.1 filter is located beyond the AR. However, the source of the main continuum coincides with the maximum of the SXR burst. Each subsequent SXR image shows new bright sources both inside and beyond the main burst region; this points to the magnetic reconnection of the flare loop with neighboring loops. Probably, it is for this reason that repetitive bursts of radio emission at 327 and 408 MHz (Triest observatory) had different polarizations. The maxima of the SXR brightness occurred at the same place (in the center of the AR over the neutral line) at 09:59 UT (before the type II burst) and at 10:08 UT (during the type III burst). Sigmoid shape of the SXR burst followed the shape of the neutral line of the magnetic field. It was supposed in Manoharan *et al.* (1996) that the flare triggered a large-scale magnetic reconnection.

In this event, the ZP was observed in the frequency range 130–210 MHz against the background of type III bursts drifting from 400 to 150–125 MHz. Let us note

the principal issues in Figure 31 that elucidate the event dynamics. The initial frequency of type III bursts varied between 300 and 450 MHz with a period gradually increasing from 10–15 to 30–35 s during a series of type III bursts. This was possibly related to slow MHD oscillations of the region where the fast particles were accelerated. The lowest frequency of type III bursts varied asynchronously with their initial frequency and decreased to about 125 MHz between 10:08:12 and 10:08:30 UT.

An explicit indication of a new perturbation was that the frequency drift terminated abruptly between 10:07:38 and 10:07:57 UT at a frequency of 170 MHz (see the lower spectrum in Figure 31). About 3 s later, a ZP arose at frequencies of 140–170 MHz. By the end of the 8th min (10:08 UT), the ZP frequency range expanded to 130–210 MHz, whereas type III bursts gradually disappeared (their intensities and frequency bandwidths steadily decreased). In the time interval from 10:08:17 to 10:08:24 UT, within which the ZP was most pronounced, seventeen emission stripes with a frequency separation gradually increasing from 1.7 MHz at 140 MHz to about 2.2 MHz at 170 MHz were observed. The degree of polarization of radio emission in the ZP and type III bursts was rather moderate (25–30%) and reached its maximum in the ZS at the end of the 8th min. The right sign of polarization of radio waves emitted from the source above the southern-polarity tail spot corresponded to the predominance of ordinary waves.

A part of the ZP dynamic spectrum recorded with the Potsdam spectrograph is shown in Figure 32. It is almost identical to the spectrum recorded at IZMIRAN. The lower part of Figure 32 shows the contour lines of the South-North (SN) distribution of the radio emission intensity at a frequency of 164 MHz (NRH). The maximal intensity corresponds to the center of the ZP source after 10:08:33 UT or to a type III burst before this instant. The solid line that passes through the source centers shows the spatial drift of the sources at a fixed frequency. We note that the centers of the sources of the ZP and type III bursts coincide not only in the NS direction but also in the East-West (EW) direction (i.e., on the Sun disk).

The III type sources (at the beginning of spectrum) drift from south to north, whereas the ZP sources (at the end of spectrum) drift from north to south. In all the ZP absorption stripes, the source drifts is the same way as in the type III bursts (one such instant corresponding to 10:08:33.4 UT is shown in Figure 32 by the heavy vertical line). The labels on the vertical axis correspond to the numbers of the spatial channels of the Nançay radio interferometer. At a frequency of 164 MHz, one channel in the SN direction provides resolution of about $3.2'$. Therefore, the average full width at half-maximum of the radio source (about $4.8'$) corresponds to one-and-a-half channel for both the ZP and type III bursts, whereas the maximal velocity of the spatial drift turns out to be $>90000 \text{ km s}^{-1}$ (about $170\,000 \text{ km s}^{-1}$ for the last source). Taking into account the projection onto the disk, the actual velocities of the source are always $>10^{10} \text{ cm s}^{-1}$ (i.e. close to the speed of light). Thus, the measured source size is actually the AR size and the observed drift velocities can only be attributed to fast (relativistic) particles. Approximately the

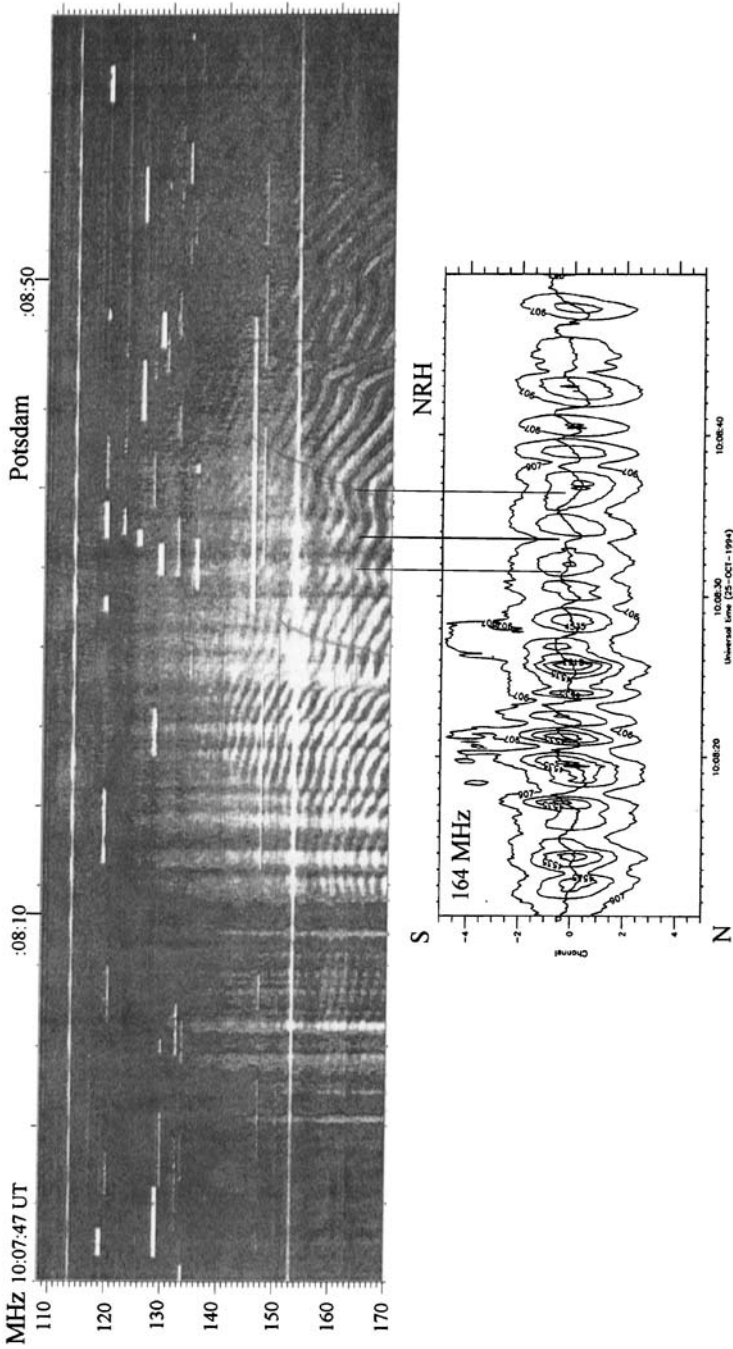


Figure 32. (Top): Dynamic spectrum of ZP against the background of periodic type III bursts in a part of the frequency range 110–170 MHz of the Potsdam spectrograph. (Bottom): One-dimensional (S–N) contour plots of the relative brightness distribution at 164 MHz (Nançay RH). The solid line passing through the maxima of the sources shows their spatial drift (from Chernov, 2005).

same drift velocities of the ZP sources were observed earlier during the June 5, 1990 event (Chernov *et al.*, 1994).

We also note the following important feature of the dynamic spectra: there are several humps in the ZP where the frequency drift changes its sign. The change in the sign of the frequency drift correlates with the change in the direction of the spatial drift of the ZP source. The negative frequency drift corresponds to the same source drift as for type III bursts. The change in the direction of the source drift is accompanied by the change in the sign of the frequency drift (see, e.g., the instants 10:08:32 and 10:08:36.5 UT in Figure 32, which are marked by light vertical lines). These results allow one to choose model of the ZP generation and to explain the width of the frequency band occupied by the ZP in the dynamic spectrum (see Discussion). In the URAP experiment, the *Ulysses* satellite recorded one type III burst at 10:10 UT at frequencies below 1000 kHz. This burst was caused by an electron beam accelerated at the beginning of the flare.

2.4. ZP IN MICROWAVE RANGE: FIRST ZEBRA

In recent years because of the observations with the high resolution by the Chinese spectrometers, data about the detailed spectra of ZP in the microwave range (2.6–7.6 MHz) have appeared (Ning *et al.*, 2000).

2.4.0.1. The event of October 29, 2000. The analysis of many cases of ZP near 3GHz in some events shows the full variety of fine structure similar to that seen in the meter range. In the event of October, 29 2000, for about 20 minutes ZP and fiber bursts (FB) were followed by intermittent pulses of some seconds. An example of ZP evolution is shown in Figure 33. This event was connected to the H_{α} 2B M4.4 flare in AR NOAA 9209, located at S25E35. The ZP shows different frequency drifts: slow negative, positive or switches between the two. The FB often overlap the zebra pattern, and the emission frequency band is about the same for both structures. After some fluctuations of ZP a strong series of FB with different periodicity and a constant frequency drift of -240 MHz s^{-1} was observed. The FB and ZP have about the same spectral parameters, e.g. the frequency bandwidth of emission stripes $\Delta f_e \approx 20\text{--}30 \text{ MHz}$ and the frequency separation between emission lines is 50–80 MHz in the range 2.6–2.8 GHz.

In Figure 34 after some ZP wiggles we can see a series of strong fibers with different periodicities and almost constant frequency drift rate $\sim -240 \text{ MHz s}^{-1}$. However, the multi-channel profiles in the *bottom panel* show the small retarding of the drift rate of some fibers, drifting from 2.83 to 2.60 GHz, which seems completely natural, in accordance with formula (1) (frequency drift is proportional to magnetic field strength). We see that the high frequency IDB are found to be identical in their relative characteristics with FB in the metric range.

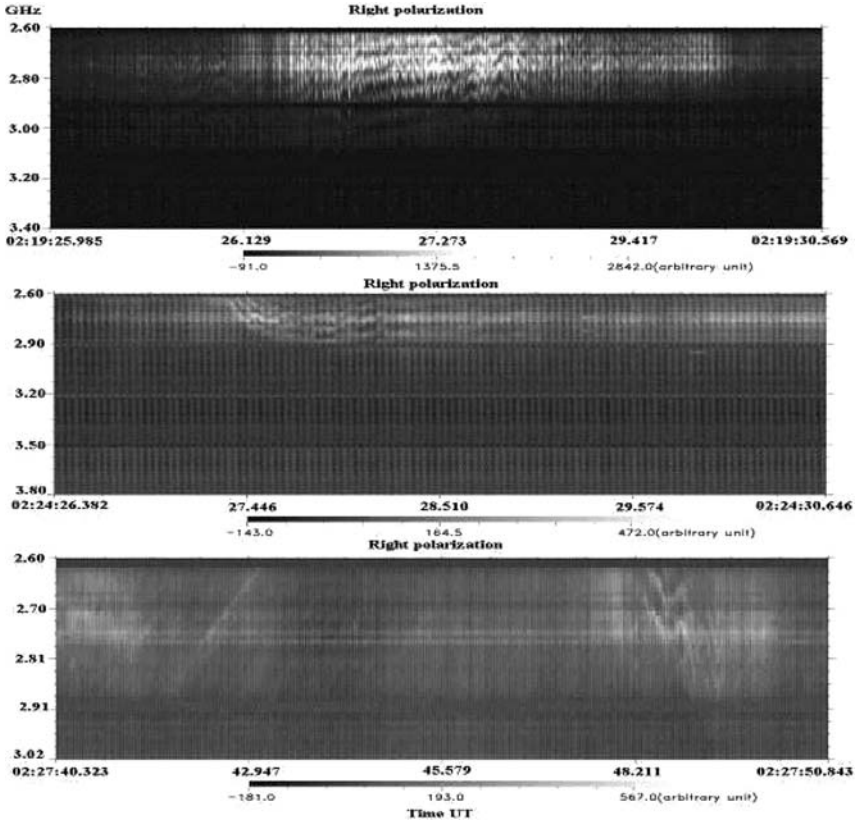


Figure 33. Radio spectrograms of zebra patterns and fiber bursts during the evolution of the event of 29 October 2000 between 02:19–02:28 UT in right polarization recorded by the spectrometer of NAOC (2.6–3.8 GHz). The frequency difference between the 5 regular zebra stripes in the top panel depends weakly on the frequency (from Chernov *et al.*, 2001b).

A detailed analysis of the multi-channel time profiles (see Figure 3 in Chernov *et al.*, 2001b) shows that the intensity level in the black stripes (between emission stripes) could be lower than the emission level of the main continuum (without ZP). Thus, the black zebra-stripes are visible not due to the absence of bright stripes, but due to an absorption of the main continuum emission (a modulation effect). In this connection the main parameter of ZP and FB is not frequency separation between emission stripes ($\Delta f_s \approx 60\text{--}70$ MHz on an average), but the frequency separation between the emission and the adjacent low frequency absorption with a mean value $\Delta f_{ea} \approx 30\text{--}40$ MHz. Therefore we can assume that both of the fine structures have the same origin.

2.4.0.2. *The event of April 21, 2002.* The eruptive long duration X1.5 class flare event of April, 21 2002 occurred in AR 9906 close to the western solar limb

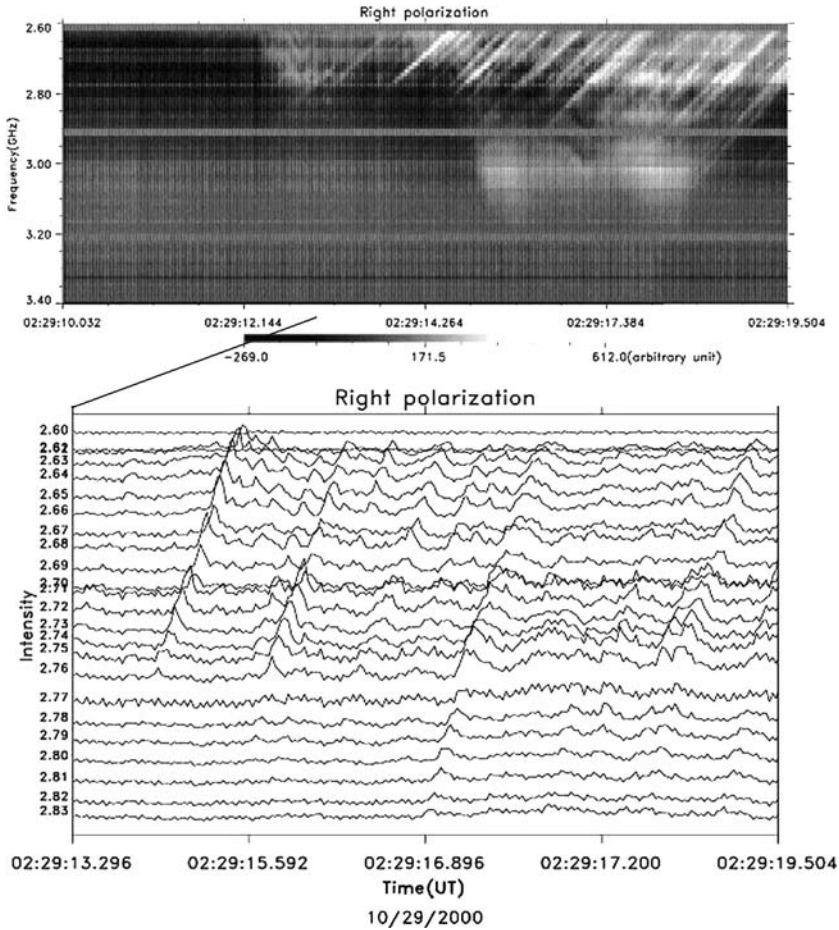


Figure 34. Radio spectrograms of fiber bursts in the event of 29 October 2000. The multi-channel profiles (*bottom panel*) show irregular character of fibers in time and almost constant frequency drift. (from Chernov *et al.*, 2001b).

(S14W84) between 00:43 and 02:38 UT. Images of TRACE data in the EUV 195 Å line show the formation of a bright post-flare arcade in the flare site (Gallagher *et al.*, 2002). From 01:34 to at least 02:15, dark matter is seen falling onto the arcade from above. The dark matter apparently occults bright arcade loops.

The entire prolonged event was divided into two phases in the radio data and in hard X-rays: in the growing flow of soft X-rays (GOES) there was a first maximum in hard X-rays (about 01:15–01:18 UT, MTI/HXRS) and in the radio range (near 01:30 UT). In this phase the maximum energy release occurred in the decimeter wave band, which indicates magnetic reconnection at heights of the decimeter range. According to the data of radio-spectrographs (Hiraiso and IRS, Korea (Cho, personal communication)) high flux levels were recorded in the meter range (between 01:18–01:30), possibly with fine structure.

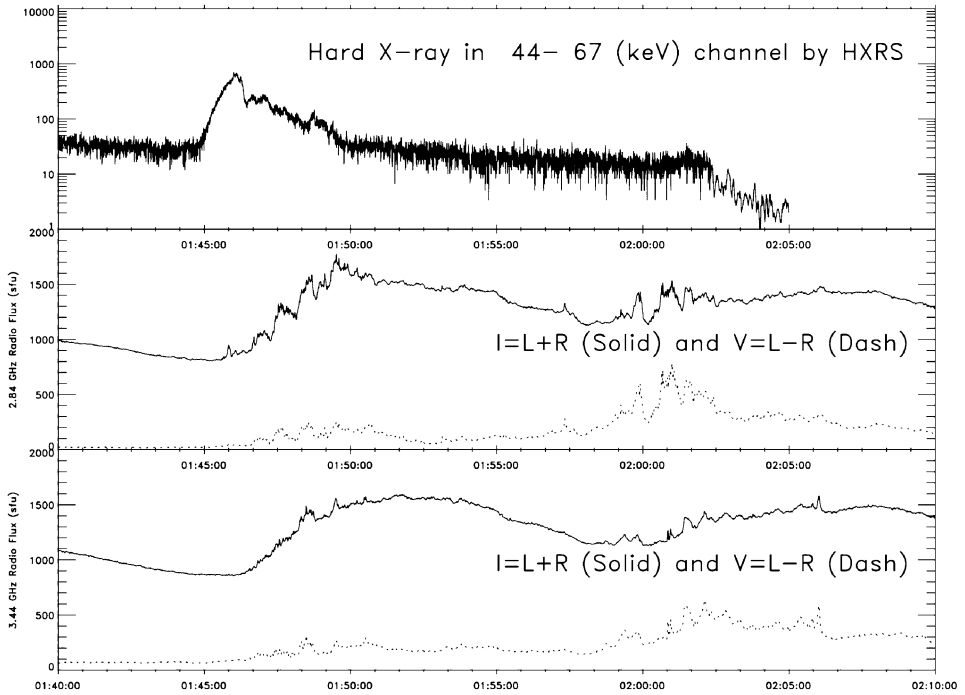


Figure 35. The hard X-ray burst in the 44–67 keV channel of the HXRS during the period of ZP in 2.6–3.8 GHz. The Huairou radio profiles at 2.84 and 3.44 GHz showing the radio flux intensity ($I = L + R$) and the polarization component ($V = L - R$) are indicated by *solid* and *dashed* lines respectively (from Chernov *et al.*, 2005).

In the microwave range the maximum of the first phase was above that of the second phase. However, no fine structure in the first phase was registered around 3 GHz. The arcade of loops began to form only after approximately 01:30 UT.

The ZP are observed only during the second phase, between 01:44 and 02:05 UT, during the second phase of the HXR (MTI, HXRS) burst presented in Figure 35. In the loop arcade we see during this phase two new bright centers as X-points of magnetic reconnection (see top left panel in Figure 36). During the interval 01:51–01:53 UT the ZP was very weak. At this time in the TRACE 195 Å image some bright centers disappeared (see right top panel in Figure 36). The difference image between 01:50:57 and 01:48:16 shows many bright loops (middle left panel in Figure 36), where the radio sources of ZP could be located. At the same time three new sources of HXR (RHESSI, Gallagher *et al.*, 2002) appeared under the mentioned two X-points of the magnetic reconnection visible in the bottom left panel of Figure 36. Such a proposal is confirmed by radio source positions with SSRT data at 5.7 GHz for polarized emission (the parameter V , see two centers shown by isolines in the bottom right panel in Figure 36). White and black contours in the bottom left panel of Figure 36 show source positions of

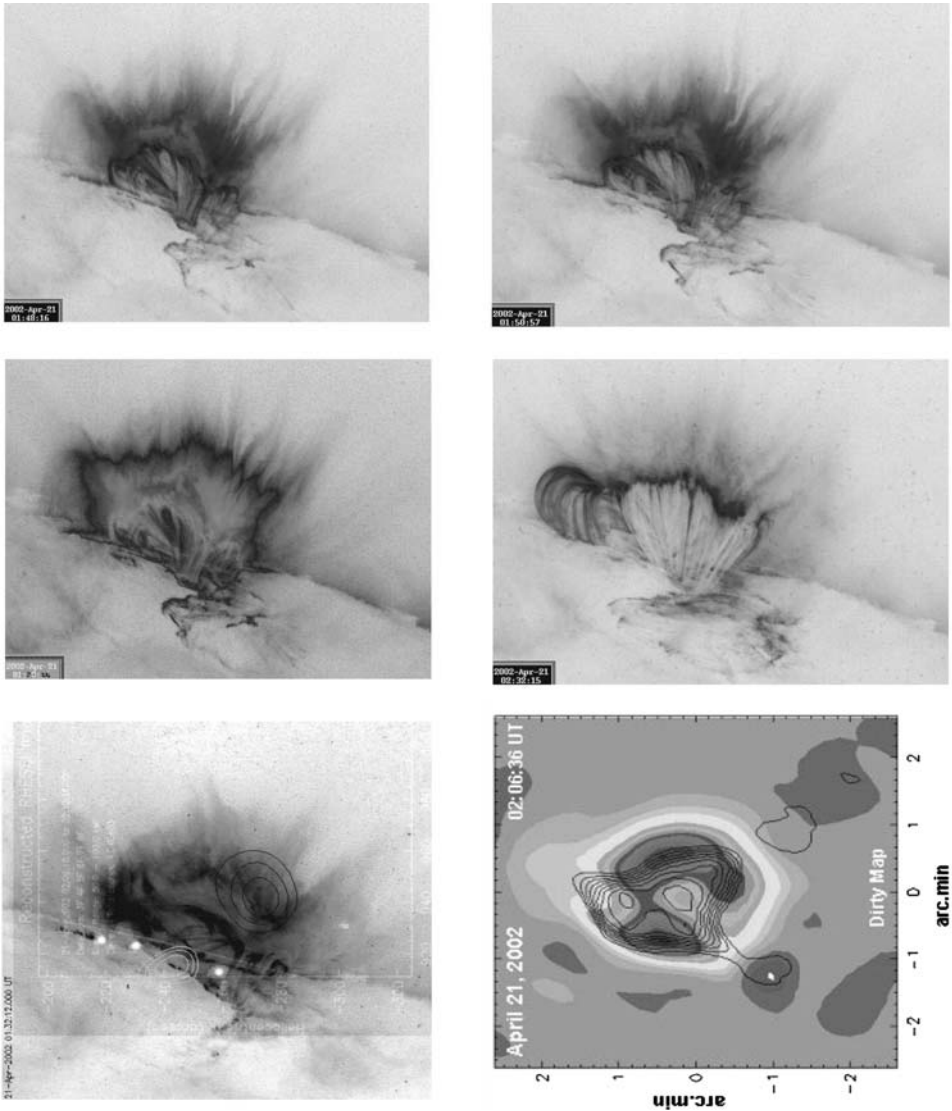


Figure 36. The evolution of the flare of April 21, 2002 with TRACE data in EUV line 195 \AA and RHESSI HXR data. The difference image between 01:50:57 and 01:48:16 UT is shown in (*middle left panel*). The *bottom left panel* shows three new sources (*white points*) of HXR (RHESSI, Gallagher, 2002). The *bottom right panel* shows radio source positions with SSRT data at 5.7 GHz (courtesy of R.Sych) in intensity (parameter I, shown by the *grey and black background*) and in polarization (parameter V shown by *contours*) (from Chernov *et al.*, 2005).

RHESSI/HXR energy channels respectively at 50–100 and 12–25 KeV (Gallagher *et al.*, 2002). Radio sources of continuum emission in intensity with SSRT data (parameter I) have approximately the same positions. After 02:09 UT the arcade of bright loops in the line 195 \AA rose to high altitudes (*middle right panel*

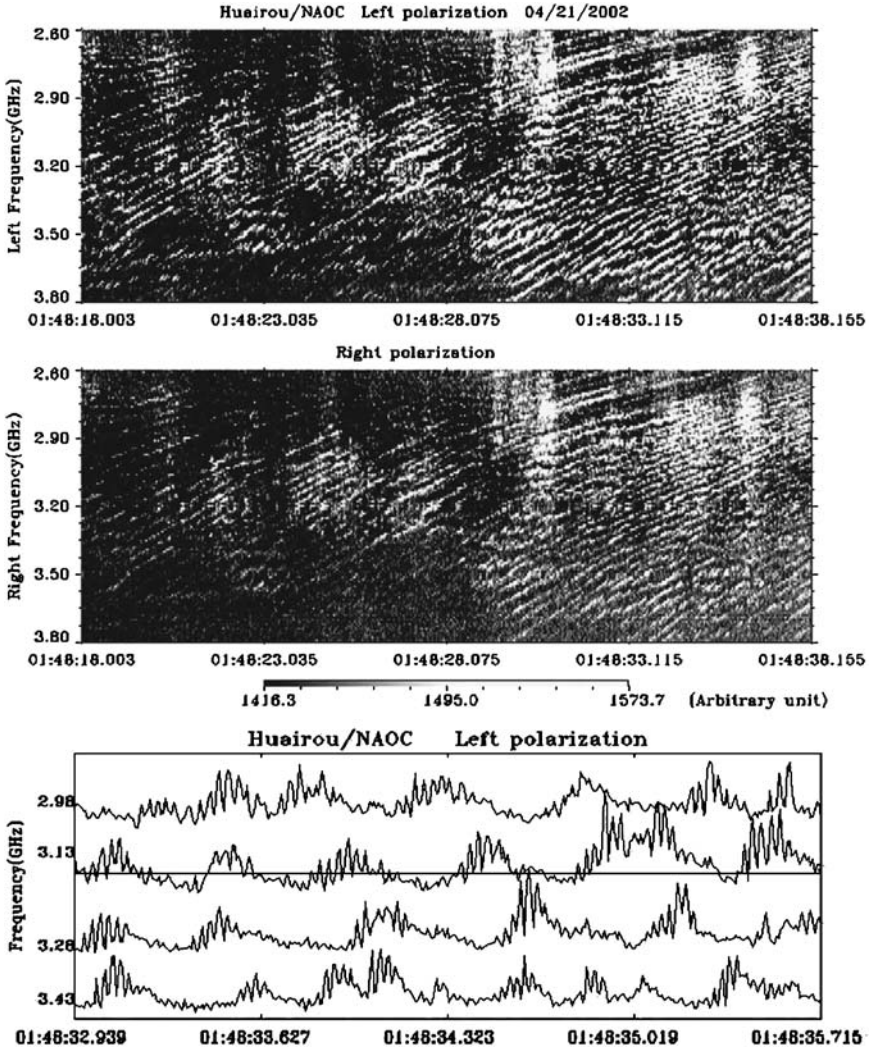


Figure 37. Zebra structure in the event of April 21, 2002. The two upper panels show the Huairou radio spectrograms in the 2.6–3.8 GHz range in the left and right polarization components with a zebra pattern at 01:48:18–01:48:38 UT, in which 34 stripes can be distinguished and whose frequency separation grows smoothly with frequency. The lower panel shows profiles of the intensities at four fixed frequencies. The profiles confirm the spike-like structure of each zebra stripe in emission. The dark stripes do not contain a spike-like structure, and the radiation level proves to be lower than the average level of continuum, shown by the straight line at a frequency of 3.13 GHz (from Chernov *et al.*, 2005).

in Figure 36), and the maximum of activity was displaced into the decimeter range.

All series of the ZP in this event represented zebra stripes with negative frequency drift, which is more inherent to fibers. In Figure 37 and 38 two intervals with the

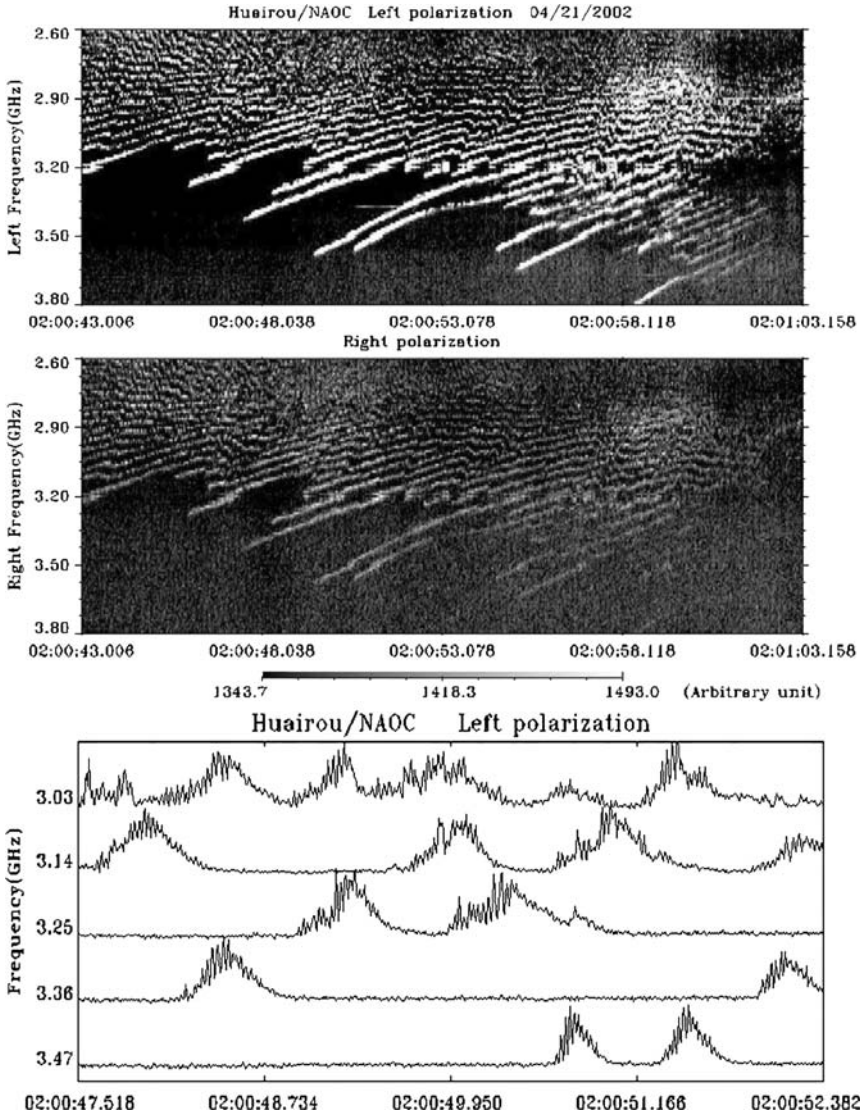


Figure 38. Zebra structure in the event of April 21, 2002 at 02:00:43–02:01:03 UT. The zebra stripes on the high-frequency edge of the spectrum are more similar to isolated fibers without any strict periodicity. The multichannel time profiles (in the bottom panel) show stripes in emission consisting of spikes as before. However, in the dark stripes the residual emission remains at a fixed level (from Chernov *et al.*, 2005).

most pronounced ZP are shown, taken with the NAOC spectrometer at 2.6–3.8 GHz. In the first fragment of 20 second duration from 01:48:18 UT 34 zebra stripes are counted in the range 2.6–3.8 GHz with a barely noticeable increase in frequency separation between stripes from 27 MHz at 2.8 GHz to 43 MHz at 3.7 GHz. It is

remarkable that the relative value of the frequency separation proves to be about the same as in the meter range $\Delta f/f \approx 0.012$.

The frequency drift of zebra stripes was negative and almost constant ≈ -120 MHz s⁻¹ between 3.8–3.4 GHz, which is more characteristic of fibers. At the low frequency part of the spectrum a small deceleration of the frequency drift is observed. However, each 1–2 s, stripes undergo failures and jumps of frequency drift, covering several adjacent stripes with a small time delay. Sometimes shifts in the frequency lead to merging or splitting of stripes. Such effects are well known in the meter wave band. In the bottom of Figure 37 a short fragment of intensity time profiles of about 3 s duration is shown at four frequencies. A detailed analysis of multichannel time profiles shows that each zebra stripe in emission has a spike-like structure. In the dark stripes (between the bright zebra stripes) the emission level can be lower than the level of burst background (lower than the average level of continuum, shown by a straight line at 3.13 GHz). Thus the presence of dark stripes is connected not with the absence of bright stripes (in emission), but with an absorption of background microwave emission. The polarization degree was weakly left-handed. We propose that two polarized radio sources at 5.7 GHz were located above the leading spot (the left polarized source) and above the tail spot (the right source in the bottom right panel of Figure 36). Therefore due to the limb position of the AR it is difficult to precisely define the magnetic polarity of the corresponding radio sources to define the type of radio wave.

The fragment in Figure 38 shows some changes of ZP properties: the polarization degree becomes stronger and it grows with time and frequency; the frequency drift almost stops in the low-frequency part of the spectrum (sometimes the stripes are almost parallel to the time axis); however, in the high-frequency part of the band they are more similar to isolated fibers with a negative frequency drift (there is no strict periodicity). The multichannel time profiles (in the bottom panel of Figure 38) show that stripes in emission consist as before of spikes, however, in the dark stripes, deep dips in emission are not observed; the residual emission remains at a fixed level.

ZP was also observed in the pulsating regime, but almost all series of ZP were prolonged; in the examples in Figure 36 and 37 the duration exceeded 1 minute. The evolution of zebra stripes in several series began from a cloud of millisecond spikes with the gradual shaping of zebra stripes, as is shown in Figure 39.

2.4.1. *A Superfine Spiky Structure of ZP in Microwave Bursts*

In this section we present observations of a new property of ZP. According to Chernov (2003), in 7 microwave bursts with ZP and FB a new effect was discovered by broadband radio spectrometer at Huairou station (Beijing, NAOC) (Fu *et al.*, 1995) in the frequency range 2.6–3.8 GHz: zebra-stripes had own super fine structure, they were consisted of numerous fast spikes with duration at a limit of the time resolution of spectrometer ≤ 8 ms. The same superfine structure was present in Figures 36–38 in the event of April 21, 2002.

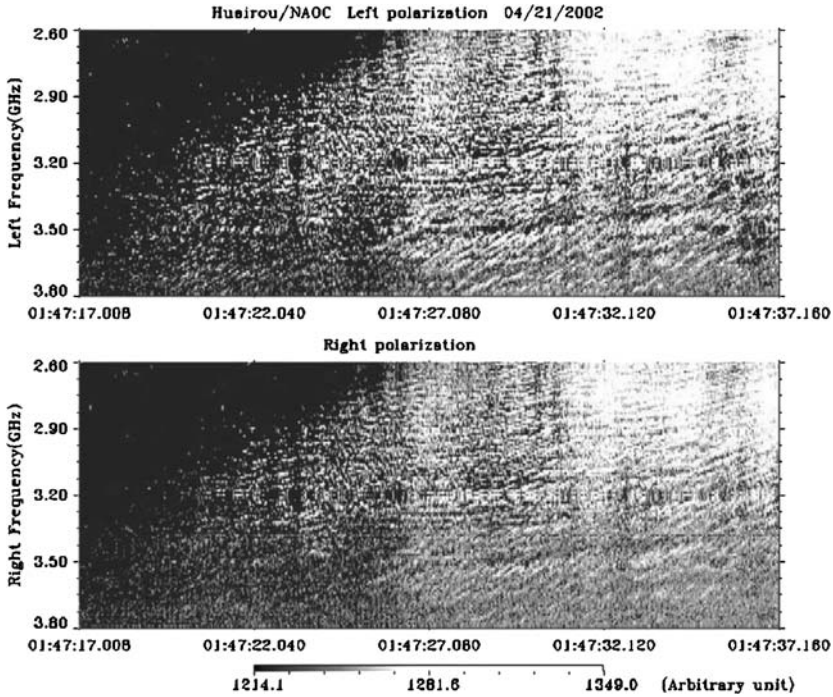


Figure 39. Some series of ZP began from a cloud of millisecond spikes with gradual formation of zebra stripes (from Chernov *et al.*, 2005).

At two top panels of Figure 40 two spectra of the weak event January 21 2000 in left and right hand polarization are shown (the degree of polarization was moderate). A cloud of the emission (in the form of apple) consists of spikes, as well as zebra-strips with negative and positive frequency drift. The emission bandwidth of zebra – strips is equal about to the bandwidth of spikes (50–100 MHz), practically vertical white traits with duration at the limit of the time resolution 8 ms. In this connection we could conclude, that the source dimension of an isolated zebra stripe is about equal to the source dimension of spikes, and therefore their brightness temperatures are also about the same $T_b \geq 10^{13}$ K.

A fragment of similar structure in the strong radio burst November 25, 2000 is present at the bottom panel of Figure 40. The spectrum is shown in one left polarization channel, because the emission was full polarized at this moment. The emission on the whole includes numerous spikes, as well as zebra-strips showing the oscillating frequency drift. The frequency separation between stripes and bandwidth of each stripe are smaller than at upper panels (~ 50 MHz).

The event November 24, 2000 was very dynamic, and 20 seconds after the first strong polarized ZP with the spiky structure a zebra stripes with moderate left polarization appeared (Figure 41), as well as two zebra stripes around 3 GHz

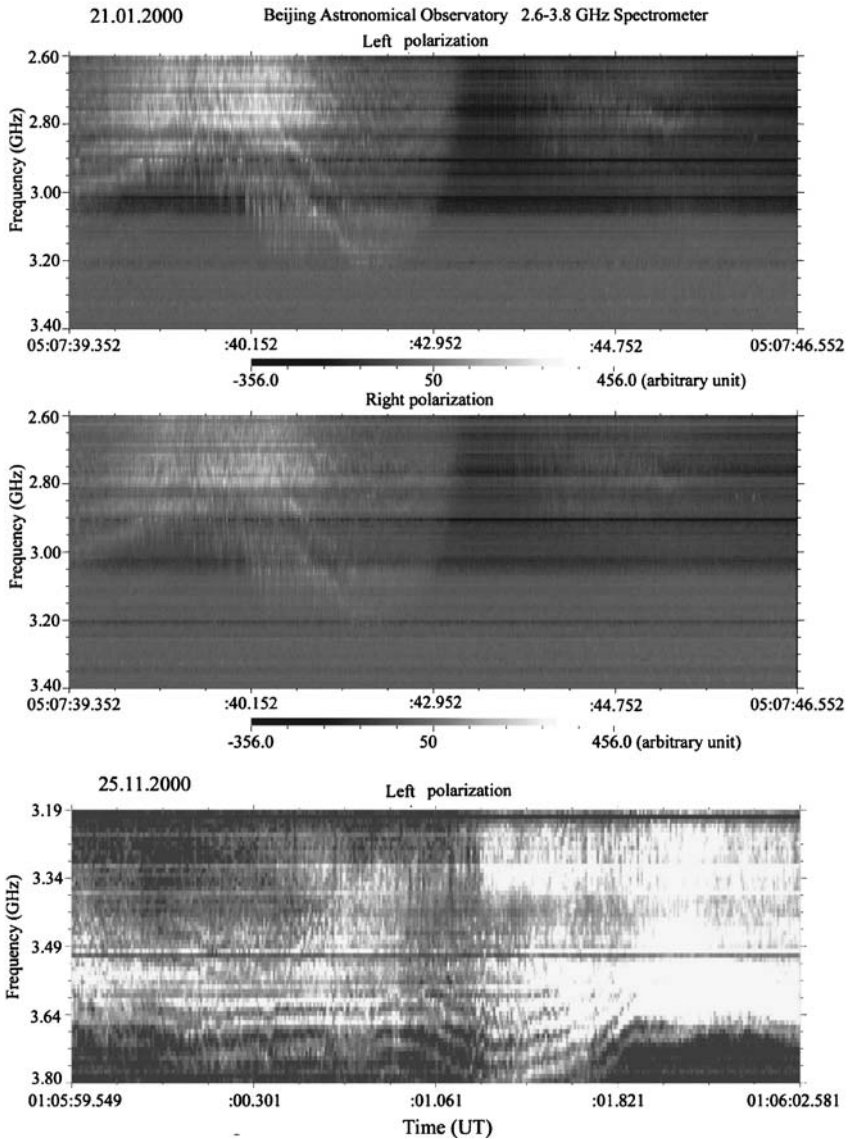


Figure 40. Dynamical spectra of super fine structure of zebra-pattern in two events: 21 January 2001 (two top panels in left and right circular polarization in the frequency range 2.6–3.4 GHz) and 25 November 2000 (bottom panel of ~ 3 s duration in left polarization in the range 3.19–3.8 GHz) (from Chernov *et al.*, 2003).

at 05:00:56 UT that became more pronounced in right polarization, and at this time they consisted of spikes. The Nobeyama data show at this moment a double radio source above the neutral magnetic line, and the main, stronger radio emission (L-sign) corresponds to the ordinary mode. An enlarged fragment (3.54 s) of zebra

Beijing Astronomical Observatory 2.6–3.8GHz Spectrometer (11/24/2000)

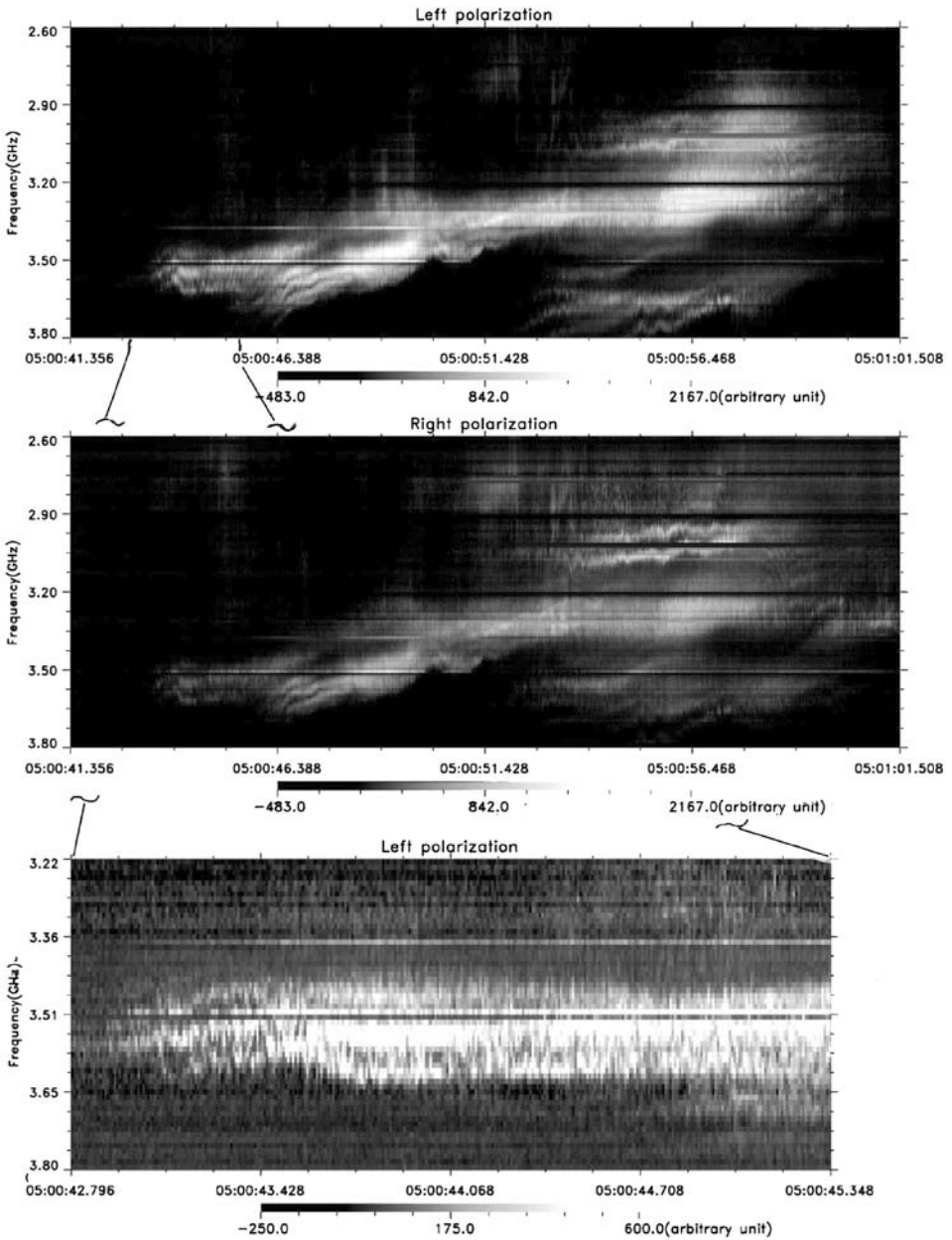


Figure 41. The continuation of the event of 24 November 2000 showing a complex zebra-pattern with superfine structure. An enlarged fragment (3.54 s) of zebra-stripes in left polarization at the beginning of this interval is shown on the bottom panel. The radio emission on the whole has a moderate left polarization, but two zebra stripes around 3 GHz and 05:00:56 UT have a moderate right polarization (from Chernov *et al.*, 2003).

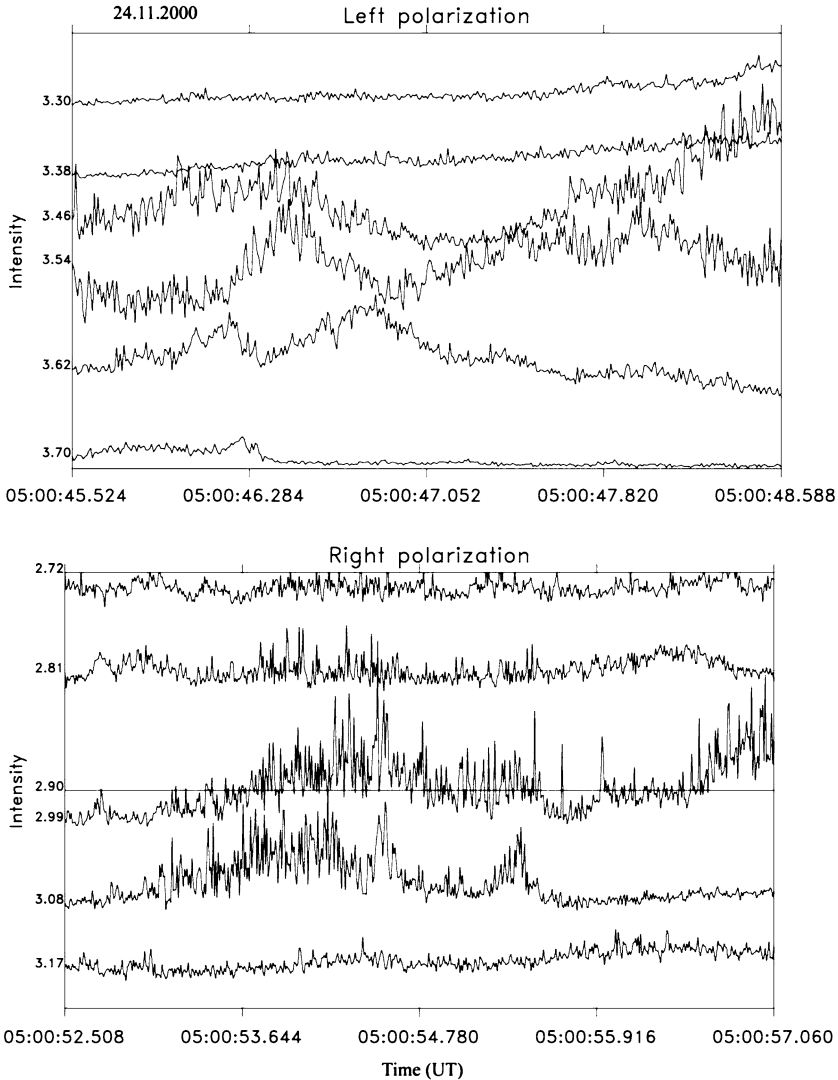


Figure 42. A multichannel presentation of two fragments of ZP from Figure 41 with a duration of 3 s (in left polarization) and 4.5 s (in right polarization). The frequencies of channels were chosen almost along zebra-stripes in emission (from Chernov *et al.* 2003).

stripes at the beginning of this interval is shown at the bottom of Figure 41. We can see that the majority of spikes have a duration of one pixel, i.e. ≤ 8 ms.

The bandwidth of spikes is equal to about 35–45 MHz, and $\Delta f_e \approx 60$ MHz. Spikes in two neighboring zebra-stripes do not have any correlation, as shown in Figure 42 with a multichannel presentation of two short fragments of zebra patterns from the Figure 41: between 05:00:45.5–05:00:48.6 UT in left polarization and

between 05:00:52.5–05:00:57.0 UT in right polarization. The frequencies of channels were chosen almost along zebra-stripes in emission. We see obvious chaotic behavior of spikes, as in practically all such events. Multichannel intensity profiles show also a very important result: the intensity between zebra stripes (in absorption stripes) remains lower than the intensity between spikes in emission stripes, but slightly higher than in parts of the spectrum without the background burst emission. Spikes almost disappear in absorption stripes, but the intensity level there testifies to a modulation effect. The flux density of spikes in the composition of zebra-stripes is usually about 20–50% (in different events) of the radiation of the background burst.

Another important observation was that the spiky structure is not pronounced in FB, when fibers appear simultaneously with ZP (October 29, 2000, see Figures 34). Zebra stripes as well as fibers can appear as isolated stripes, and all other parameters of both stripes in emission and in absorption are similar (Chernov *et al.*, 2001b). We conclude that the spiky structure of ZP is seen almost in all events, when the time resolution of the spectrometer is high enough: some ms. In this connection the rapid frequency variations in the range 0.8–1.3 GHz observed by Karlicky *et al.* (2001) with 0.1 s resolution (called Lace-bursts) are possibly similar structures if observed with millisecond resolution.

The wealth of fine structure does not always correspond to the importance of the chromospheric flares and the intensity of the radio bursts. The relatively weak event of April 15, 1998 was very rich in spikes and ZP (see Chernov *et al.*, 2001b). Zebra patterns were usually observed after the burst maximum in all events.

Chernov *et al.* (2006) present the results of the first simultaneous observations of zebra patterns with superfine spiky structure in the microwave range made at two observatories 1000 km apart (Beijing and Nanjing, China). The fine structure was recorded by Huairou station with a spectra polarimeter in the 5.2–7.6 and 2.8–3.6 GHz ranges and by the Purple Mountain Observatory spectrometer in the 4.5–7.5 GHz range (Figure 43).

Identical spectra of zebra stripes with superfine structure (within the limits of instrument resolutions) obtained simultaneously at two observatories, confirm a solar origin of the ZP superfine structure.

The circular polarization degree was very weak for the burst background radio emission and moderate to strong for the fine structure. The polarization sign in all the cases probably corresponds to the extraordinary wave mode (see source positions with SSRT in Figure 44). But, these attempts show the difficulties involved in determining the wave mode for the fine structure. In all our cases the sources were located near the neutral magnetic line, and their positions at 15–20 thousand km do not necessarily correspond to the magnetic polarity sign at the photosphere level. Therefore it is not possible to regard our conclusions about the prevalence of the X-mode as absolute. The same note is also applicable to the conclusion made by Altyntsev *et al.* (2005) (see below Figure 47).

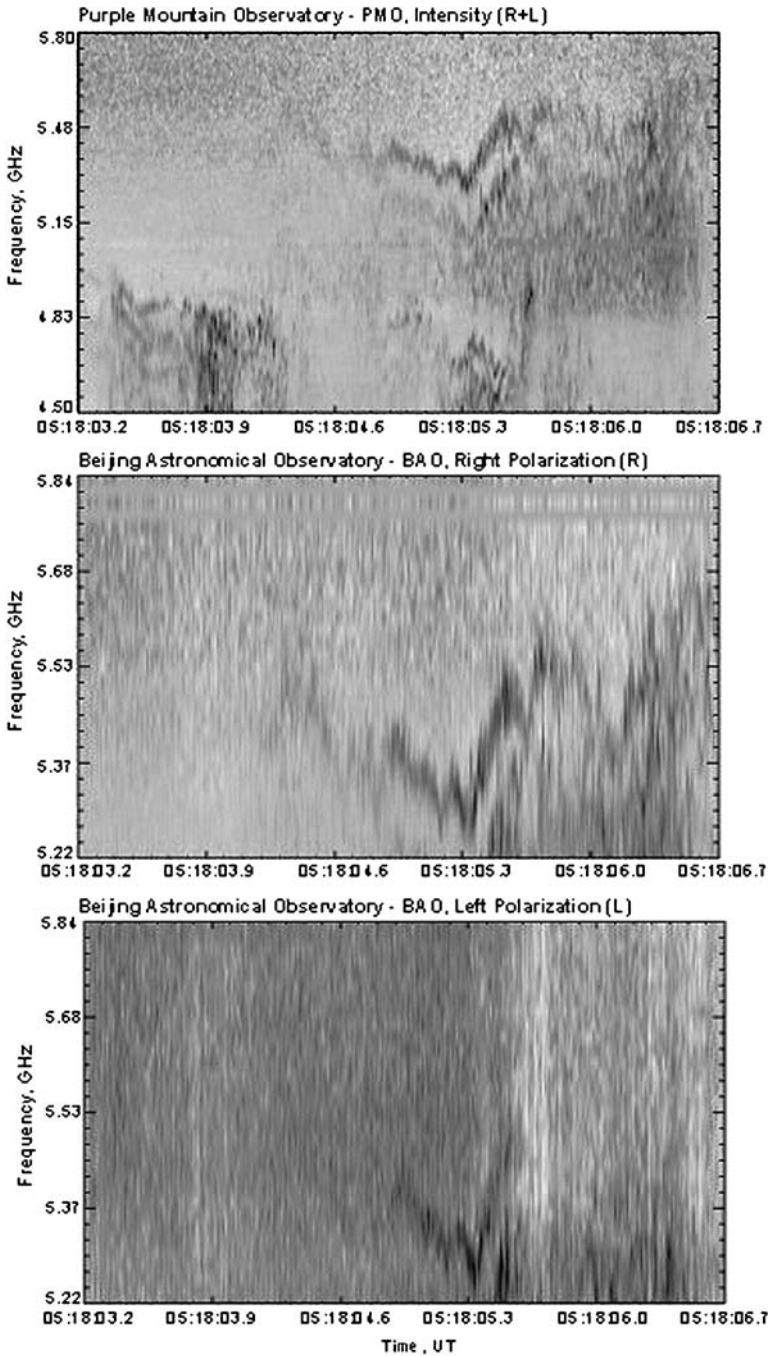


Figure 43. Dynamic spectra of the zebra pattern in the April 10, 2001 event observed simultaneously by two observatories: Purple Mountain Observatory in intensity (*top*) and Huairou/Beijing Observatory in left (L) and right (R) polarization channels (*middle and bottom panels*) (from Chernov *et al.*, 2006).

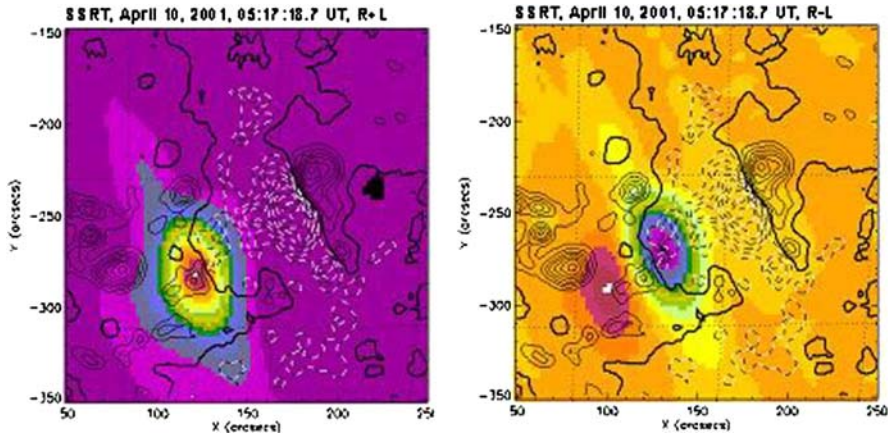


Figure 44. SSRT 5.7 GHz source positions overlaid on the magnetic map from SOHO/MDI. *Solid thick line* is the neutral magnetic line. In the *left panel* the brightness distribution of intensity (parameter $I = R + L$) is presented. In the *right panel* the polarized sources (parameter $V = R - L$) are shown. To the left is the R radio source shown in halftone with a brightness center above the N magnetic polarity; to the right is the L radio source (*solid color contour*) above the S magnetic polarity. The radio emission corresponds to the extraordinary mode (L e S) (from Chernov *et al.*, 2006).

The top panel of Figure 45 shows that all the spikes have peaks simultaneously in both R and L channels of the spectrometer, which proves the absence of any group delay between them within the limits of the spectrometer time resolution (5.0 ms). Thus, in this case, the degree of partial polarization is not related to the delay between ordinary and extraordinary wave modes discovered by Fleishman *et al.* (2002) (as for spikes of some events).

Two adjacent stripes of the zebra are shown in the lower panel of Figure 45. Although a strict correlation between spikes in the adjacent stripes is not observed, the largest elements of the superfine structure reveal the specific correspondence with small delays in the low-frequency stripe. Straight, inclined lines connecting such details prove to be strictly parallel, suggesting the propagation of some agent. The speed of the frequency drift (df/dt) of the straight, inclined lines is approximately equal to 15 GHz s^{-1} , and in a realistic density model above the sunspot with a height scale: $L_n = 2n(dn/dh)^{-1} \sim 10^9 \text{ cm}$, we obtain the speed of the agent $\sim 5.8 \cdot 10^9 \text{ cm s}^{-1}$, which is suggestive of beams of fast particles.

In the whistler model the frequency separation between the stripe in emission and the adjacent absorption (Δf_{ea}) is approximately equal to the whistler frequency $f_w \approx 0.1 f_B$, and we obtain, for $\Delta f_{ea} = 70 \text{ MHz}$ at 5.2 GHz (Figure 40), $B = 250 \text{ G}$ and consequently the plasma $\beta \approx 0.03$.

2.4.2. ZP at Frequencies Around 5.7 GHz

ZP was barely observed at frequencies higher than 5.5–6 GHz. Only one and very weak event was registered by China spectrometer (5.2–7.6

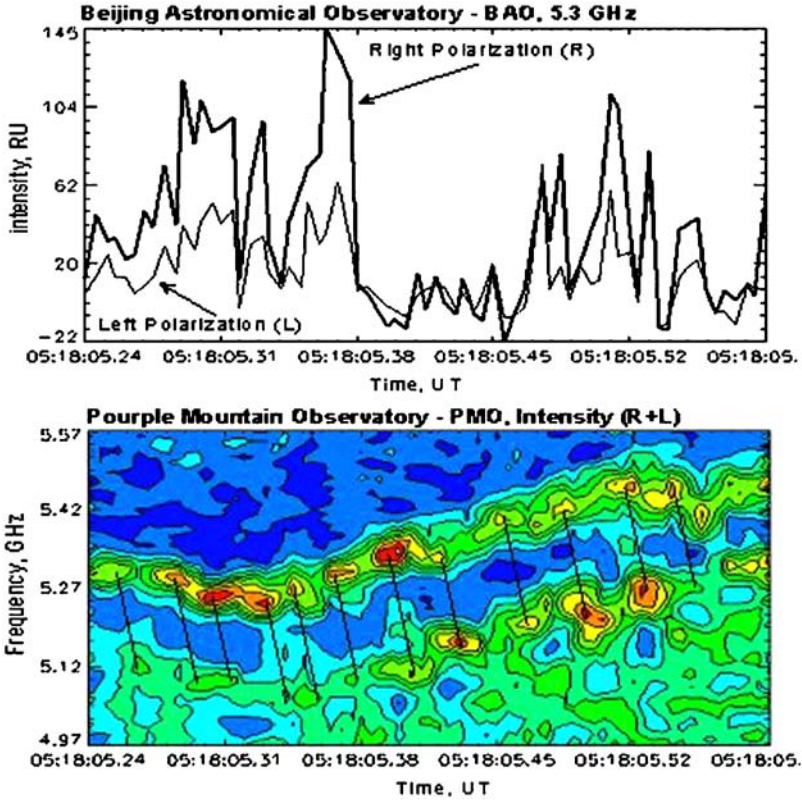


Figure 45. Profiles at 5.3 GHz in the *top panel* show that all spikes (superfine structure of the zebra stripes) have peaks simultaneously in both R and L channels, proving the absence of any group delay between them within the time resolution of the spectrometer (5.0 ms). Two adjacent stripes of the zebra of the PMO spectrum are shown in the *lower panel*. Although no strict correlation between the spikes in the adjacent stripes is observed, the largest elements of superfine structure reveal specific correspondence with the low-frequency stripe, although with a small delay (from Chernov *et al.*, 2006).

GHz) (Altyntsev *et al.*, 2005; Kuznetsov, 2005). The radio flux of zebra stripes reaches only 2–3 s.f.u. above the burst background of 25 s.f.u. (Figure 46).

The position of the radio source of ZP is shown by crossed straight lines at the background of SOHO/MDI magnetogram in Figure 47.

The main conclusions from these observations are:

- the frequency interval between adjacent stripes has almost constant value of 160 MHz;
- the instantaneous bandwidth of stripes is about 60 MHz;

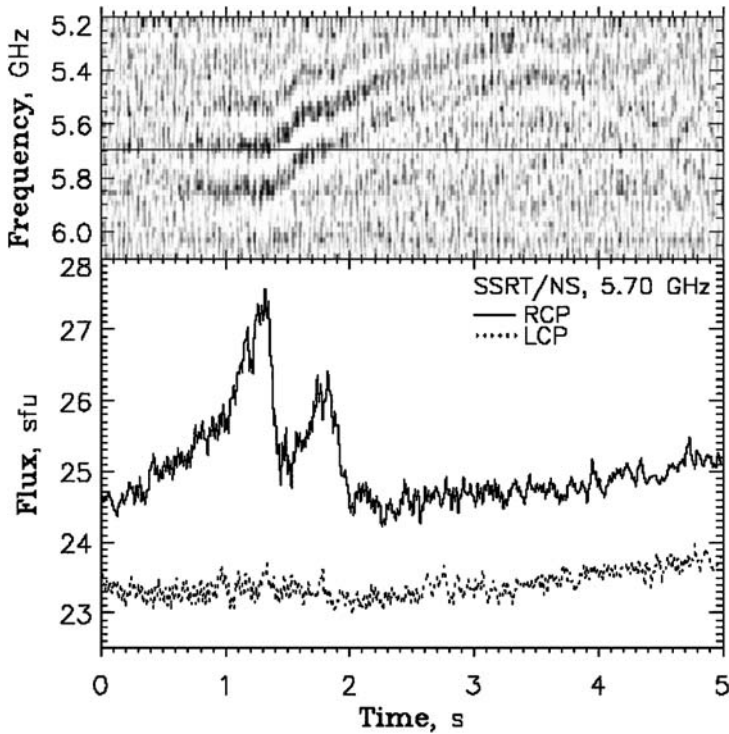


Figure 46. *Top*: NAO dynamic spectrum with zebra pattern, recorded on January 5, 2003 (06:06:10.3 UT). Darker areas correspond to the higher intensity of emission. The horizontal lines show the frequency 5.7 GHz. *Bottom*: the corresponding temporal profiles of emission with right (RCP) and left (LCP) circular polarization at 5.70 GHz, recorded by the SSRT linear interferometer. The circular polarization degree of the ZP reaches 100% (from Kuznetsov, 2005).

- the apparent source size does not exceed 10 arcsec (7 thousand km), and the sources of the different stripes of the zebra structure coincide spatially (but at one frequency);
- the circular polarization degree reaches 100%, and the polarization sense corresponds to the extraordinary wave.

In connection with this rare event one should nevertheless note: first, during the precise study of the dynamic spectrum it is possible to note a smooth increase in the frequency separation between the five stripes with frequency; in the second, the identical position of the radio sources of different stripes was determined at one frequency, therefore it is not amazing, that they coincide. In this case the sources of different stripes at different frequencies (at one time moment) can quite locate at the different heights, as in the distributed source (see below Figure 60b); in the third, the stripes reveal superfine structure (as millisecond spikes), and the authors in no way discuss it.

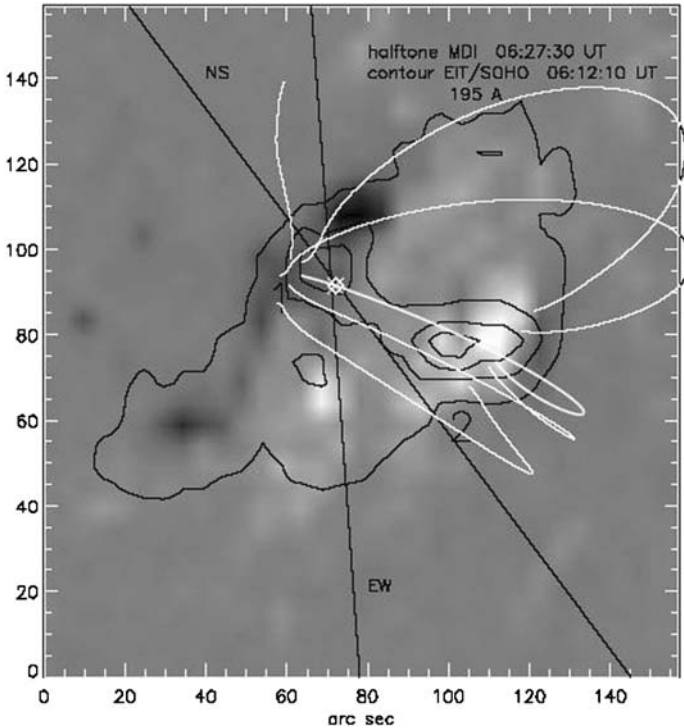


Figure 47. The SOHO/MDI magnetogram (half-tone) and the UV emission map (contour) of the AR 0243 flaring region. The crossed straight lines show the scanning directions of the EW and NS linear interferometers. The intersection point corresponds to the position of the zebra source. The contour levels are 45%, 60%, 75% and 90% of the maximum values. (From Altyntsev *et al.*, 2005).

3. Models of Fiber Bursts (FB) and Zebra Pattern ZP

Concerning the interpretation of of FB and ZP, the theory always lagged behind from obtaining of ever more diverse observational data.

3.0.2.1. Theory of the continuum emission. Our description of the theory would be incomplete, if we shall not illuminate briefly the mechanisms of the continuum radio emission against the background of which the fine structure develops. Type IV bursts are believed to originate from closed magnetic structures (magnetic traps) at heights up to $\approx 0.5R_{\odot}$. Winglee and Dulk (1986) indicate that the distribution of fast particles tends to be peaked at large pitch angles when the electrons are injected impulsively into a closed field loop, whereas loss-cone distributions tend to develop if continuous injection occurs. Kuijpers in his review (Kuijpers, 1980) concluded that the most important high-frequency instability in stationary magnetic traps in the solar corona is the loss-cone kinetic instability of upper hybrid waves. This conclusion was specified by Winglee and Dulk (1986):

after a broad consideration of different aspects of the continuum emission in the Introduction, and after the numerical simulation of the electron cyclotron maser instability, they conclude that the continuum emission results if the maser instability with the loss-cone distribution is saturated. Because zebra-stripes and continuum bursts are produced by the same mechanisms, his theory is able to account for the simultaneous continuum enhancement and ZP appearance (when the maser instability is not at saturation). But in any case the precise knowledge of the distribution function is of prime importance in determining the properties of the instability. In particular, (Kuijpers, 1980) gives an example of the loss-cone distribution when the generation of cyclotron waves become possible at frequencies above the hybrid band in contrast with conclusion of Zheleznyakov and Zlotnik (1975a).

The theory of Winglee and Dulk (1986) is well suited for a homogeneous plasma, and it is not known how it works under the conditions relevant a case when the dense background plasma is assumed to be locally in a highly turbulent state with a number of density irregularities. In plasmas of this kind it has been shown by Fleishmann (2001), referring to earlier suggestions of Ginsburg and Tsytovich (1984), that energetic particles moving across a turbulent plasma emit so-called transition radiation at frequencies above the average local plasma frequency. The first indications of the importance of the account of the transition emission were made by LaBelle *et al.* (2003) in connection with a new theory of ZP.

3.1. THEORY OF FIBER BURSTS

The interaction of plasma electrostatic waves (l) with whistler waves (w) (generated by the same fast particles with loss-cone anisotropy) is a well-accepted emission mechanism for fiber bursts: $l + w \rightarrow t$ with freely escaping electromagnetic waves (t) in the ordinary (O) mode. This model was proposed by Kuijpers (1975a, c). He calculated some principal whistler parameters in the case of longitudinal propagation for conditions in the solar corona: linear instability, cyclotron damping, coupling with Langmuir waves (admissibility) and a possibility of propagation in the form of discrete wave packets (with dimensions $\approx 10^8$ cm), called as solitons. This name, however, refers no to concept of the soliton within the framework of strong turbulence. He estimated that the whistlers must be generated in a periodic manner due to the quasilinear development of loss-cone instability with time interval exceeding ≈ 0.2 s.

The calculations of linear increments for loss-cone distribution (shown in the Figure 48) are one of the very crucial points of theory of Kuijpers (1975c). The calculation were made for typical conditions in the middle corona: the ratio of densities of hot particles to cold plasma ($n_h/n_c = 10^{-3}$, $T_e = 10^6$ K and velocity $v_h \approx 10^{10}$ cm s $^{-1}$).

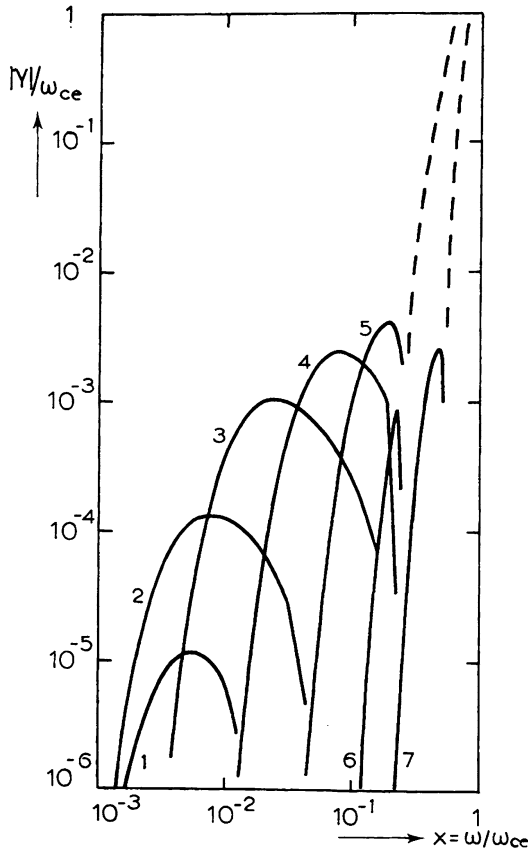


Figure 48. Whistler growth rates in dependence of wave frequency with loss-cone distribution function. The numbered curves (1–6) correspond to increasing loss-cone angles $\alpha = 8^\circ \div 86^\circ$ and fixed ratio $\omega_p/\omega_B = 30$; the curve 7 – to $\alpha = 90^\circ$ and $\omega_p/\omega_B = 10$. The dashed curves present part of the cyclotron damping: at the left is common to cases 1–6, at the right – to case 7 (from Kuijpers, 1975c).

3.1.1. Other Models

The modulation of the emission into IDB was interpreted by a whistler wave packet propagating through a region of enhanced Langmuir waves. In the mean time this model has suffered criticism from several sides: (i) Melrose (1975) has pointed out that the parametric conditions of $l + w \rightarrow t$ are difficult to be met by beam-driven Langmuir waves, making this process very inefficient. (ii) Using nonlinear wave packets (solitons), Bernold and Treumann(1983) have demonstrated that a nonlinear $l + w \rightarrow t$ process operates, but the emission of a single soliton is far too weak since whistler solitons have a small volume. Instead, they proposed the nonlinear process as the emission mechanism involving a large number of whistler solitons, but another process for the modulation producing IDB is required. As a possible candidate, they proposed Alfvén solitons changing the emission properties

of the whistler solitons in a large volume and thus producing the observed drifting absorption and emission. Thus the drift rate would not be the whistler group velocity as assumed by Kuijpers (1975a), but the velocity of the Alfvén soliton.

Güdel *et al.* (1988) and Treumann *et al.* (1990) have investigated stationary solutions for Alfvén solitons propagating obliquely to the magnetic field in a two component (hot and cold) corona. They apply a super-Alfvénic solution to modulate the emission and relate the observed range of drifts to velocities between 1 and 3 times the local Alfvén velocity. Another line has been followed by Mann *et al.*, (1987), who proposed a different modification of the original model. They consider low-frequency, form-stable whistler wave packets for both emission and modulation of IDB. The proposed wave packets do not satisfy the conditions for solitons, but are much larger. The ponderomotive force induces a density hump causing the observed absorption feature at the low-frequency side of IDB. The wave packets originate at the bottom of magnetic loops that trap energetic electrons and near the level where the whistler frequency equals the lower-hybrid frequency. The wave packets then propagate upward with the local whistler group velocity. Thus we are faced with two models of the IDB phenomenon interpreting the drift rate by a few times the Alfvén velocity and the whistler group velocity, respectively. The magnetic field derived from the observations differs by an order of magnitude for the two models. If the interpretation of IDB were settled in either way, the magnetic field in the source could be determined with accuracy.

Thus we have different understanding about the role of whistlers in the formation of FB. Moreover, a model is developed for explaining FB generally without participation of whistlers: Kuznetsov (2006) proposes modulation of upper-hybrid waves by the propagating MHD wave (sausage mode).

3.2. WHISTLER MODE

In connection with different understanding of the participation of whistlers in the formation of FB one should first dwell on the general representation of the whistler mode, and mainly, on the conditions for their generation and propagation in the solar corona, since all attempts at the use of whistlers are introduced from the field of research of the magnetospheric whistlers.

It is known that whistlers are almost transverse waves which carry their energy predominantly along the magnetic field in both directions. The rotation of the electric vector of a whistler corresponds to the extraordinary wave (X-mode) (some renaming of the waves is allowed for oblique propagation (Gershman and Ugarov, 1960). In contrast with other low-frequency waves, whistlers are purely electron oscillations at frequencies $\omega_w \ll \omega_B$ and $\gg \omega_{B_i}$ and can propagate in a dense plasma $\omega_w \ll \omega_p$ (ω_p - electron plasma frequency, ω_B - electron cyclotron frequency, ω_{B_i} - ion cyclotron frequency). The expression for the index of refraction in the quasi-longitudinal approximation (valid for enough big angles) has a form (Edgar, 1972;

Chernov, 1976):

$$\mu^2 = \frac{k_w^2 c^2}{c^2} = \frac{\omega_p^2 \omega_B^2}{M \omega^2 \cos \theta - -(\delta \omega / \omega_B)(1 + \omega_B^2 / \omega_p^2)}, \quad (2)$$

where $\delta = 1 - \omega_{LHR}^2 / \omega^2$, θ is the angle between the wave normal and the direction of the magnetic field, ω_{LHR} is the frequency of the lower hybrid resonance

$$\omega_{LHR}^2 = \frac{\omega_B \omega_B^2 / M + \omega_p^2}{M \omega_p^2 + \omega_B^2}. \quad (3)$$

M is the ratio of the proton (i) and electron (e) masses, k_w is the whistler wave number and c is the velocity of light. Under conditions of the middle corona $\omega_p^2 \gg \omega_B^2$ and (2) is simplified: $\omega_{LHR} \approx \omega_B^2 / M^{1/2} \approx \omega_B^2 / 43$. The frequency ω_{LHR} is the resonance frequency in the case of $\delta \approx 0$ when θ approaches $\pi/2$, then $\omega \approx \omega_{LHR}$ and $\mu \rightarrow \infty$.

For quasi-longitudinal propagation at frequencies $\omega \gg \omega_{LHR}$, $\delta \approx 1$ and the dispersion relation is simplified (Edgar, 1972):

$$\omega = \frac{\omega_B k_w^2 c^2 \cos \theta}{\omega_p^2 + k_w^2 c^2}. \quad (4)$$

The dispersive branch of the whistler wave is the high frequency extension of the fast magnetosonic wave (Kaplan and Tsytovich, 1972), but the analysis of just high-frequencies whistlers ($\omega_B > \omega \gg \omega_{Bi}$) excites the greatest interest, since at these frequencies the Cherenkov damping is exponentially small and whistlers can propagate in a dense plasma without appreciable absorption. The collisional damping is also small since the collisional decrement of whistlers (Kaplan and Tsytovich, 1972) $\gamma_v = \omega \omega_p \sin^2 \theta / (\omega_B \cos \theta N_e d_e^3)$ will be $\ll 10$ through the whole corona (d_e – Debye length). The whistler branch is not altered at the transition from cold plasma to a plasma with hot electrons.

It is known that in the quasi-longitudinal case the effect of the ions is not important, and a simplified equation is obtained for the group velocity of whistlers:

$$v_{gr} = 2c \frac{\omega_B}{\omega_p} \sqrt{x(1-x)^3}, \quad (5)$$

where $x = \omega / \omega_B$. The values of v_{gr} calculated from Equation (4) for the values of the ratio $f_p / f_B \approx 1 \div 20$ are plotted in Figure 49. We can see that v_{gr} is always $> 10^8 \text{ cm s}^{-1}$ and in the middle corona $\sim 10^9 \text{ cm s}^{-1}$. The qualitative decrease of v_{gr} for large angles θ is shown by a dashed line. The frequency $f_{LHR} \approx f_B / 43$ is marked by a vertical dashed line.

For low-frequency whistlers (more exactly for $x / \cos \theta \ll 1$) and in quasi-longitudinal approximation the whistler group velocity does not deviate from the direction of magnetic field more than on an angle $19^\circ 29'$ (the theorem of Storey (Storey, 1953)).

It is known from the magnetospheric whistler propagation that in the quasi-transverse case the effect of the ions comes down to the fact that the index of

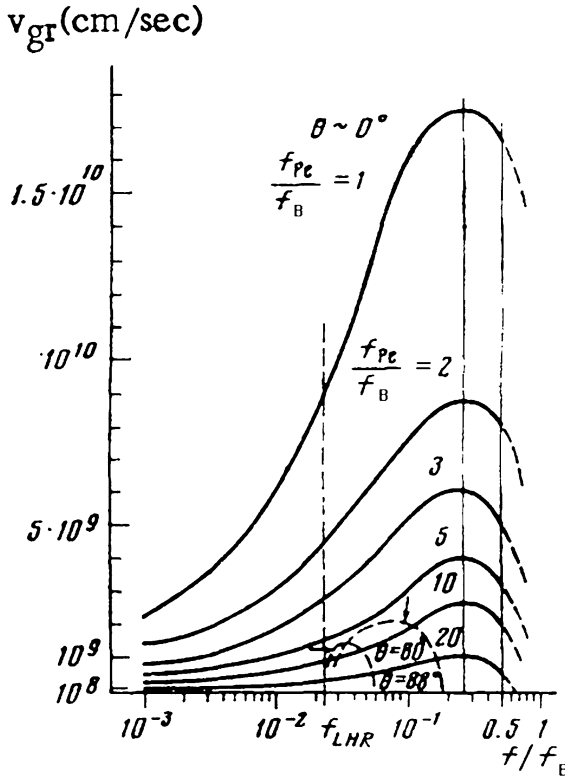


Figure 49. Group velocity of whistlers in quasi-longitudinal propagation for values of ratio $f_p/f_B = 1-20$ as a function of the relative frequency of whistlers f/f_B . The qualitative decrease in v_{gr} for angles $\theta \approx \pi/2$ is shown by a dashed line (from Chernov, 1976b).

refraction does not go to infinity, thanks to which at a frequency $f \approx f_{LHR}$ in a very narrow height interval the group velocity reverses direction with insignificant damping of the wave (Edgar, 1972). This is a linear refraction effect described by Snell's law. Furthermore, probably, nonlinear decay interactions are possible, causing low-frequency plasma turbulence. In Molchanov *et al.* (1974) such processes are examined for the explanation of the disturbances of linear refraction of the magnetospheric whistlers, when instead of the reflection, the wave packet can penetrate through the appropriate level of lower hybrid resonance. Probably, analogous behavior of whistlers should also be characteristic of magnetic traps in the solar corona.

3.2.1. Cyclotron Damping

Whistlers undergo strong cyclotron damping on the cold plasma. The first estimations of cyclotron damping for the solar corona were made by Kuijpers (1975a,c). Under coronal circumstances ($T_e = 10^6$ K, $\omega_p/2\pi = 300$ MHz, $\omega_p/\omega_B = 30, 10$

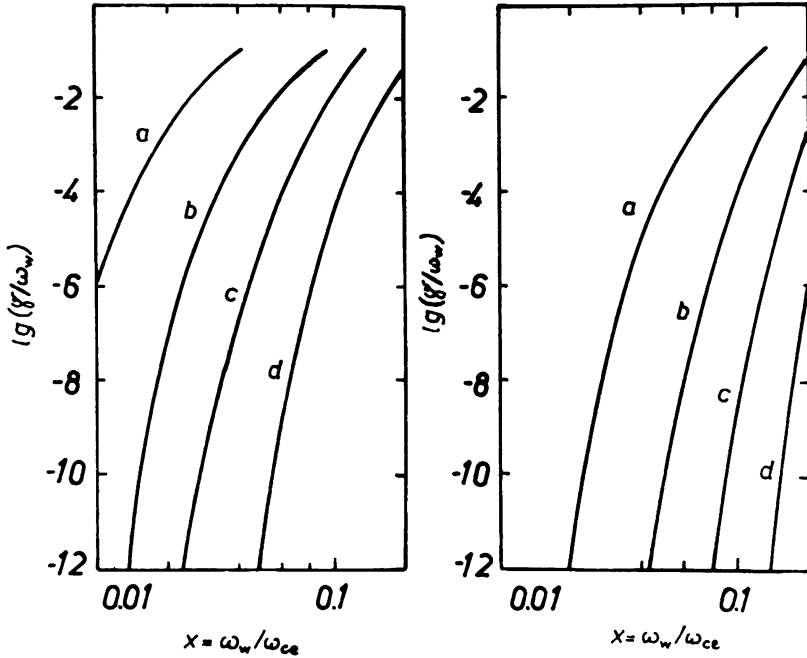


Figure 50. Frequency dependence of the decrement of the electron cyclotron damping for whistler waves propagating along the external magnetic field in the case of $\omega_p/\omega_B = 43$ (left) and $\omega_p/\omega_B = 20$ (right) for various temperatures: (a) 10^7 K, (b) $4 \cdot 10^6$ K, (c) $2 \cdot 10^6$ K, (d) 10^6 K (from Mann *et al.*, 1987).

and in the absence of a loss-cone distribution the role of the cyclotron damping is so important that the propagating whistlers will not occur above $0.5\omega_B$.

Such calculations were repeated by Mann *et al.* (1987) (Figure 50) with more various plasma parameters. But these authors overestimate the importance of the cyclotron damping, so that they draw a conclusion about the impossibility of the whistler propagation in the corona and on this basis they developed the new model of FB (above mentioned) with the ponderomotive force as a main factor inducing a density hump causing the observed absorption feature. The interpretation was later revised (Benz and Mann, 1998; Aurass *et al.*, 2005) where the initial version of model on whistlers of Kuijpers (1975) is accepted.

Nevertheless, Figure 50 shows a strong dependence of the cyclotron damping on the ratio ω_p/ω_B and especially on the plasma temperature. Therefore, if a chosen distribution function does not ensure maximum excitation at frequencies to the right of curves of the cyclotron damping, that indeed, the propagation of whistlers cannot be considered. At the same time one must take into account, that when this condition is satisfied, whistlers experience scattering on the background plasma with the transmitting to the low frequencies. Then, with the propagation to the side of the decrease of external magnetic field this transmitting detains the moment

of switching on of the complete cyclotron damping. Moreover according to the contemporary representations, the magnetic field changes very slowly with the height in the narrow magnetic loops (Aschwanden, 2004).

3.2.2. Whistler Interaction With Langmuir Waves

In the Kuijpers model the analysis of the interaction of Langmuir waves with whistlers was rather semi-qualitative, and there was no detailed analysis of such an interaction and its efficiency in the solar corona before the appearance of a theory of Fomichev and Fainshtein (1988). They showed that the observed fiber radio fluxes are explained in frameworks of weak plasma turbulence. Therefore, alternative models with solitons of Alfvén waves (Bernold and Treumann, 1983) and the strong whistler turbulence (Benz and Mann, 1998) are not required (in greater detail see Chernov (1990b)).

Following a formalism of Fomichev and Fainshtein (1988) first let us consider the kinematics of a three-wave interaction between a plasma wave (ω_l , k_l), a whistler ω_w , k_w and an electromagnetic wave (ω_t , k_t). As is well known, the condition of spatio-temporal synchronisation (conservation laws)

$$\omega_l + \omega_w = \omega_t, \quad \mathbf{k}_l + \mathbf{k}_w = \mathbf{k}_t \quad (6)$$

must be satisfied in such an interaction. The frequencies and wave numbers must satisfy the dispersion relations for the corresponding branch of oscillations in a plasma for the case of longitudinal propagation:

$$\omega_w = \frac{\omega_b k_w^2 c^2 \cos \theta_w}{\omega_p^2 + k_w^2 c^2}, \quad (7)$$

$$\omega_l^2 = \omega_p^2 + 3k_l^2 V_T^2 + \omega_B^2 \sin^2 \theta_l, \quad (8)$$

$$\omega_t^2 = k^2 c^2 + \omega_p^2 (1 + (\omega_B/\omega_t) \cos \theta_t)^{-1}. \quad (9)$$

Here $v_T = (k_B T/m_e)^{1/2}$ is the thermal velocity, k_B is Boltzmann constant, θ_w , θ_l , θ_t - the angles between the direction of propagation of corresponding waves to the external magnetic field \mathbf{B} , $\omega_B = eB/m_e c$ - the electron gyrofrequency, $\omega_p = (4\pi e^2 n_e/m_e)^{1/2}$ - the electron plasma frequency (c - the velocity of light, e and m_e - charge and mass of the electron), n_e - the electron density. Equation (9) correspond to the ordinary wave (O-mode).

For a realistic case in the corona where $\omega_t > \omega_p \gg \omega_B$ and using the geometrical relations between wave vectors

$$k_t^2 = k_l^2 + k_w^2 \pm 2k_l k_w \cos \theta, \quad (10)$$

(where θ is the angle between the directions of wave vectors of whistlers and plasma waves) one can obtain from Equations (7)–(10) the expression for $\cos \theta_t$. In Equation (10) the sign ‘-’ before the third term to the right corresponds to the decay process $l \rightarrow t + w$ at the difference frequency $\omega_t = \omega_l - \omega_w$, $\mathbf{k}_t = \mathbf{k}_l - \mathbf{k}_w$.

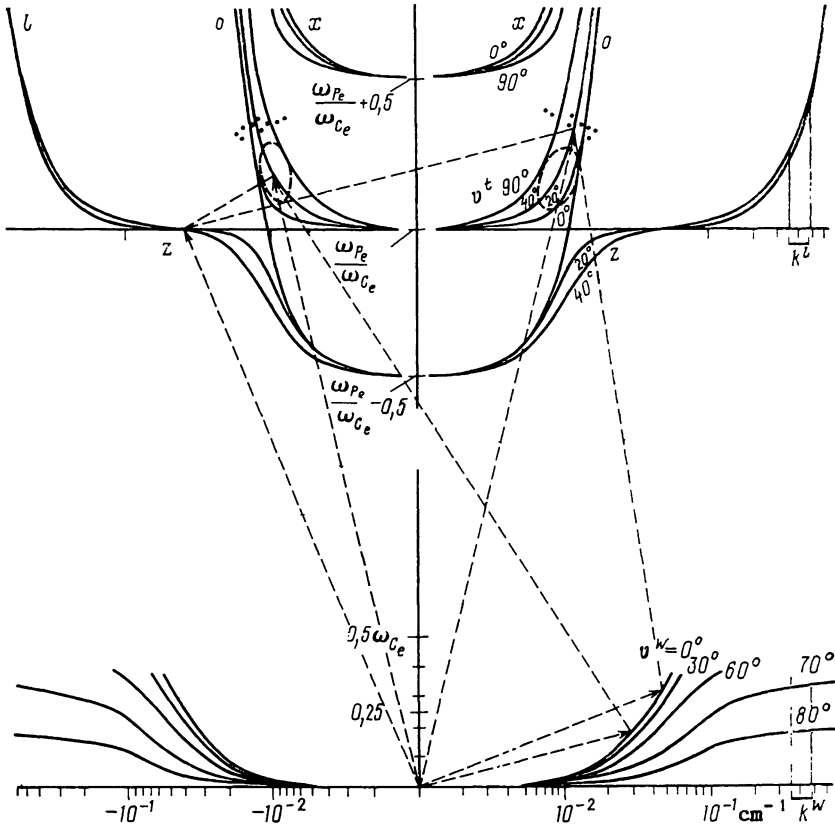


Figure 51. Dispersion curves for electromagnetic (O- and X-modes), Langmuir waves (l) and whistlers (*bottom*) for different propagation angles (θ^i) with respect to the magnetic field. A graphic diagram of the $l + w \rightarrow t$ interaction at the sum frequency is shown by dashed lines for two whistler wave numbers and $\theta_w = 0^\circ$. The domains of values ω_t, k_t for the $l \rightarrow t + w$ decay process at the difference frequency are encircled by dashed curves on the branches for the ordinary wave. The corresponding values of k_l and k_w are marked by segments on the k -axes (from Chernov, 1990b).

As shown by Chernov and Fomichev (1989) and Chernov (1990b) such a process is quite possible, if the thermal additive (to the plasma frequency) in the dispersion relation in Equation (8) will be more than the whistler frequency. Such a condition can be realized for the ratio $\omega_p/\omega_B > 8$ for the whistler frequency $\omega_w \approx 0.1\omega_B$.

From the natural requirement $|\cos \theta_i| < 1$, the range of possible values k_l/k_w was obtained. It was shown that the interaction is possible for both relations $k_l/k_w > 1$ and $k_l/k_w < 1$ with $k_l \simeq k_w$ and $\mathbf{k}_l = -\mathbf{k}_w$, i.e. Langmuir wave and whistlers with approximately equal and oppositely directed wave vectors take part in the interaction. For the interaction at the difference frequency the vectors \mathbf{k}_l and \mathbf{k}_w must be in the same direction with a very small angle between them $\theta < 1.28^\circ$, but with a limitation of the angle $\theta_w, \theta_l > 70-80^\circ$. Chernov and Fomichev (1989) obtained the maximum plausible angles $\theta_l \leq 84^\circ$ at the difference frequency. In Figure 51

we show the dispersion curves and a graphic representation of the interaction of l , w and O-mode, $l + w \rightarrow t$ for the typical conditions in the middle corona: $\omega_p/\omega_B = 30$ and $T_e = 10^6$ K. The branches of whistlers for $\theta_w = 0^\circ$ and $\theta_w = 30^\circ$ are cut off at the frequency $\omega_w = 0.37 \omega_B$, since the strong cyclotron damping sets in at higher frequencies, and ω_w does not exceed $0.17 \omega_B$ for $\theta_w = 80^\circ$. The interaction of waves at the sum frequency is shown schematically by dashed lines for two whistler wave numbers. The sum values ω_t and k_t for different frequencies ω_w are denoted by dots on the branches of O-mode (similar to Figure 5 in Kuijpers (1975c)). The intervals of values of k_l and k_w for which the conservation laws are satisfied at the difference frequency are denoted by segments on the wave number axes. The domains of values of ω_t and k_t at the difference frequency are encircled by dashed curves on the branch of O-mode.

The synchronization conditions (conservation laws) are not satisfied for extraordinary (X) wave with any values k_l and k_w (Fomichev and Fainshtein, 1988). Therefore the polarization of the radio emission generated through the interaction plasma waves and whistlers will correspond to the ordinary wave, which agrees with observations.

For the interaction at difference frequency significant constraints are imposed on the range of wave numbers k_l and $k_w \approx 0.23 \div 0.45$ and consequently on the propagation angles $\theta_l, \theta_w \gtrsim 80^\circ$. Specifically these factors may explain the rare appearance of radio emission at the difference frequency (Figures 7 and 22). Oblique whistlers can be generated only at anomalous Doppler resonance, (see below the Section 3.2.5.) which can be realized rather during quasi-linear diffusion of whistlers on fast particles.

The conservation laws will be carried out analogously for interaction of plasma upper hybrid waves and whistlers with the escape of ordinary wave for the case, when both wave vectors \mathbf{k}_{uh} and \mathbf{k}_w are directed at large angles toward the magnetic field.

The estimation of effectiveness of the interaction of plasma waves and whistlers presents the main result of work of Fomichev and Fainshtein (1988), for the first time they solved the system shortened equations for complex amplitudes of interacting waves (in the steady-state case with $\partial/dt = 0$). In the case of fixed wave phases the amplitude of the electromagnetic wave increases linearly with distance. But the case with random wave phases is more realistic in the sources of type IV radio bursts. Performing the averaging over the wave phases the initial system of equations for the wave amplitude (a_i) is transformed into equations for the dimensionless wave intensities $N_i = \langle a_i^2 \rangle \Delta\omega_i$. Here $\Delta\omega_i$ is the bandwidth of wave of type i .

In the general case, the solution of the system for the wave intensities was too unwieldy, and a numerical simulation were carried out. Taking into account the subsequent estimations of the interaction at the difference frequency (Chernov and Fomichev, 1989) we can state that coalescence and decay at the frequencies $\omega_t = \omega_l \pm \omega_w$ can be equally efficient in an optically thick source, and the maximum

electromagnetic radiation intensity is given by the expression:

$$N_t \leq \frac{N_l N_w}{(\omega_p/\omega_B)N_w \pm \sqrt{\omega_B/\omega_w}(\omega_B/\omega_p)N_l} \quad (11)$$

Here ‘-’ in the denominator – for the decay process at the difference frequency.

Melrose (1983) has shown that four-plasmon coalescence and decay processes in an optically thick source at the combination frequencies $\omega_t = \omega_l \pm \omega_w \pm \omega_{w'}$ are also possible in the corona.

3.2.3. *Weak or Strong Turbulence of Whistlers*

Fomichev and Fainshtein (1988) have estimated one important parameter, the turbulent level of whistlers in the source. The fiber fluxes $\sim 10^{-19}$ W m⁻² Hz⁻¹ and brightness temperatures $\sim 10^{14}$ K for the plasma wave power $W_l \approx 10^{-5}$ – 10^{-6} erg cm⁻³ require a whistler power $W_w \approx 2 \cdot 10^{-10}$ erg cm⁻³, which is only four to five orders of magnitude higher than the thermal noise of the whistlers and as many orders of magnitude lower than the energy of the plasma waves. Thus, a more detailed analysis of the interaction $l + w \rightarrow t$ confirms the result of Kuijpers (1975a,c), that usually observed radio fluxes in FB are explained in the context of weak turbulence.

However, observations of FB in very strong type IV bursts are stimulating many authors to employ strong turbulence of whistlers. On the basis of of an expression for the functional form of a one-dimensional whistler soliton obtained by Karpman and Washimi (1977) it was proposed in Treumann and Bernold (1981) and Bernold and Treumann (1983) that all the energy of the whistlers is concentrated in such solitons. This model subsequently encountered new difficulties.

- (i) It turns out that the emission of $\sim 10^{14}$ solitons from a volume of $\sim 10^8$ km³ is required to explain the observed fiber fluxes. The absorption cannot be explained in the usual way in this case, since the individual solitons in such a volume cause emission (and absorption) at frequencies which much differ, due to their very small size.
- (ii) For attaining strong turbulence at the reflection points of whistlers, the whistler frequency $\omega_w \approx \omega_{LHR} \approx \omega_B/43$, that contradicts to the condition for the formation of whistler soliton, $\omega_w \gtrsim \omega_B/4$.
- (iii) A simple decrease in the group velocity cannot result in the formation of whistler solitons. Multiple reflections of whistlers are observed in the earth’s magnetosphere, but solitons were not recorded. The reflection of whistlers occurs with a gradual reversal of \mathbf{k}_w through the interaction with the electrostatic mode. A strong wave can therefore result in the formation of lower-hybrid solitons, which propagate perpendicular to the magnetic field and could interact with upper-hybrid waves.

It is thought that the level of strong turbulence of whistlers (and plasma waves, incidentally) may be reached in powerful events. But the analysis of the linear stage of modulational instability in Karpman and Washimi (1977) does not at

all mean that all the energy of whistlers is concentrated in solitons. For FB it is necessary to consider the non-linear stage of modulation instability, and even more its saturation. Such a two-dimensional problem was solved numerically in Karpman and Shagalov (1988). They showed that the field of a powerful wave is concentrated in two types of narrow structure drawn out along field lines: fast magnetosonic waves with decreased density and magnetic field, propagating with whistler group velocity, and slow magnetosonic waves with increased density, moving with a very slow velocity ($< V_T/43$). The first structures containing density cavities can be used to interpret the usual classic FB, and the slow magnetosonic structure can be used to interpret unusual slowly drifting fibers.

3.2.4. Formation of Stripes in Emission and Absorption

Let us examine in more detail the yield of radio radiation in this process. First of all we enforce that the radiation at a fixed frequency can be generated in the corona in an extended region. This extent can be connected with the finite width of the spectrum of plasma waves due to the thermal spread of the background plasma and velocity dispersion of the fast particles. We designate the dimension of the emitting region at fixed frequency in the direction of ∇n_e as L , assuming that the intensity of the radiation of a given frequency declines exponentially in this region with height h : $W \sim \exp -(h/L)^2$. This means that from each level in the corona a spectrum of frequencies $\Delta\omega$ should be emitted. A realistic dimension of L can be of $\sim 10^8$ cm. And about the same value can be the dimension of whistler wave packet L_w , if to judge on the duration of fibers at a fixed frequency ≈ 0.5 s (Figure 7), taking into account the group velocity of whistler $v_{gr} \approx 10^9$ cm s $^{-1}$ for the ratio $\omega_p/\omega_B \approx 20$ (Figure 49).

Figure 52 shows qualitative diagram of formation of stripes in emission and LF-absorption for different relation between L and L_w : (a) $L_w > L$, $\omega_w > \Delta\omega$; (b) $L_w < L$, $\omega_w \gtrsim \Delta\omega$; (c) $L_w \sim L$, $\omega_w \lesssim \Delta\omega$. In all cases the frequency separation between neighboring maxima in emission and absorption equals the whistler frequency ω_w . The condition of frequency separation of stripes in emission (from neighboring whistler wave packet) means that the distance between packets must be greater than L . The stripes in emission will be separated by stripes in absorption if the condition for their formation is satisfied: $\omega_w > \Delta\omega = L \cdot \nabla\omega_l$.

The reality of the formation of stripes is confirmed in Chernov (1976) by the numerical calculations of intensity relative to continuum, based on the comparison of effectiveness in the processes of interaction $l + w \rightarrow t$ and induced scattering of l plasmons on ions. The modulation depth in the calculated profiles agrees with that observed in FB in the event May 3, 1973 (Figure 5) and in ZP in the event July 3, 1974 (Figure 19). The calculations show that the necessary whistler wave energy is much less than the energy of plasma waves.

The possibility of the escape of radio emission as on the sum, so at the difference frequency it is confirmed by the observations of FB and ZP. In the Figure 21 the

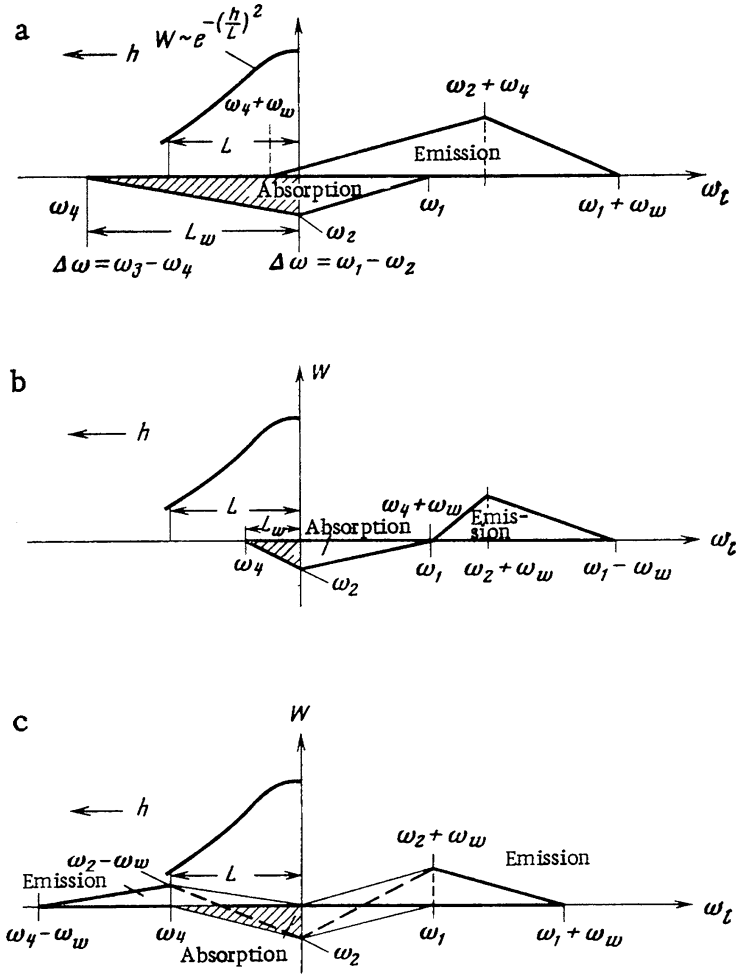


Figure 52. Qualitative diagram of formation of stripes in emission with LF-absorption for different dimension of wave packets of whistlers (L_w), ω_l – Langmuir frequency and h -height in the corona. (a) $L_w > L$, $\omega_w > \Delta\omega$, regions of emission and absorption are overlapped in frequency; (b) $L_w < L$, $\omega_w \gtrsim \Delta\omega$, these regions are separated; (c) $L_w \approx L$, $\omega_w \lesssim \Delta\omega$, regions produce a form of a “tadpole” type owing to the yield of radiation at the difference frequency. In all cases the frequency separation between neighboring maxima in emission and absorption equals the whistler frequency ω_w (from Chernov, 1976b).

absorption is located from the HF edge of fiber in the emission in the event on July 28, 1999. In the Figure 7 the exchange of the position of absorption from HF to LF is shown in the course of the drift of one fiber. In Figures 21 and 22 the position of absorption changed to the reverse one in one series the ZP during about 1 minute. Here, the different directivity of emission in these processes plays the dominant role.

3.2.5. Linear Whistler Instability

Linear cyclotron instability was investigated in some detail in application to magnetospheric whistlers by Kennel (1966) and Kennel and Thorne (1967). Jamin *et al.* (1974) analyzed firehose and mirror whistler instabilities for a large temperature anisotropy. They showed that the whistler wave field has the form of sporadic irregular oscillations with a transfer of energy inside the spectrum. The spectrum of whistlers in coordinates $[\gamma t; kx]$ resembles to a braided zebra patterns (see Figure 3 in Chernov (1976b)). Yip (1970) calculated the first possible frequency and angular spectra of whistler at normal and anomalous Doppler resonance by electron streams in the solar corona. And in application directly to FB Kuijpers (1975a,c) calculated linear increments for loss-cone distribution with different plasma parameters (shown in the Figure 48). Berney and Benz (1978) used much more various loss-cone distribution function, and they confirmed in general calculations of Kuijpers. They compare also whistler and electrostatic instabilities, and conclude that the growth of electrostatic waves is at least an order of magnitude faster. However, according to Sharma and Vlahos (1984), the growth rates of Langmuir and upper hybrid waves for the loss-cone distribution are less than for whistlers.

In all papers above mentioned the instability was calculated only for the longitudinal whistlers at the normal Doppler resonance with monoenergetic electron distribution. In order to examine the amplification of whistlers propagating in coronal plasma at arbitrary angles to the magnetic field, Mal'tseva and Chernov (1989) use an anisotropic Maxwellian distribution with a loss-cone in the perpendicular velocity v_{\perp} and with the presence of a beam along the magnetic field \mathbf{B} :

$$f_h(v) = \frac{n_h v_{\perp}^{2j}}{\pi^{3/2} v_{T_{\parallel}} v_{T_{\perp}}^{2j+2} (j+1)} \exp \left[-\frac{(v_{\parallel} - v_b)^2}{v_{T_{\parallel}}^2} - \frac{v_{\perp}^2}{v_{T_{\perp}}^2} \right], \quad (12)$$

where n_h is the concentration of hot electrons, $v_{\perp} = v \sin \alpha$, $v_{\parallel} = v \cos \alpha$, α is the pitch angle, $v_{T_{\perp}}$ and $v_{T_{\parallel}}$ are the rms transverse and longitudinal velocities, v_b is the velocity of the beam along \mathbf{B} and j is the positive index of the loss-cone in v_{\perp} . In this case $f_h \sim \sin^{2j} \alpha_{lc}$, where α_{lc} is loss-cone angle. The temperature anisotropy is introduced by the parameter $a = 1 - v_{T_{\parallel}}^2 / v_{T_{\perp}}^2$. The cold background plasma is specified by the same Maxwellian distribution with $j = 0$, $a = 0$, $v_b = 0$ and the temperature $T_e \sim 10^6$ K.

A beam distribution with the loss-cone yields a beam with $v_{\parallel} > v_{\perp}$ (if $a < 0$, and $j \lesssim 0.5$, which can be realized at the top of the magnetic trap), in which case Cherenkov and cyclotron resonances on the anomalous Doppler effect contribute to emission (Kennel, 1966; Gendrin, 1981). In such a case in the cyclotron resonance relation

$$\omega - k_{\parallel} v_{\parallel} - s \omega_B = 0 \quad (13)$$

the harmonic number $s = -1$. With a strong transverse anisotropy ($a > 0$, and $j \approx 2$, we obtain $v_{\perp} > v_{\parallel}$ (rather at the base of the magnetic trap), and the resonance

on the normal Doppler effect will basically responsible for whistler emission ($s = 1$ in Equation (13)).

In the expressions for local growth rates of whistlers excitation by hot electrons (γ_h) and for damping decrements by cold plasma (γ_c) the three main resonances (Cerenkov and cyclotron on normal and anomalous Doppler effects) were summed.

The calculations were carried out for large series of the parameters of anisotropic beam and cold plasma. For the energy of hot electrons $E \approx 30$ keV ($v \approx 10^{10}$ cm s^{-1}) and energy dispersion $\Delta E \approx 30$ keV the maximum growth rates locates near the relative whistler frequency $x = f_w/f_B = 0.1 \div 0.15$ (for large loss-cone angles and velocity anisotropy $a = \pm 0.5$). Specifically, at this frequency the minimum of the absorption (γ_c) is located. This result confirms calculations of Kuijpers (1975c) for the longitudinal propagation. However, the account of three resonances made it possible to reveal the maximum of absorption (Landau damping) at the smaller frequencies, $x = 0.03 \div 0.05$.

The main new inference to be drawn from calculations of Mal'tseva and Chernov (1989b) is complex behavior of instability as function of the angle of propagation (here the angle ψ) shown in Figure 53. The anisotropic high-energy beams produce emission at all angles ($0^\circ < \psi < 90^\circ$) for $x \lesssim 0.1$ but only up to angles $\psi \approx 45^\circ - 50^\circ$ for $x > 0.1$. The sign change of the velocity anisotropy from $a = 0.5$ to $a = -0.5$ at the high loss-cone anisotropy ($j = 1.5$) cause a pronounced shift of the curves towards larger ψ .

The complex behavior of $\gamma_c(\psi)$ (γ_c curves are intersected twice) is explained by the increase in Landau damping as ψ increases at low frequencies. But for $x > 0.1$ and angles ψ near $\pi/2$, the cyclotron absorption begins to dominate and the curves are crossed again at $\psi \approx 80^\circ$.

It was found that the Landau damping peaks at intermediate angles $\psi \approx 30^\circ \div 50^\circ$ (although it remains small even there), and that the damping decreases with increase of ψ to $80^\circ \div 90^\circ$. Therefore whistlers can be reflected without appreciable damping in low-hybrid resonance regions. The Landau damping decrement begins to decrease as ψ approaches 90° , since the components of the antihermitian part of the permittivity tensor ϵ_{yy} , ϵ_{yz} and ϵ_{zz} which are exponentials $\exp(-X_o^2)$ with coefficients of different signs, contribute to it for $s = 0$ (see Appendix in Mal'tseva and Chernov (1989b)). There is a definite similarity between these calculations and the results of Hashimoto and Kimura (1977).

The actual variation of the wave amplitude (A_o) during propagation at group velocity is determined by the integral gain $\gamma_\Sigma = \int_o^l (\gamma/v_{gr}) dl'$, in which the amplification (damping) contributions from hot particles and damping by the cold plasma along the path l are summed. Large negative values of γ_Σ (when $|\gamma_\Sigma| \gg 1$) characterize instantaneous damping of the wave, since its amplitude will decrease in accordance with the law $A = A_o \exp \gamma_\Sigma$.

Figure 4 in Mal'tseva and Chernov (1989b) shows small damping along whistler trajectory during 10–20 s even for extreme conditions for the instability with $E = 3$ keV, $\Delta E = 0.01$, $n_h/n_c \sim 10^{-7}$. As a final result of calculations of Mal'tseva

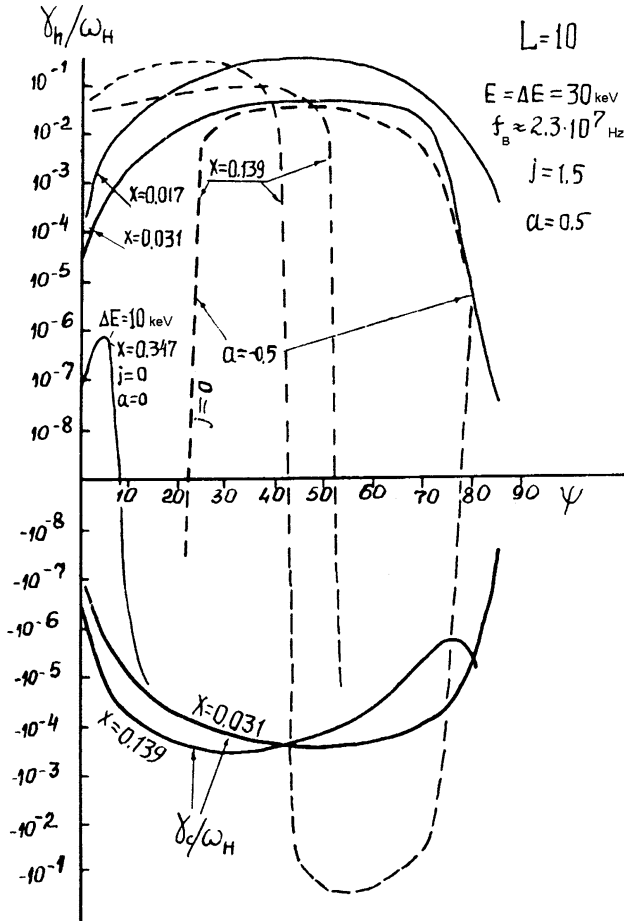


Figure 53. Curves of γ_h and γ_c for several frequencies x . A negative velocity anisotropy shifts the γ_h curves towards larger ψ (the anomalous Doppler effect) (from Mal'tseva and Chernov, 1989b).

and Chernov (1989b) Figure 54 shows the frequency range of the positive total increments of whistlers, obtained on the totality values of γ_Σ along 60 trajectories for different values of f_p/f_B . The amplified whistler propagation is possible only, if $\gamma_h \gg |\gamma_c|$ (by two – three orders of magnitude with a maximum in the frequency interval $x = 0.022 \div 0.1$. This result is differed from those of Kuijpers (1975c) (see above Figure 47) and Berney and Benz (1978) in terms of cutting curves by low frequencies (due to Landau damping) and in terms of smoother decrease from the side of the high frequencies (due to contribution of three resonances).

Thus Mal'tseva and Chernov (1989b) showed that whistlers excited by anisotropic beams (as the most real distribution in the solar magnetic traps) can propagate in arbitrary angles to magnetic field in course of tens of seconds.

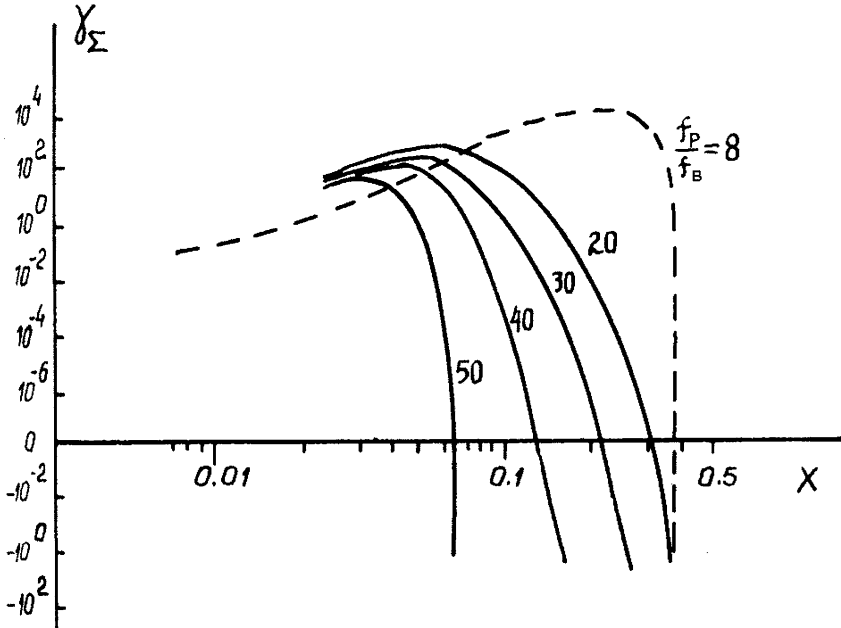


Figure 54. Frequency range in which amplified whistler propagation is possible (with maximum positive gain to the first reflection) (from Mal'tseva and Chernov, 1989b).

In connection with the new observations of FB in the microwave range, it is important to estimate the possibility of the excitation of whistlers in the dense hot flare plasma. The calculations of increments for such conditions were carried out by Yasnov *et al.* (2002). The position of the radio source near the acceleration region of particles justifies the use of the same distribution function (12) in the form of anisotropic beam. One example of calculations for $a = -0.5$ and $j = 0.2$ (the anomalous Doppler effect with a small loss-cone anisotropy) and different temperatures (to 10^7 K) is shown in the Figure 55. We can see, the whistler growth rates increase with T and the maximum is shifted with T to the lower frequencies, from $x = 0.13$ to $x \approx 0.1$ for $T = 2 \cdot 10^7$ K. The absolute values of increments prove to be even higher, than in the upper corona for the meter range.

3.2.6. Whistler Ray Tracing in the Solar Corona

Accordingly Kimura (1966) as a result of the account of ions in the dispersive relationship, refractive index at the mirror point acquires large, but end value. Only account of ions made it possible to calculate the trajectories of magnetospheric whistlers with the multiple reflections (Walter, 1969). The form of trajectory at the mirror point depends on the frequency of the whistlers: it is smooth oval, if $\omega \ll \omega_{LHR}$, sharp, if $\omega \sim \omega_{LHR}$, or even with the overlap, if $\omega > \omega_{LHR}$, (Edgar, 1972).

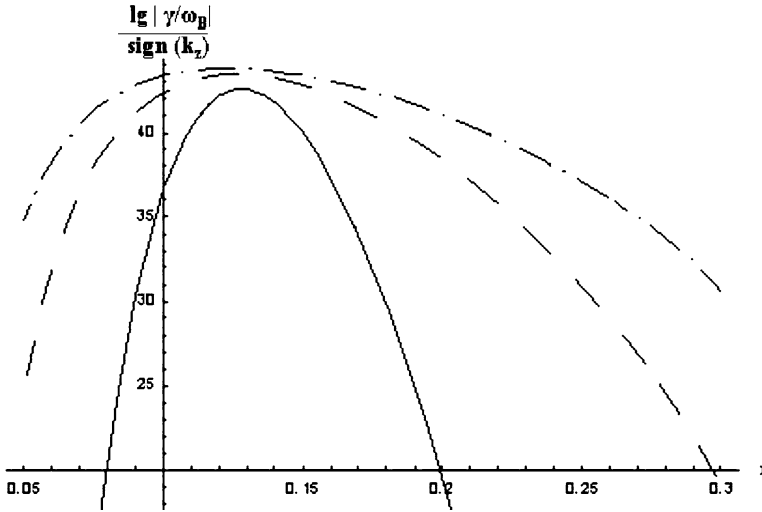


Figure 55. Increment of whistler instability relative ω_B on the dependence of whistler frequency x for three values of the coronal temperature, from below to upward $T = 2 \cdot 10^6$ K, 10^7 K, $2 \cdot 10^7$ K (from Yasnov *et al.*, 2002).

However, the simple transfer into the corona of all effects characteristic for the magnetospheric whistlers will be not completely correct, since coronal plasma is denser, hotter, and the relation of plasma frequencies changes in the larger interval of values (1–50). It was therefore very important to verify the possibility of reflections of whistlers in the solar corona.

The possible whistler trajectories in the solar corona were calculated by Mal'tseva and Chernov (1989a). The standard program of numerical integration of Haselgrove two-dimensional equations (usual for earth's magnetosphere) was used. This is system of four differential first order equations in the polar coordinates (r, Θ) . The equations of ray are obtained from the differential form of Snell's law with the propagation of wave with the group velocity through the medium with the smoothly varying parameters (Haselgrove, 1955). The double Newkirk model of the electron density was chosen, as a convenient analytical form above the active region (Newkirk, 1961),

$$n_e = 16.52 \cdot 10^4 \cdot 10^{4.32/h}, \quad (14)$$

where h is the height from the center of the Sun in solar radii. And the dipole model of magnetic field above an active region was selected for the analogy with magnetospheric calculations, with a depth of the position of dipole under the photosphere $L = 20000$ km, which was utilized as the parameter of McIlwain with the calculation of the course of force line according to the formula: $r = L_0 \cos^2(90 - \Theta)$, where L_0 is the maximum height of the force line. The magnetic field strength at

the photosphere level was chosen of 300 G for force lines in the height interval $0.015\text{--}0.1 R_{\odot}$ and of 1000 G for heights $>0.1 R_{\odot}$.

The calculations of Mal'tseva and Chernov (1989) showed that the trajectories of whistlers in the solar corona can be such complex, with the multiple reflections, like magnetospheric ones. Mal'tseva and Chernov (1989) were limited to the most probable frequency range of whistlers, $0.02 \lesssim x \lesssim 0.25$ in which the propagation is possible without appreciable attenuation. With the inclined excitation and propagation of the whistlers (more precisely, when the angle between the wave vector \mathbf{k} and the ray polar coordinate r , $\delta < 20^\circ$) they can experience reflections at the points of lower hybrid resonance and repeatedly intersect the source of radio emission. Figure 56 shows two of numerous trajectories beginning at the top of magnetic loops and interesting rather for the interpretation of ZP, when the oblique whistler wave is excited at anomalous Doppler effect. The lower trajectory is seized in the corona after numerous reflections, seven rays in the interval of 32 000 km. The periodic whistler wave packets are prove to be seized at a certain level in the corona in the time interval compared with one minute, then this can be used for the interpretation of the stationary stripes of zebra almost without the frequency drift.

If the longitudinal whistlers are excited in the base of magnetic trap (at the normal Doppler resonance), they propagates along the magnetic field and they can be responsible for FB.

The parameters of ducts capable of canalizing whistlers with the increased density and magnetic field strength (in 2–5 times) represent a special interest. The greatest cross size of duct should not exceed $2 \div 3 \cdot 10^8$ cm. A critical angle of capture of whistlers in the duct is found: $\psi \lesssim 70^\circ$ (ψ is the angle between \mathbf{k} and \mathbf{B} in a point of whistler excitation).

3.2.7. *Scattering of Whistlers on Thermal Plasma and Coupling With Ion-Sound Waves*

In the course of the propagations in the corona the whistlers undergo by the induced scattering on thermal ions and electrons. According to Livshits and Tsytoich (1972) the predominant scattering of whistlers by ions occurs only in strong magnetic field, more precisely for the coronal conditions, when $\omega_p/\omega_B < 12$ (see in detail Chernov (1989)). During scattering by ions whistlers transfer to lower frequencies (to $\omega_w \approx 0.1\omega_B$) and became aligned along the magnetic field. However this process is slow. The scattering by electrons is much faster, (approximately by a factor 43) and the continuous transfer to larger angle θ_w occurs.

Under conditions of a non-isothermal plasma $T_e \gg T_i$ the main process consists in the inter-conversion of ion-sound wave (s) (at frequency $\omega_s \approx \omega_{pi}$ - ion plasma frequency) into whistlers and back. Here there is a strong constraint on the angle between \mathbf{k}_w and the magnetic field $\theta_w \gtrsim 70^\circ$. Angular scattering of whistlers by electrons to satisfy this condition, although the main role plays the angles θ_w under which whistlers are excited.

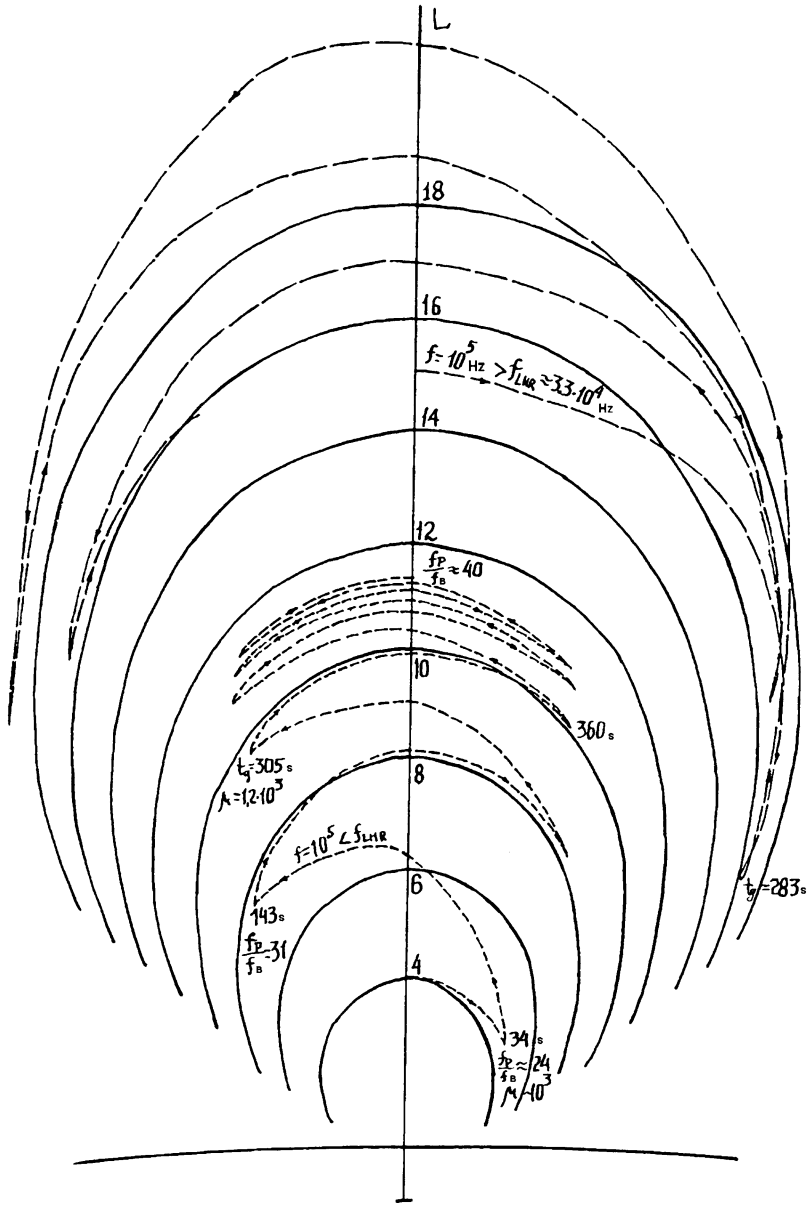


Figure 56. Whistler trajectories (broken line) with repeated reflections against the background of dipole force lines (solid line). $L = 20000 \text{ km}$ is the depth of the position of dipole under the photosphere. The scale in the horizontal direction is the same (in L). The lower trajectory is seized at the level of $L \approx 11.5$. In some reflection points the parameters of trajectories are marked: time of group propagation t_g , ratio f_p/f_B and value of the refractive index μ (from Mal'tseva and Chernov, 1989a).

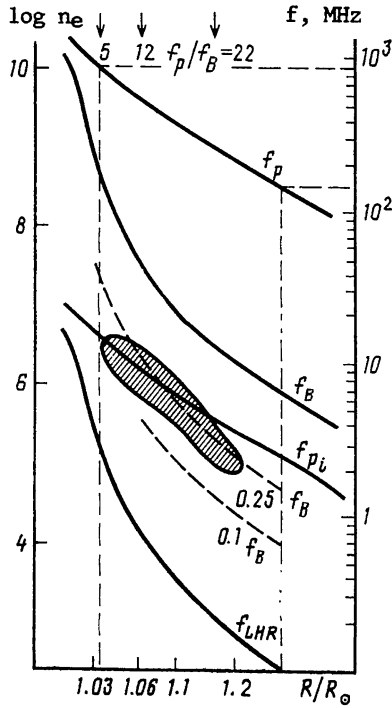


Figure 57. Variation of characteristic frequencies with distance R in the corona. The interaction ($s + s' \leftrightarrow w$) is most efficient in the hatched region (from Chernov, 1989).

The maximum increments for coupling and decay of whistlers and s -waves occur only when their frequencies almost coincide, which means that $0.25\omega_B \approx \omega_{pi}$. Just such relation is satisfied in the solar corona. The approximate behavior of the main plasma frequencies in the corona is shown in Figure 57. The plasma frequency f_p is approximated by double Newkirk model. It is seen that the $0.25 f_B$ curve intersects the f_{pi} curve in the vicinity of $f_p \approx 300$ MHz, so this level is the middle of the range where rapid conversion of whistlers into ion-sound waves and back in a pulsating regime can occur ($s + s' \leftrightarrow w$). This region is hatched in Figure 57.

This mechanism will useful to understand the nature of the superfine structure of zebra stripes consisting of millisecond spikes (Chernov, 2003). Couplings and decays of s -waves and whistlers are observed in the laboratory experiments and are used for the interpretation of radio emission in the active rocket experiments with the injection of the electrons (Mishin *et al.*, 1989).

3.2.8. Problem with Magnetic Field Estimations Using FB

Benz and Mann (1998) the first time presented IDB above 1 GHz (Figure 58) and they investigated the variation of the frequency drift rate with frequency as well as the magnetic field estimations in different models. In Figure 58 we see that (df/dt)

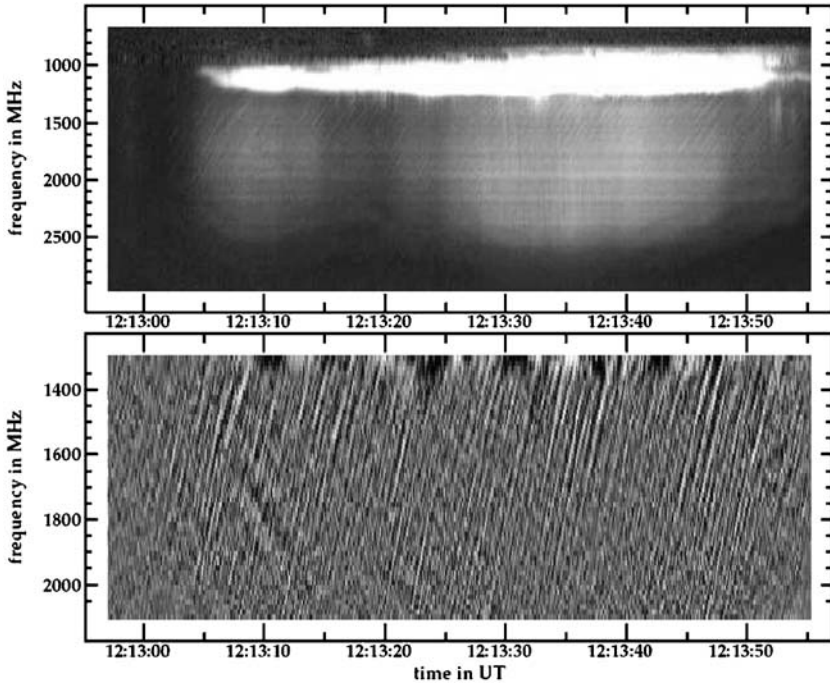


Figure 58. *Top*: Spectrogram of a decimetric type IV burst observed with the Phoenix radio spectrometer of ETH Zurich on March 20, 1993. *Bottom*: The IDBs in the range 1200–2400 MHz; the intensity has been enhanced by subtracting a gliding average in frequency and time (from Benz and Mann, 1998).

is almost constant with frequency and high frequency IDB are found to be identical in their characteristics with FB below 1 GHz. The quantitative results on the first derivative (drift rate) and second derivative have been used to test the two existing models. At the newly accessible high frequencies, the Alfvén soliton model by Treumann *et al.* (1990) predicts very high magnetic fields that are inconsistent with plasma emission.

The other model, suggesting whistler waves (e.g. Mann *et al.*, 1987), predicts relations of \dot{f} and \ddot{f} with frequency dependences that are not consistent with the observations. However whistler wave model gives the reasonable magnetic field strengths using the whistler group velocity and df/dt : 212 G at 2000 MHz and 5.7 G at 200 MHz. But these estimations depend strongly on relative whistler frequency (x) and density model (L_n).

Dulk and Mclean (1978) did not include the estimations of the magnetic field strength using the frequency separation ($\Delta f_{ea} \approx f_w$) between emission stripe and LF absorption in FB due to a large arbitrariness in the choice of x . In Chernov (1990b) a special attention is given to the choice of x where the whistler growth rate is maximal.

At meter wavelengths ($f_p/f_B \approx 30$) the distribution function should have a narrow loss-cone and the generation maximum falls at frequencies $x \approx 0.1$ (see Figure 48). In this case the fast differential scattering of whistlers on thermal electrons is predominant with transfer over the spectrum to low frequencies which may compensate the increase of x with upward whistler propagation toward lower magnetic field. Since the scattering on electrons has a low frequency limit $x \approx 0.1$ this value remains almost constant during life time of the fiber.

In the decimetric range fast electrons have larger loss-cone angle (near the magnetic mirror) and the maximum of the growth rate takes place at $x \approx 0.25$. For $f_p/f_B \lesssim 12$ the differential scattering on ions is predominated and the value $x \approx 0.25$ should be conserve along the fiber. By this reason the value Δf_{ea} usually hardly varies during life of one fiber (e.g. see Figures 6, 22).

Thus, in the metric range $x = 0.1$ must be used and in the decimetric range $x = 0.25$. The estimations of B with these values of x satisfy condition that plasma β would be $\lesssim 1$ and they are close to model of Dulk and McLean (1978):

$$B = 0.5(h - 1)^{-1.5} G, \quad (1.02 \leq h \leq 10) \tag{15}$$

where h is the height in solar radii. The reliability of this procedure is checked by the simultaneous testing of the obtained estimations according to the frequency drift of fiber using the formula (1), obtained by Elgarøy (1982) via equating v_{gr} of whistlers (formula (5)) and speed of an agent, determined from the frequency drift

$$V \approx 2 \frac{(df/dt)}{f} \frac{n_e}{dn_e/dh} \tag{16}$$

For determining of the agent speed V the simple double Newkirk model (formula (14)) is traditionally used. Coefficients in the formula (1) must be different for different x .

3.3. THEORY OF ZEBRA PATTERNS

Zebra-patterns are more complicated structures, and many mechanisms have been proposed to explain them (Kuijpers, 1975; Zheleznykov and Zlotnik, 1975; Chernov, 1976; Mollwo, 1983, 1988; Winglee and Dulk, 1986; Ledenev *et al.*, 2001; Karlicky *et al.*, 2001). The majority are based on electrostatic emission at double plasma resonance (DPR):

$$\omega_{uh} = (\omega_p^2 + \omega_B^2)^{1/2} = s\omega_B \tag{17}$$

with ω_{uh} - upper hybrid frequency, ω_p -electron plasma frequency, ω_B -electron cyclotron frequency and s -integer harmonic number. The most advanced model in this category, proposed by Winglee and Dulk (1986), is based on cyclotron non-saturated maser emission of electrostatic waves by a loss-cone electron distribution. However some difficulties remain with all these versions: the frequency separation between zebra stripes Δf_e must comprise certain portion of the electron cyclotron

frequency (depending on the relationships of the scale heights of density and magnetic field in the corona), and this is hard to reconcile with its often irregular variation with frequency; the magnetic field deduced from Δf_e seems too low for the flare region and we are faced with the difficulty of having plasma $\beta \approx (v_s/v_A)^2 \leq 1$ (a well accepted value for magnetic traps in active regions). Practically all models explain only stripes in the emission, although the stripes are sometimes observed predominantly in the absorption. An important property of distribution with the loss-cone was missed in all models: it generates also whistlers, and interaction of whistlers with the fast particles changes radically the velocity distribution function, when the transverse anisotropy decreases, but a beam on the longitudinal velocities appears.

Probably, the noted difficulties always stimulated the new authors to the search for other mechanisms. For example, Fomichev and Fainshtein (1981) proposed the generation of zebra pattern due to the excitation of nonlinear ion-sound waves and their scattering on fast particles.

3.3.1. *Electrostatic Waves Perpendicular to the Magnetic Field*

For the description of double plasma resonance (DPR)-model we will address to the primary sources of the theory of kinetic excitation of electrostatic plasma waves in the solar corona (Zheleznyakov and Zlotnik, 1975a) and on the motion of account we will note the subsequent specifications and additions of the different authors. For the brevity of account we will not repeat long computations, requiring detailed descriptions and appendixes, which exist in the original papers.

If we assume that the density of non-equilibrium electrons is small compared to background plasma and if the wave length is much smaller than the gyroradius of thermal electrons (a parameter $\lambda = \frac{k_{\perp}^2 v_T^2}{\omega_B^2}$, where k_{\perp} is the transverse component of the wave vector \mathbf{k} , v_T is the thermal velocity), that the dispersion properties of the waves are determined by the equilibrium component and can be described by well-known equations (the equation (2.5) in Zheleznyakov and Zlotnik (1975a)):

$$\epsilon_{\parallel}^0 = 1 - \frac{\omega_p^2}{\omega^2 - \omega_B^2} - \frac{3\omega_p^2 \omega_B^2 \lambda}{(\omega^2 - 4\omega_B^2)(\omega^2 - \omega_B^2)} - \frac{\omega_p^2}{\omega^2 - s^2 \omega_B^2} \frac{s}{(s-1)} \left(\frac{\lambda}{2}\right)^{s-1} = 0, \quad (18)$$

(s is the harmonic number). Equation (18) has solutions at the frequencies close to the cyclotron harmonics $s\omega_B$ (the so-called Bernstein modes):

$$\omega^2 - s^2 \omega_B^2 = \frac{\omega_p^2 \omega_B^2}{[(s^2 - 1)\omega_B^2 - \omega_p^2]} \frac{s(s+1)}{(s-2)!} \left(\frac{\lambda}{2}\right)^{s-1} \quad (19)$$

and close to the upper hybrid resonance frequency ω_{uh} :

$$\omega^2 = \omega_{uh}^2 + 3\lambda \omega_B^2 = \omega_{uh}^2 + 3k_{\perp}^2 v_T^2. \quad (20)$$

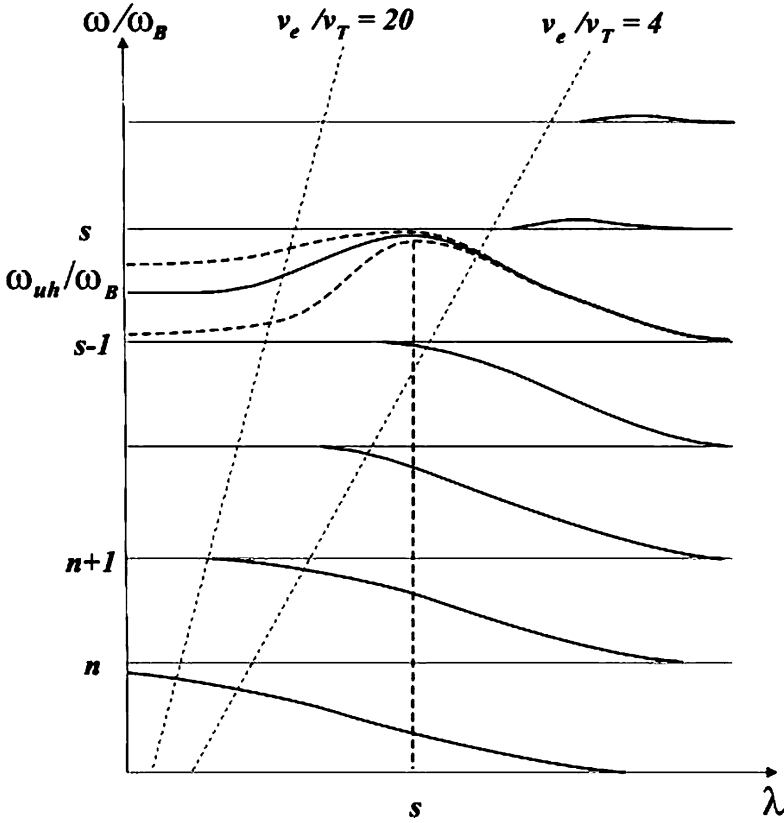


Figure 59. Qualitative dispersion curves for Bernstein modes and plasma waves at the frequency of upper hybrid resonance. Straight lines mark the instability boundaries for two ratios of velocities v_e/v_T (from Zlotnik *et al.*, 2003).

The dispersion curves $\omega(\lambda)$ for the ratio $\omega_{uh}/\omega_B = 15$ are shown in Figure 59.

The Bernstein modes have anomalous dispersion passing from one harmonic to the other. A qualitative difference is present for the plasma waves in the vicinity of the hybrid frequency at $\lambda < s$: they have normal dispersion. Three curves inside the hybrid band correspond to different location of ω_{uh} within the given interval. The curves in Figure 59 at $\lambda \ll 1$ show that the dispersion relation (20) is valid only inside the hybrid band $(s - 1)\omega_B < \omega < s\omega_B$ determined by $s \simeq \omega_{uh}/\omega_B$. It cannot be extended to the adjacent band to the hybrid band from above, as done by Winglee and Dulk (1986). Zlotnik *et al.* (2003) affirm that Winglee and Dulk (1986) neglected the resonance term in (18). This remark should shake (or reject) the subsequent statements of Winglee and Dulk (1986) about an opportunity of contributions from various harmonics to the emission at a fixed frequency as well as the numerical result of growth rates, represented in Figure 2 in Winglee and Dulk (1986): flat “piling” of 17 harmonics.

In Appendix B in Zlotnik *et al.* (2003) the calculation of growth rates for DPR instability is specified for non-relativistic case important for ZP. Zlotnik *et al.* (2003) consider the distribution function of fast electrons in the DGH form (Dory *et al.*, 1965) without a loss-cone:

$$f(v_{\parallel}, v_{\perp}) = \frac{v_{\perp}^2 c^3}{4\pi \sqrt{2\pi} v_e^5} \exp\left(-\frac{v_{\parallel}^2 + v_{\perp}^2}{2v_e^2}\right), \quad (21)$$

where v_{\parallel} and v_{\perp} are the longitudinal and transverse components of electron velocity \mathbf{v} relative to the magnetic field. The DGH distribution function (sometimes named as ring distribution) is too specific, in the sense that the maximal instability develops only for a strictly fixed velocity of fast electrons which sharply limits the possibilities of its use. ZP is usually observed in the post flare phase, when the energy particles manage repeatedly to be reflected from magnetic mirrors, as a result of which the loss-cone distribution is formed. Winglee and Dulk (1986) examine both these distributions in a comparative aspect, in order to show, what distribution and with what velocities can excite the isolated harmonics, not being merged together into the continuum. Zlotnik *et al.* (2003) repeat all calculations of the growth rates from Zheleznyakov and Zlotnik (1975a), in order to precise the instability limits and to respond on some remarks of Winglee and Dulk (1986).

The growth rate of longitudinal waves (γ) is determined only by the nonequilibrium fast electrons (when a small addition of fast particles does not change the dispersive properties of plasma: $\gamma \ll \omega$) and is given by

$$\gamma = \text{Im } \omega \approx -\frac{\text{Im } \epsilon_{\parallel}^{(1)}}{[\partial \epsilon_{\parallel}^{(0)} / \partial \omega]_{\epsilon_{\parallel}^{(0)}=0}}, \quad (22)$$

where $\epsilon_{\parallel}^{(1)}$ is the antihermitian part of the dielectric tensor. For positive γ the value $\text{Im } \epsilon_{\parallel}^{(1)}$ should be negative which defines the instability boundaries: $\lambda > \lambda_{cr} \approx (sv_T/v_e)^2$, shown in Figure 59 by dotted lines. A strong instability is realized at sufficiently great velocities v_e , when the instability boundary is located in the region of normal dispersion ($\lambda_{cr} < s$). Zlotnik *et al.* (2003) emphasized that the Doppler shift (the value $k_{\parallel} v_{\parallel}$ in the resonance term in $\epsilon_{\parallel}^{(1)}$) was taken into account as necessary condition of such an instability in contrast of the statement of Winglee and Dulk (1986), that Doppler shift was neglected by Zheleznyakov and Zlotnik (1975a).

In Appendix B of Zlotnik *et al.* (2003) it was confirmed the following peak growth rate of upper hybrid waves in the hybrid band for $v_e/v_T = 20$ and $\omega_p/\omega_B = 15$: $\gamma_{\max} \sim \omega_B(N_e/N_o)$. This value is one to two orders of magnitude greater than the growth rate of Bernstein modes. However the estimation of the relative frequency bandwidth of the excited waves

$$\delta\omega/\omega_B \sim (3/2s)(v_T^2/v_e^2) \quad (23)$$

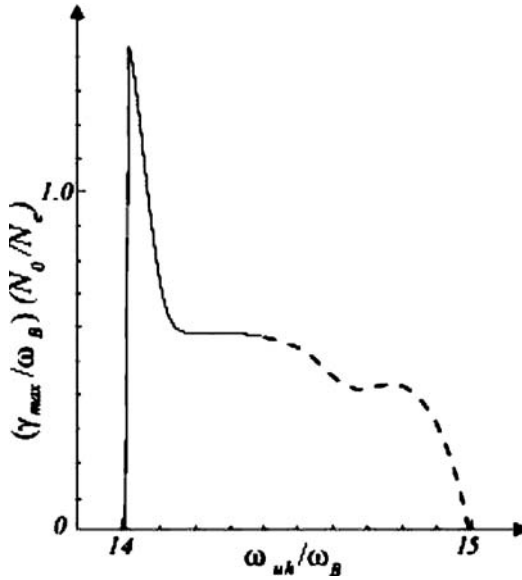


Figure 60. The dependence of maximum growth rate on the position of ω inside the hybrid band (from Zlotnik *et al.*, 2003).

for used values $s = 15$ and $v_T/v_e = 1/20$ gives a too small unrealistic value $\delta\omega/\omega_B \sim 2.5 \times 10^{-4}$. And the reason is that at the estimation of $\Delta k_{\perp}/k_{\perp}$ (the expression B.15) the velocity dispersion $\Delta v_{\perp}/v_{\perp}$ was missed as the infinitesimal quantity. In this connection the main qualitative conclusion that the frequency interval of enhanced generation is much less than ω_B (represented in Figure 60) causes the doubt. Such a behavior of increment will be correct only for a distribution being peaked at large pitch angles and with the velocity dispersion $\Delta v_{\perp}/v_{\perp} \ll 1$.

This remark is confirmed by new calculations carried out by Yasnov and Karlicky (2004) for the same distribution function of (21). The growth rate of the upper hybrid waves was computed for different velocities of fast electrons considering a finite temperature of the background plasma and relativistic corrections. One of examples of calculation is shown in Figure 61 for $s = 6$. We see a noticeable maximum of γ only for greater velocities $v = 0.3-0.5 c$, but the bandwidth of the maximum occupies more than a half of ω_B and its value decreases on more than one order. The maximum of the growth rate appears only on harmonics $s = 5-10$. According to results of Stepanov *et al.* (1999) the frequency interval of plasma wave excited in the DPR conditions occupies also about 0.3–0.5 part of the distance ω_B between the adjacent harmonics.

In such a case a problem arises with the overlapping of harmonics. The frequency bandwidth $\Delta f/f_B$ of γ should be less than the frequency separation between harmonics which depends on the relative relationship of the height scales in the corona of the density $L_n = 2n(dn/dh)^{-1}$ and the magnetic field $L_B = B(dB/dh)^{-1}$

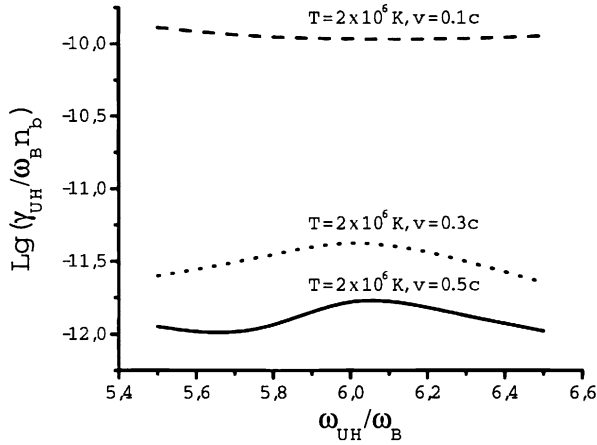


Figure 61. The growth rate of the upper hybrid waves for the harmonic number $s = 6$ and different temperature and velocities of fast particles (from Yasnov and Karlicky, 2004).

(Winglee and Dulk, 1986; Zlotnik *et al.*, 2003):

$$\delta f/f_B < L_B/(L_n - L_B). \quad (24)$$

For realization of DPR-levels it is required, that the height scales would noticeably differ, and usually $L_n \gg L_B$ (the magnetic field changes with height faster than the electron density). However if even $L_n/L_B = 4$, we obtain the values $\Delta f/f_B$ and $\delta f/f_B$ of one order, thus harmonics will merge into a continuum emission. Taking into account the given above valid remarks of Zlotnik *et al.* (2003) it should be nevertheless recognized to be accurate with the basic conclusion of Winglee and Dulk (1986): in most cases the emitted harmonics overlap in the continuum radiation and zebra stripes can appear only if the maser instability is not at saturation, if the fast electrons have a loss-cone distribution and their velocities are close to $0.1 c$. This result seems natural, if we will compare resonance curves on both distribution functions, DGH and loss-cone distribution, represented in Figure 62: the resonance curve in the loss-cone distribution is located at the maximum of distribution near loss-cone with the lower perpendicular velocities, and on DGH – with the higher velocities without the maximum of distribution, that will require the higher concentrations of non-equilibrium particles.

Mollwo (1983, 1988) explained smooth changes of frequency drift by a movement of fronts of fast particles at various angles to the magnetic force lines. Thus, a certain restriction is imposed for the cross-section size of these fronts, so that the stripes are not merged into the continuum.

Up to now two versions of the radiation source of cyclotron waves are allowed for the explanation ZP: the first version is the excitation due to the kinetic cyclotron instability in a small-size source of Bernstein modes (Figure 63a). Such a scheme is apparently responsible for quasi-equidistant on frequency ZP stripes. The second

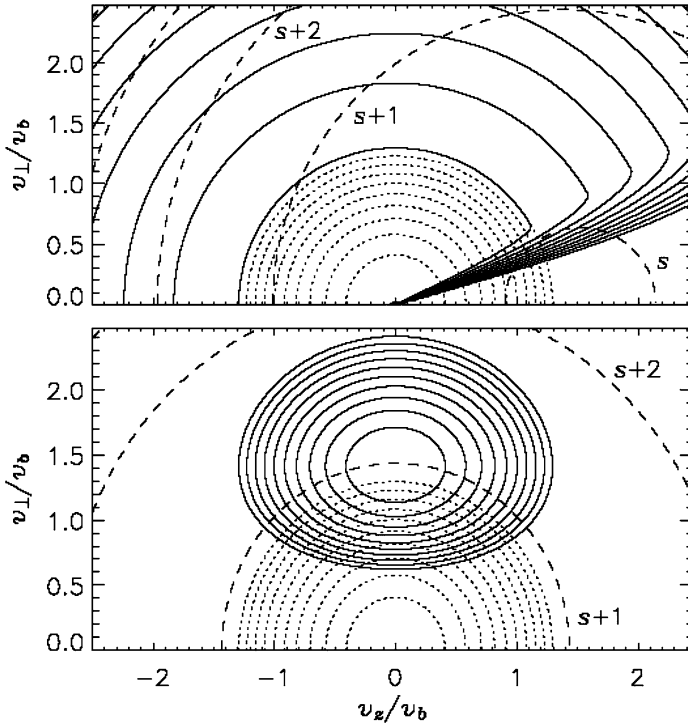


Figure 62. Distribution functions of fast electrons with loss-cone (*top*) and DGH (ring) type (*bottom*). The dashed lines show the resonance curves corresponding to the maximal growth rate for Bernstein modes with frequency $s\omega_B < \omega < (s + 1)\omega_B$. The dotted contours show the distribution of background plasma electrons (from Kuznetsov, 2005).

and more common version is the generation in a distributed source in the magnetic flux tube filled with hot electrons. Here the emission stripes are formed at the levels of DPR in the different regions of the source (Figure 63b). In this case ZP stripes may be of essentially non-equidistant character.

Independently and almost simultaneously Kuijpers (1975a,b) suggested one of the possibility of ZP generation. His model coincides with Zhelnyakov and Zlotnik (1975c) model of the distributed source: excitation of cyclotron waves takes place in the region of DPR. However Kuijpers (1975) considers the hydrodynamic instability. His model permits to explain in a unified way the origin of the background continuum and zebra stripes. The background generates in regions between the levels $\omega_{uh} = s\omega_B$ and the enhanced emission of zebra stripes emerges from these discrete levels. A version of the hydrodynamic instability was also developed by Berney and Benz (1978).

The hydrodynamic instability seems rather attractive to explain the ZP (due to the high increment). However, as Zlotnik (1979) shown, for the hydrodynamic approximation to be valid, it is necessary that in solving the dispersion equation in

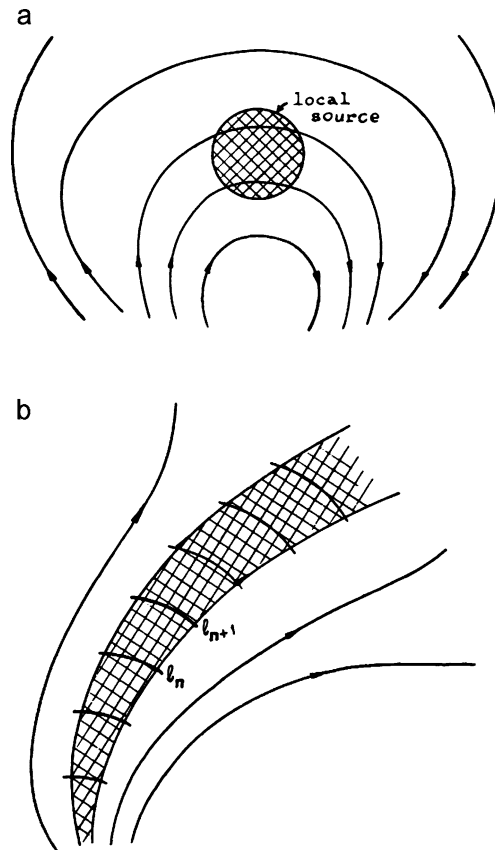


Figure 63. (a)- Model of the local source localized at the apex of magnetic trap. (b)- Model of the distributed source extended along of flux tube (from Zheleznykov and Zlotnik, 1975b).

the integral which determines the imaginary part of the dielectric permittivity one could neglect the pole in the denominator of the integrand. Physically, this means that all non-equilibrium electrons interact similarly with a wave and in this sense the distribution function may be replaced by δ -function. Then, Zlotnik (1979) obtains the applicability limits of hydrodynamic approximation: $|\omega - s\omega_B| \gg v_e^2 s \omega_B / 2c^2$. It is seen from this inequality that for weakly-relativistic electrons the number of observable harmonics cannot be greater than ten, since for large s the mistuning $|\omega - s\omega_B|$ exceeds the distance ω_B between the harmonics. Moreover, even at low harmonics the hydrodynamic instability is unlikely excited under coronal conditions, because it is realized with impossibly large values of the hot electrons density $n_h \gg 0.05n_o$.

The kinetic instability has no density threshold to occur, and under conditions in the coronal magnetic trap it is realized at rather low densities: $n_h \geq 10^{-6}n_o$. And one more argument in favor of the kinetic instability in the double resonance

region: it gives a possibility to explain absorption stripes near low frequencies of emission stripes. It is this frequency dependence which the kinetic increment has for cyclotron waves in the hybrid band in the normal dispersion region (Figure 4 in Zheleznyakov and Zlotnik (1975a)). In the hydrodynamic approximation the dispersion equation has purely real solution in that parameter region where the instability does not exist, and the absorption stripes cannot be explained.

The same argument is offered by Zlotnik (1979) not in favor of model suggested by Fedorenko (1975), according to which the ZP appears in a point source due to the kinetic instability of Bernstein modes at the harmonics above the hybrid band. In this frequency region Bernstein modes are closely adjacent the harmonics themselves (in a narrow part of the interval ω_B , (Figure 59)) where one may obtain only the amplification band. Besides, additional calculations show that the increments of Bernstein modes at the harmonics above the hybrid band are rather small. They are less by an order of magnitude than the increments under the hybrid band and by several orders less than the increments of plasma waves in the double resonance region in the hybrid band.

3.3.2. *The Role of the Relativistic Effects*

Zheleznyakov and Zlotnik (1975a) considered also the role of relativistic electrons (the velocity dependence of electron mass) in the kinetic instability of cyclotron waves in plasma and possible manifestation of this effect in the occurrence of the so-called “tadpoles” (Figure 18) in ZP (Zheleznyakov and Zlotnik, 1975b).

The relativistic effects are most important for the waves propagating perpendicularly to the magnetic field. This is easily seen from the Doppler resonance condition:

$$m\omega - sm_o\omega_B - k_{\parallel}mv_{\parallel} = 0 \quad (25)$$

which determines the interaction between particles and a wave. Really, for $k_{\parallel} = 0$ the bunching and re-distribution of particles affected by the wave field may be only due to the velocity dependence of mass. For Bernstein modes with anomalous dispersion the electrons with comparatively small velocities ($v_e/c \lesssim 0.1$) perpendicular to the magnetic field excite the waves in the narrow frequency interval $\Delta\omega \simeq s\omega_B v_o^2/c^2$, where for the inclined waves the absorption takes place. The maximal relativistic increment amounts to a value

$$\gamma_{\max} = 10^{-3}\omega_B n_h/n_o, \quad (26)$$

which about one order less than for inclined waves, however in both cases the space amplification coefficients ($\mu = \gamma/v_{gr}$) can be comparable.

For Bernstein modes at the frequencies $\omega < \omega_{uh}$ (with anomalous dispersion) the absorption stripe is at the higher frequencies. It is this relative position of the frequency intervals of amplification and absorption takes place for “tadpoles”, and it was the reason to use Bernstein modes with anomalous dispersion for interpreting its frequency spectrum with emitting tail, absorption body and bright eye. The

relativistic amplification interval is situated in a place where the inclined waves are absorbed. In such a way a relativistic eye appears on the high frequency part of the absorption body (Zheleznyakov and Zlotnik, 1975b).

Thus, the relative position of absorption and amplification stripes in the ZP may serve as an indicator what model – point source with Bernstein modes or distributed source with plasma waves at DPR frequencies – is responsible for the origin of ZP.

In this connection, we could however mention, that in some events we observed simultaneously different positions of the absorption relatively the amplification (Figure 22), moreover this position could change during one interval of ZP.

And else a doubt arises with a such statement, when we see in Figure 18 some “tadpoles” almost simultaneously with eye and without it though the relativistic effect should be always present, then may be there are not Bernstein modes which are responsible for the appearance of the “tadpoles”. In other events an isolated “tadpole” appear sometimes in the interval of the non-stationary ZP (Figure 19).

3.3.3. Polarization

The longitudinal cyclotron waves cannot escape outside the corona therefore one of the main processes is the conversion (coalescence) of plasma waves into the electromagnetic radiation. According to observations the polarization of ZP can be as very weak as well as very strong and in both polarization modes, but more often in ordinary mode than extraordinary.

The polarization is defined by escaping conditions and for cyclotron plasma wave was considered by Zlotnik (1977). The radio emission at the second harmonic due to the combinational scattering of plasma waves on each other may appear to be considerably stronger than the fundamental occurred as a result of spontaneous scattering by thermal ions. Then one can hardly expect the emission with a marked polarization since the condition of escaping at the frequency $\omega \simeq 2\omega_p$ are practically the same for ordinary and extraordinary waves.

Another situation will be in the case when the level of excited plasma waves is sufficiently high and the efficiency of conversion into the radio emission of the fundamental is determined by induced process rather than spontaneous one. Then the emission at the fundamental may be stronger than at the second harmonic and we may expect the radio emission with a considerable polarization.

The problem of the induced scattering in plasma wave source in the corona was clarified by Zaitsev (1975). In particular he obtained the critical value W_l^{cr} of the energy density of plasma waves above which the processes of induced scattering are essential. A re-calculation of the criterium obtained under the conditions typical for ZP generation region leads to the estimation $W_l^{cr} \sim 10^{-8}$ erg cm⁻³. For the comparison, one can estimate the plasma wave level from the observed radio emission intensity and from the known formula for the possibility of the combinational plasma wave scattering in the DPR conditions. For example, for the typical value of the emission flux density $f_\omega \sim 4 \times 10^{-17}$ erg s⁻¹ cm⁻² Hz⁻¹ (observed

in the March 2, 1970 event (Slottje, 1972)) the necessary energy density has to amount to $W_l \sim 2 \times 10^{-7} \text{ erg cm}^{-3}$. This value is close to W_l^{cr} , that means that depending on specific conditions in the ZP source the plasma wave scattering may be both spontaneous and induced process. Accordingly, we can observe mainly the unpolarized emission at the second harmonic or the fundamental emission with essential polarization with the sign of the ordinary mode.

As the point source model when the electromagnetic radiation occurs as a result of coalescence of Bernstein modes with plasma waves at the hybrid frequency $\omega = \omega_{uh} + s\omega_B$, the situation there is nearly the same. A detailed analysis of this process of conversion (Zlotnik, 1976) shows that the intensity of the radio emission is proportional to $(1 \mp \cos\theta)^2$, where θ is the angle between the wave vector of electromagnetic wave and the magnetic field, the signs ‘-’ and ‘+’ correspond to extraordinary and ordinary modes. The circular polarization degree is determined by the relation

$$p_c = \frac{2 \cos \theta}{1 + \cos^2 \theta}, \quad (27)$$

and depending on the angle θ changes from zero to unity (of the ordinary mode). In Chiuderi *et al.* (1973) an incorrect conclusion was made that the resultant electromagnetic radiation is unpolarized since they did not take into account a weak non-longitudinality of Bernstein modes. The dependence of polarization in accordance with the formula (27) should be reflected in the decrease of polarization degree with an increase in the source heliolongitude. However, in the observations the strong polarization was sometimes recorded in the limb events.

Thus, both models of ZP generation (of distributed and point source) may provide the appearance of both unpolarized and circularly polarized radio emission. However the increments of the upper-hybrid waves exceed significantly increments of Bernstein modes (by one-two orders of magnitude) therefore from all possible combinations of waves two main nonlinear coupling remain as the most probable to explain ZP: (1) the generation of plasma waves in a distributed nonuniform source, at levels of DPR with the escaping ordinary mode; (2) the generation of Bernstein modes in a point-like source and the coupling process ($\omega = s_1\omega_B + s_2\omega_B$) with the escaping extraordinary mode (Mollwo and Sauer, 1977; Willes, 1999).

In spite of fact, that the increments of Bernstein modes are considerably less, than for the plasma waves, Altyntsev *et al.* (2005), Kuznetsov (2005) utilizes precisely Bernstein modes for interpretation of ZP, although the distribution function is selected with a large limitation on the particle energy. In any cases Kuznetsov (2005) calculated more detailed dependence of the growth rates of Bernstein modes on frequency (with a fast decrease after $s = 10$), and he shown effectiveness of the nonlinear coupling of modes between themselves. There are a very weak flux (1.5 s.f.u.) against the background (20 s.f.u. at 5.7 GHz in discussed event of January 5, 2003), the defined extraordinary wave mode and the same space positions of radio sources of all zebra stripes which remain certain positive arguments in favor of this model.

In a number of last works the DPR mechanism continues to be improved. Ledenev *et al.* (2001) have chosen a scale of heights of a magnetic field much less than the scale of heights of plasma density. They have assumed that radiation originates in the second harmonic of f_{uh} and they have determined higher values of magnetic field strength B (comparable with values from Chernov *et al.* (2001b) in models with whistlers). However, ZP is usually strongly polarized and very seldom has moderate polarization, suggesting radiation in the fundamental frequency. Thus values (B) appear overestimated by more than twofold as the number of harmonics s is arbitrarily chosen. In Sawant *et al.* (2002) for the first time the fragment of ZP on harmonic frequencies (1700 and 3400 MHz) is discussed; such a trend was predicted in the model of Ledenev *et al.* (2001). However in the absence of information on polarization and also in the absence of any conformity of zebra-stripes at harmonic frequencies, a certain doubt remains about the reality of harmonic structure.

For braided zebra (or lace bursts) Karlicky *et al.* (2001) proposed a version of DPR mechanism for flare plasma, when the radio source is considered to be in a turbulent state. Authors for the first time assume, that the different zebra lace lines can be generated in different magnetic flux tubes.

3.4. DETAILED EXAMINATION OF THE RECENT MODELS OF ZP AT DPR

We are forced to examine in more detail interpretation of ZP in the event October 25, 1994, since below an alternative interpretation of this event will be presented.

In two papers, Aurass *et al.* (2003) (I. Observations) and Zlotnik *et al.* (2003) (II. Source model, theory), the DPR mechanism was used for the interpretation of the short type IV burst with ZP that occurred on October 25, 1994. In the first article, the results of the force-free extrapolated magnetic field of AR 7792 in the corona are presented. The extrapolated magnetic force line starting from the head spot and used in paper II is not connected to the radio source of ZP, since the positions of the fine structure radio sources are far to the NE of AR 7792.

The authors of paper II do not address the conclusion of paper I (at the end of section 3.2.2.) that particle acceleration took place most likely above the NE part of the loop LS1, instead of the SW part. The statement about the position of particle acceleration in the SW part of the loop LS1, made in II, contradicts Figure 5 in (I) where it is shown that the radio sources of type III bursts at 164 MHz are far to the NE of the bright area in which the main flare took place. The positions of radio sources of type III bursts and ZP coincided, therefore particles responsible for type III bursts should move upwards on the NE part of the loop LS1 and those responsible for ZP should move downwards in the same part of the loop.

In paper II, the opposite problem is solved: using multiple crossings of the calculated cyclotron harmonics with the fixed frequencies of ZP stripes (at a fixed time point) a dependence $f_p(h)$ is constructed (Figure 5). The authors have considered

an arbitrary selected force line in the center of the coronal loop LS1. They assert that the electron density over height follows a barometric law.

From Figure 5 in paper II it is visible that for the extrapolated magnetic force line the cyclotron frequency drops approximately 4 times faster than the plasma frequency (for example, for the gyroharmonic number $s = 15$). More precisely, the scale height for the magnetic field $L_B = B(dB/dh)^{-1}$ appears to be 4 times lower than the scale height for the electron density $L_n = 2n(dn/dh)^{-1}$. Thus, these relations satisfy a condition for realization of DPR with a large number of harmonics $L_n/L_B \gg 1$. However, it does not satisfy a condition for the separation of zebra stripes on the continuum background, namely $\delta f/f_B < L_B/(L_n - L_B)$, at least for the nonrelativistic case.

In Appendix A, B of paper II the main formulae for the theory of growth rates for DPR instability are presented with some newer details than Zheleznyakov and Zlotnik (1975a) and Zheleznyakov (1995). In particular, these authors voice two objections, relating to Winglee and Dulk (1986). First, the dispersive curves of longitudinal electrostatic waves at the frequency of DPR (shown in Figure A1 in II) $\omega^2 = \omega_{uh}^2 + 3k_{\perp}^2 v_T^2$ are valid only inside the hybrid band. This cannot be extended to the band adjacent to the hybrid band from above, as done by Winglee and Dulk (1986).

Furthermore, in the footnote of Appendix A (in II) it is noted that Winglee and Dulk (1986) considered only the first order of the small parameters $k^2 v_T^2 / \omega^2$ in the “thermal” dielectric tensor. That corresponds to neglecting the important resonance term. However, they do not discuss to what inaccuracies this leads in the final analysis. Thus, the main result, represented in Figure 2 in Winglee and Dulk (1986) is inaccurate: a piling or comb of harmonics cannot be equal in intensity for $s = 6-20$.

However, in II, all formulae for similar estimations (after (B.7)) show only the qualitative behavior of the growth rate of upper hybrid waves in DPR conditions. If we choose (in more detail) the optimal value of the wave number k^{opt} (where the growth rates are maximal) for the velocity of fast particles $v_e \approx 5 \times 10^9$ cm s⁻¹ and if we take into account the velocity dispersion $\Delta v_e / v_e \approx 1$ we obtain the relative bandwidth of the maximum growth rate inside the hybrid band $\delta f / f_B$ approximately equal to the frequency separation between stripes $\Delta f / f_B \approx L_B / (L_n - L_B) \approx 0.3$. According Stepanov *et al.* (1999), the frequency interval of a plasma wave excited in DPR conditions also occupies about 0.3–0.5 of the distance ω_B between the adjacent harmonics. The value of $\delta f / f_B \approx 1/10$ (see Figure 60) is obtained only for an unrealistically narrow velocity dispersion $\Delta v / v \ll 1$, since in the expression (B15) the term $\Delta v / v$ is omitted (i.e. as the infinitesimal).

Thus, for the calculated magnetic force line, the ZP stripes in Figure 5 (in II) should merge in a continuum, and the plotting of the dependence $f_p(h)$ becomes almost arbitrary. The authors of II discuss merging of zebra-stripes in a continuum (in Section 4.2.), but do not check this condition further in the construction of Figure 5.

Therefore the explanation of frequency drift of stripes due to a change of magnetic field and temperature cannot be accurate. The barometric formula: $f_p = f_{p0} \exp(-h/10^4 T)$ (the formula (10) in II) is written by analogy to formula (3.9) in Priest (1982) for constant temperature, thus it is impossible to define from it a change of T . The real dependence on T is given by the much more complex expression (3.8) in Priest (1982). Heating and cooling of plasma are slow processes (in the coronal loop they last some minutes), therefore it is impossible to explain a change of frequency drift of stripes on time intervals of less than 1 second by these processes. The authors in II have obtained an underestimated electron concentration of almost two orders relative to any other model ($f_{p0} = 234$ MHz for $h = 0$), and the footnote on this account (that in the base of a corona other temperatures could exist) only aggravates this question, since the local parameters will not be coordinated with the global parameters for the entire corona. The authors were forced to make this assumption because of the unrealistically calculated magnetic force line.

Thus, it was necessary to determine to what other density distributions the fitting corresponds better (for example, to the Newkirk model). If it is possible to choose any force line and to vary s , this method is not suitable for the solution of such a problem.

Smooth changes of frequency drift are explained by a movement of fronts of fast particles at various angles to the magnetic force lines (Mollwo, 1983, 1988). Thus, a certain restriction is imposed for the cross-section size of these fronts, so that the stripes are not merged into the continuum.

In the recent paper devoted to perfection of the DPR model of Yasnov and Karlicky (2004), the calculations of the growth rates of the upper hybrid waves are carried out for various velocities of fast particles and various temperatures of the background plasma. From Figure 61, it is seen that the large width of the maximum of the growth rates does not satisfy the same condition $\delta f/f_B < L_B/(L_n - L_B)$, so that the zebra-stripes would not merge in the continuum.

In II the question of real absorption of the background continuum in dark ZP stripes is in no way discussed, although Zheleznyakov and Zlotnik (1975a,b) relate absorptions to the negative relativistic growth rates of cyclotron waves in the hybrid band at the low frequency edge of the positive growth rates. Winglee and Dulk (1986) do not discuss this at all due to the too large differences of the scale of negative and positive increments (of about two orders). Winglee and Dulk (1986) conclude that in most cases the emitted harmonics overlap in the continuum radiation and zebra stripes can appear only if the maser instability is not at saturation, if the fast electrons have a loss-cone distribution and their velocities are close to 0.1 c .

3.5. NEW THEORIES OF ZEBRA PATTERN

In search of an elimination of the difficulty with small values of magnetic field strength in the DPR model the new theory of ZP based on the radiation mechanism

of auroral “choruses” – magnetospheric bursts observed at ground stations on frequencies of 2–4 MHz, with the fine structure similar to ZP is offered in LaBelle *et al.* (2003). It is supposed, that the Z-mode is radiated by the cyclotron maser mechanism (by the analogy with Winglee and Dulk (1986)). And though the Z-mode at the upper hybrid frequency does not escape from the source, it can be transformed in ordinary (O) mode at discrete frequencies (quasi-harmonics or eigenmodes) with the presence of density enhancements of the appropriate scales. The task is reduced to the solution of the equivalent Schrödinger equation for the Z- mode captured in a density inhomogeneity of an idealized cylindrical form. The Wentzel-Kramers-Brillouin approximation is used on the basis of the previous papers of co-authors. Harmonics will be derived due to the quantization in eikonal conditions with the leakage of the wave for appropriate quantum numbers in the eikonal conditions, azimuthal (m) and radial (n).

This complicated theory demands a some clarification of the physical sense of those numbers. With an analogy with quantum mechanics the azimuthal quantum number ‘ m ’ is a number of potential holes in a single inhomogeneity. The number ‘ m ’ defines the number of the angle modes along the coordinate ‘ r ’, and ‘ n ’ – the number of wave periods inside of the potential hole, i.e. the frequency of an eigenmode at a fixed level (the propagation is excluded in the consideration). Therefore ‘ m ’ defines the number of zebra stripes, and ‘ n ’ – the frequency separation between neighboring stripes. However, the numerical solution of dispersion Equation (12), represented on Figures 2 and 3 in LaBelle *et al.* (2003), reveals an increase of the frequency separation with the decrease of the frequency, while the observations testify about the inverse dependence.

According the estimation in LaBelle *et al.* (2003) the maximum number $m \approx \delta^{1/2}/\rho$, where the positive value $\delta < 1$ is a density increase inside the inhomogeneity, $\rho = \rho_e/L$ – the ratio of the electron gyroradius ρ_e to the size of the inhomogeneity L . Thus, bigger number of gyroradii gets in the scale of a single density enhancement bigger harmonic number m (the number of zebra stripes may approach to $m \approx 100$).

Thus generation of the Z- mode can occur in a point source at one level of the double plasma resonance ($s - \text{const} = 2$ or 3 in (17)). Main difference and advantage of this model will be, that it provides generation of the big number of harmonics (up to 100) with the small frequency separation $\Delta f_s \approx 0,01 f_{Be}$. In LaBelle *et al.* (2003) the estimations of parameters of density inhomogeneities ($\sim 20\%$) and sizes $L = 1 - 100$ m are obtained. The such density irregularities can form dispersing ion-sound waves. However authors do not discuss an important point: the time dependence of the own harmonics (dynamics of ZP), it is spoken only about a possible stability of irregularities during $\sim 10s$. The generation conditions of ion-sound waves (a main condition – exceeding of the electronic temperature above ionic one $T_e \gg T_i$), are not discussed also, which in the solar coronae is realized only in turbulent plasma with an anomalous resistance (in current layers, in fronts of shock waves) (Kaplan and Tsytovich, 1973). Besides the total picture from the

set of discontinuities (they form by extending ion-sound waves) should lead to a merging of stripes into a continuous spectrum (continuum) taking into account, that approximately 10^8 of the such point sources are required to produce the observed power of the zebra emission. The simultaneous appearance of fibers bursts on background of ZP and also the stripes in absorption remain still away from the consideration.

There is also a doubt in applicability of model LaBelle *et al.* (2003) in the meter wave range, when the length of a wave becomes of one order of size with the size of irregularities ($\lambda \sim L$), as only the opposite relation ($\lambda \ll L$) is the basic condition of applicability of geometrical optics for the writing of the eikonal conditions (the equations (4) and (5) in LaBelle *et al.* (2003)).

In this connection, we note that the zebra-structure model of LaBelle *et al.* (2003) is not able to explain the continuous transition between zebra structure and fiber bursts (shown in Figures 13 and 22), since only a stable point source is considered. It is not clear what variations of the positions of the absorption stripes should be expected in this model, or what their origin would be.

In recent paper of Ledenev *et al.* (2006) a new theory of ZP is offered: it is asserted that ZP can be formed as a result of interference between direct and reflected rays coming from a source of small size in a stratified atmosphere. The emission is generated by plasma mechanism. Full emission flux is contributed from a great number of narrow-band short-lived sources of small sizes, which are formed by plasma waves captured in density minima of background plasma fluctuations.

The formalism of geometric optics for solids (from the domain of crystal optics) adapts for obtaining of a interference pattern from the direct rays and reflected ones from the coronal heterogeneities. A doubt immediately appears about the reality of interference from the rays reflected from the heterogeneities with a smooth boundary (with a transition layer). O- and X-wave modes are reflected from the different levels in such heterogeneities (Hayes, 1985), and the necessary parallelism of rays will not be reached. The radio source should be of point-like size, of $<10^6$ cm, and the sum emission from a great number of point sources should merge into the continuum.

Barta and Karlicky (2006) have proposed an interpretation of ZP close on the subject-matter to Ledenev *et al.* (2006). They show that ZP can be the result of the transillumination of the radio waves through the regular coronal density heterogeneities or the consequence of the reflection of radio waves from such heterogeneities. The same doubts appear, connected with the direct transfer of the optical properties of the propagation of the light through the crystal grid to the radio wave propagation through the coronal heterogeneities with a smooth change in the density. Moreover the dependence of the transmission coefficient on the frequency (shown in the Figure 3 in Barta and Karlicky (2006) does not reveal an increase in the frequency separation between the peaks with the frequency.

Previously, it was counted, that the propagation of the waves through the regular heterogeneities can cause diffraction pattern, (it is possible, in the form of stripes),

passing over the Earth's surface from the East to the West (with the velocity $\approx 420 \text{ km s}^{-1}$), since the diffraction "grid" co-rotates with the corona. The first estimations of the corresponding delay (per-second scale) of peaks in the diverse observatories were made still by Pisareva (1958) and were checked by Chernov (1974). No delay of the fine structure between IZMIRAN (Moscow) and Nançay then there was discovered. The precise agreement of ZP stripes on the time and on the frequency in IZMIRAN and Potsdam is shown in the Figure 5 in Chernov *et al.* (1998). See also the precise agreement of ZP in IZMIRAN and Nançay in Figures 9 and 10.

However, excluding the ray treatment (with the interference or the diffraction), it is possible to expect, that the radio waves can enter into a resonance inside the heterogeneities of the corresponding scale, locating directly above the radio source in the flare region. This approach was realized in Laptuhov and Chernov (2006).

In contrast to Ledenev *et al.* (2006) and Barta and Karlicky (2006), Laptuhov and Chernov (2006) are obtained dispersion equations for the spectrum of the eigen frequencies of the periodic medium, which can be created in the flare plasma due to the development of thermal instability in the form of nonlinear structures. The spectrum of the eigen frequencies of such periodic in the space resonators is calculated and it is shown, that they are completely capable generate tens of zebra stripes, number of which does not depend on the relationship of plasma and gyrofrequency in the source. This can remove all difficulties in the explanation of the large number of stripes ZP and low values of magnetic field. The periodic medium is a filter of frequencies with the numerous windows of transparency, divided from each other by the zones of opacity. Number and frequency of the harmonics depends on the value of the spatial period of heterogeneities, which for the typical conditions of solar atmosphere is meters and decameters. The frequency separation between emission peaks grows with frequency, in accordance with observations.

3.6. THE GENERAL SCHEME OF FORMATION OF STRIPES IN EMISSION AND ABSORPTION IN THE MODEL WITH WHISTLERS

An important point missing in previous theories is that the loss-cone distribution generates also whistlers, which in turn affect the electron velocity distribution (Chernov, 1996).

The most essential contradiction of numerous models of the ZP based on the emission of plasma waves on the DPR consists of that, that from one side, the explanation of the dynamics of the ZP stripes should assume fast changes of the magnetic field (or density of background plasma) in time (that is improbable), and on the other hand, the weak magnetic field are obtained (calculated according to the frequency separation between the stripes), insufficient for exceeding of magnetic pressure above the kinetic one ($\beta < 1$). The dark ZP stripes indicate not the simple absence of the increased emission, but a real absorption of the background continuum emission, which is modulated by ZP. New observations on TRACE

mission showed, that the flare loops (in UV lines 171, 195 Å consist of numerous narrow non-expanding upwards loops, in which density and magnetic field are barely changed with the height (Aschwanden, 2004). The existence of double plasma resonance levels in such loops is highly improbable.

The similarity of main properties of fibers and zebra stripes allows to apply the model with whistlers for zebra-stripes: both structures represent the parallel drifting stripes in emission and in absorption. This led Chernov (1976, 1989) to propose a common interpretation for these two kinds of fine structure based on the coupling of plasma wave and whistlers, but in different conditions of the whistler instability: for fiber bursts – at the cyclotron resonance with a normal Doppler effect when whistlers propagate along the magnetic loops; for zebra-stripes – with the anomalous Doppler effect, when whistlers propagate at the different angles to the magnetic force lines (Maltseva and Chernov, 1989; Chernov *et al.*, 1998). A system of quasi-standing whistler packets is driven by a loss-cone distribution of fast electrons in the entire magnetic trap at the cyclotron resonance:

$$\omega_w - k_{\parallel} v_{\parallel} - s\omega_{Be} = 0 \quad (28)$$

with $s = +1$ (the normal Doppler effect) or $s = -1$ (the anomalous Doppler effect) depending on the form of the distribution function (Maltseva and Chernov, 1989), k_{\parallel} , v_{\parallel} being the whistler wave number and fast electron velocity, both parallel to the magnetic field, ω_w - whistler wave frequency.

However, it paid little attention itself to a question of the whistler excitation in the solar corona. After Kuijpers (1975) only Berney and Benz (1978) showed the importance of examination under the solar conditions of the whistler instability in comparison with high frequency electrostatic waves. Then Sharma and Vlahos (1984) showed clearly in their calculations, that the whistler growth rates due to the loss-cone instability is higher than for upper hybrid waves.

It is important at once to note, that all previous calculations of the whistler instability are carried out by an analogy with the magnetospheric whistlers only for the longitudinal propagation at the normal Doppler effect (Kuijpers, 1975, Berney and Benz, 1978). The quasi-linear problem of the behavior of whistlers is not yet solved fully. Some special cases have been only examined also for the longitudinal whistlers. So, Stepanov and Tsap (2002) have obtained estimations of quantity and spectral indexes of the trapped electrons in relation to the precipitating ones in loss-cone for the comparison with the fast particle spectra obtained according to X-ray radiation. The oblique whistlers undergo a small Landau damping and the account of whistlers, propagating under large angles to the magnetic field and exciting on the anomalous Doppler effect, changes radically the estimations of the quasi-linear effects (Chernov, 1996).

The radiation source of type IV is usually represented as a magnetic trap, therefore it is natural to assume the distribution function of fast electrons, responsible for the continuum radiation, of a type anisotropic Maxwellian one with the loss cone

and temperature anisotropy. As such cumulative distribution function is unstable also for the generation of the whistler waves it is necessary to take into account the dynamics of the cumulative distribution function due to the diffusion of fast electrons on the whistlers. We shall remark, that the generation and the propagation of the whistlers are quite possible in the narrow flare loops. The conservation laws of the processes of the coalescence $l + w \rightarrow t$ and the decay of whistlers $l \rightarrow t + w$ are examined in the monographs, Tsytovich (1970, 1977), and for the conditions of coronal plasma they are examined in the papers Kuijpers (1975), Fomichev and Fainshtein (1988), Chernov and Fomichev (1989) and in the present brief account of basic aspects of the whistler model are considered executed.

The formation of stripes in emission and absorption is the basic property of the whistlers in the such sources of of type IV radio bursts as a magnetic trap with the loss-cone distribution of the fast electrons (Chernov, 1990b). The calculations of the whistler kinetic instability have found out a very low power threshold of excitation (Malítseva and Chernov, 1989b). It has been shown there, that for the calculations of the integrated factors of the amplification of the whistlers, propagating under any angle to the magnetic field, it is necessary to take into account three basic resonances: the cyclotron resonance at normal and anomalous Doppler effects and the Cherenkov one.

The first consideration of quasi-linear systems of the equations (Jamin *et al.*, 1974) has shown, that the basic property of linear whistler instability is its periodicity in time and space. But it is very fast (millisecond) periodicity. In the conditions of the coronal plasma in a magnetic trap the time of diffusion can be much more. Besides it should be modulated by the bounce period, (the time of the movement of fast particles between the magnetic mirrors) $l_B/2v \approx 0.5$ s, where l_B – the length of a trap.

It follows from the calculations in Malítseva and Chernov (1989b), that the anisotropic electron beams depending on the degree of loss-cone and temperature anisotropy will excite whistlers, propagating towards the beam, on the normal Doppler effect, if $v_{\perp} > v_{\parallel}$ and $s = 1$ in the relationship (28). But if $v_{\perp} < v_{\parallel}$ and $s = -1$ in (28), that whistlers are excited on the anomalous resonance and propagate to the side of beam at large angles to the magnetic field.

Let us note an important role of the type of the electrons injection: if the injection is impulse, that quasi-linear effects on the normal resonance do not work (particle and wave disperse to the different sides), and on the anomalous one the role of injection grows with it's duration (or when new particles overtake wave).

During the prolonged particle injection the regime of whistlers generation should be periodic (in the time and the space), since the instability is sharply weakened with the precipitation of electrons into the loss-cone, and with the withdrawal of particles and whistlers (with the group velocity) from the region of excitation, the loss-cone instability is restored approximately through 0.2–0.3 s (Kuijpers, 1975; Bespalov and Trahtenherz, 1974). One should consider, that the particles can be scattered not only on the whistlers, but also on the electrostatic waves (Breizman, 1987; Omura

and Matsumoto, 1987), the diffusion occurring first on the electrostatic waves to the side of an increase of v_{\parallel} . Then the diffusion on the whistlers along the diffusion curves begins to work. Accordingly Breizman (1987) the relaxation length of beam, excited whistlers:

$$l^w = \Lambda \frac{c}{\omega_p} \frac{\omega_B}{\omega_p} \frac{n^c}{n^h}, \quad (29)$$

(where $\Lambda = 25$ in the solar corona). For $\omega_p = 2\pi \cdot 1.5 \cdot 10^8$ Hz, $\omega_p/\omega_B = 30$ and for a small fraction of the energetic particles relative to the background cold plasma $n^c/n^h \approx 3 \cdot 10^6$ we obtain relaxation length $l^w \approx 0.8 \cdot 10^8$ cm. The beam relaxation length on plasma waves with the same parameters and the velocity $v_{\parallel} \approx 1/3c$ occurs considerably bigger $l^l \approx 2.3 \cdot 10^9$ cm (Chernov, 1989). Thus, the relaxation on the whistlers is considerably faster and a condition to the initial angular spread of the beam is easily satisfied: $\Delta\Theta_0 > (l^w/l^l)^{1/3}$, with which the relaxation on the Langmuir waves is insignificant (Breizman, 1987).

In the time of withdrawal out from the loss-cone of the precipitating electrons (Bespalov and Trahtenherz, 1986) $T_c \approx l_B/2v \approx 0.25$ s (for the trap length of $l_B \approx 5 \cdot 10^9$ cm) whistlers at frequency $\omega^w \approx 0.1\omega_{Be}$ pass with a group velocity of $v_{gr}^w \approx 5 \cdot 10^8$ cm s⁻¹ an interval $\Delta l_B = T_c v_{gr}^w \approx 1.25 \cdot 10^8$ cm. Thus, as a result of the quasi-linear relaxation of the beam on the whistlers the entire trap will consist of zones of the maximum whistler amplification with a thickness of l^w , divided by intervals of Δl_B . In this case the periodic packets of whistlers will create regular stripes of ZP with the frequency separation $\Delta f_s \approx (l^w + \Delta l_B)\nabla f_p$. It is known, that within the framework of the doubled Newkirk density model $|\nabla f_p| \approx 1$ MHz 10^{-8} cm, and for the frequency of 150 MHz we will obtain the frequency separation $\Delta f_s \approx 2$ MHz, coinciding with that observing in the event on 25 October, 1994.

Let us note, that the excited whistler spectra are sufficiently narrow (Kuijpers, 1975), and the group velocities along the edges of this spectrum change little with the maximum at frequency $0.25 f_B$ (especially for the oblique whistlers, see. Figure 5 in Chernov (1976) and in more detail Chernov (1990b)). This fact eliminates the group scattering of the whistler wave packet in the corona inherent for the magnetospheric whistlers. The calculations of the possible trajectories of the whistler propagation in the solar corona showed, that the whistlers in the frequency band $\approx 0.05 f_B$ do not undergo any noticeable group dispersion in the propagation time ≈ 10 s (Mal'tseva and Chernov, 1989a). The whistlers can experience reflections in the regions, where their frequency approaches the frequency of the lower hybrid resonance: $f_w \approx f_{LHR} \approx f_B/43$. In the ducts with the increased density along the magnetic trap they go tightly along the duct for the entire frequency spectrum (a capture into the duct).

Thus, if the particle injection is prolonged, and a part of the trap is filled up with the periodic whistler packets (by thickness l_w along the trap), that each packet with the narrow whistler spectrum forms the stripe of zebra-structure in the emission as a result of the process of coalescence with the plasma waves at the summation frequency. The propagation of the system of such packets with the group velocity

will cause a stripe system of the ZP, drifting in the frequency in dependence of the angle between the trajectory and the levels of the identical density. Since the ratio of frequencies f_p/f_B changes little in the height interval of a radio source, giving the zebra, that the group velocities of different packets (even on the edges of the entire interval) are close in the value and in the direction, which excludes their rapid dispersion, and almost synchronous frequency drift of zebra stripes on the spectrum ensures (Mal'tseva and Chernov, 1989a).

The preferred appearance of the ZP stripes with the positive frequency drift can be connected with the excitation of the oblique whistlers on the anomalous Doppler effect in the loop apex (where $v_{\perp} < v_{\parallel}$) and with the non-ducted propagation downward to regions of the lower hybrid resonance, in which they experience reflections and then they can reach again the region at the apex with the maximum whistler instability. The propagation of the whistlers downward to the side of the growing magnetic field tension excludes the achievement of the level of the cyclotron damping (ω_w/ω_B decreases). Therefore the separate stripes of ZP are usually prolonged than fiber bursts.

The system of fibers with the preferred negative frequency drift must be connected with the excitation of whistlers on the normal Doppler effect in the base of a trap (more precise near the plug of the reflection of particles, where the distribution function has the maximum loss-cone angle). Such longitudinal whistlers are propagated along the trap to the level of the cyclotron damping (or up to reaching of absorption on the anomalous Doppler effect nearer to the loop apex).

In this model the similarity of the basic properties of fibers and ZP stripes are naturally explained (frequency bandwidth, modulation depth, polarization of the ordinary type etc.) It makes possible to explain also a sometimes observed continuous transformation of fibers into the ZP stripes and vice versa. If the whistler trajectory goes at small angle to ∇f_p (almost along the trap), we could observe fibers. When the bent trajectory reaches the trap apex, it can be almost perpendicular to ∇f_p , and we could observe the decelerating frequency drift and a transformation of the fibers into the ZP stripes, which remain sometimes almost parallel to the time axis on the spectrum.

3.6.1. *Manifestation of Quasi-Linear Diffusion on Whistlers in ZP and FB*

The complete solution of the quasi-linear problem for the three resonances with particle sources and losses is very difficult, and has not yet been obtained either analytically or numerically. Usually, a simplified problem is posed, and quasi-linear equations are solved numerically for one resonance and one oscillation mode with a loss-cone distribution function (Ossakov *et al.*, 1973; Ashour-Abdalla, 1972; Sazhin, 1987; Bespalov and Trakthenherz, 1986; Stepanov and Tsap, 2002).

Figure 64b schematically shows the shapes of the distribution function of type anisotropic beam at small, moderate and large pitch angles for three improvised moments of time in the course of the diffusion: with large v_{\parallel} at small pitch angles,

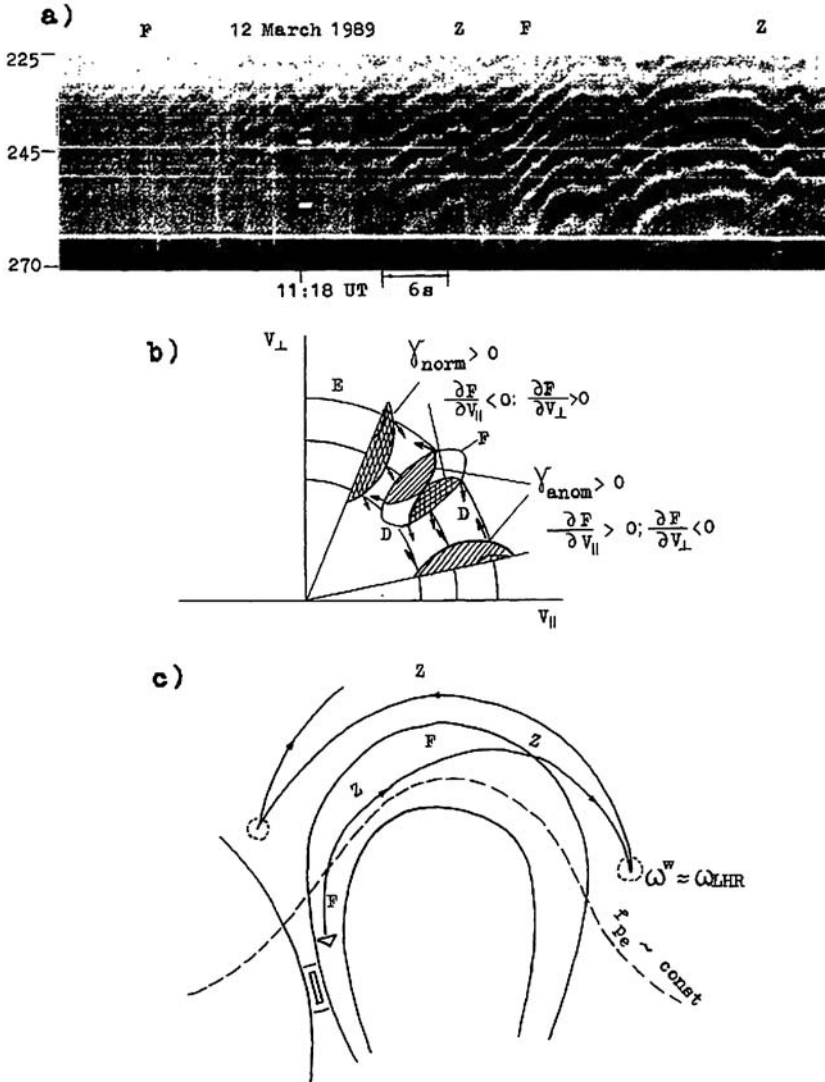


Figure 64. (a): Dynamical spectrum of ZP with wave-like frequency drift in the type IV burst of March 12, 1989. The Z, F labels above the spectrum refer to the times when zebra stripes (Z) with a constant drift toward low frequencies become similar to fibers (F). (b): Schematic presentation of the fan instability switching of whistler instability from normal Doppler cyclotron resonance (cross-hatched F regions) to anomalous resonance (single-hatched regions) due to the shift of the maximum (bump) of the distribution function F during diffusion along the diffusion curves D (arrows) from large values of v_{\perp} (where the operator $\hat{L} < 0$) to large v_{\parallel} (where $\hat{L} > 0$). (c): qualitative scheme of a whistler trajectory explaining the possibility of ZP conversion into FB and inversely (from Chernov, 1990a).

and large v_{\perp} at large angles; in an intermediate position the equal contribution of v_{\parallel} and v_{\perp} is possible.

If fast particles interact with whistlers at the cyclotron resonance (28) they move on the $(v_{\perp}, v_{\parallel})$ plane along the diffusion curves (D)

$$v_{\perp}^2 + (v_{\parallel} - \omega/k_{\parallel})^2 = \text{const}$$

in the direction of decrease of the distribution function $F(v_{\perp}, v_{\parallel})$ (Gendrin, 1981; Chernov, 1996).

Particles with the small pitch angles give their energy to the waves and they approach the loss-cone, and particles with large pitch angles increase their energy (v_{\perp}) due to the waves. However, only the part of the particles is poured out quickly into the loss-cone, directly it adjoining, and the loss-cone remains for a long time empty. Estimations of the time of life of the fast electrons with the scattering on the whistlers in the regimes of the moderate and strong diffusion give times 10–20 s (Bespalov and Trakhtenherz, 1986).

If the resulting flux of particles in velocity space is directed toward increasing particle energy, energy in the given range of velocities will be transferred from resonant waves to particles, and the wave will weaken. This physical process finds its theoretical reflection in the identity operator $\hat{\Lambda}$ (which has the meaning of a derivative along the curve D) in formulas for the whistler instability increment and the distribution function diffusion equation (Gendrin, 1981; Bespalov and Trakhtenherts, 1986):

$$\hat{\Lambda} = \frac{s\omega_B}{\omega v_{\perp}} \frac{\partial}{\partial v_{\perp}} + \frac{k_{\parallel}}{\omega} \frac{\partial}{\partial v_{\parallel}} \quad (30)$$

For positive values of the increment the operator $\hat{\Lambda}$ should be negative. In Figure 64b we show that at the normal Doppler effect the increment γ_{norm} will be positive with the derivatives $\partial F/\partial v_{\parallel} < 0$; $\partial F/\partial v_{\perp} > 0$, and at the anomalous Doppler effect γ_{norm} will be positive with $\partial F/\partial v_{\parallel} > 0$; $\partial F/\partial v_{\perp} < 0$. In the intermediate position the beam contributes in the instability at both resonances, and the parts with positive γ_{norm} are cross-hatched, and the parts with positive γ_{norm} are single-hatched.

The smooth switching of the predominant contribution from the anomalous to normal Doppler resonances (and inversely) occurs in accordance with the sign of an operator $\hat{\Lambda}$. Thus, if the entire trap is filled up with the fast particles (prolonged injection), that the continuous quasi-linear diffusion on the whistlers begins to work in a self-oscillatory regime, when it is possible a switching of the instability from the predominance of the normal Doppler resonance to the anomalous one and back (an analogy with the fan instability (Shapiro and Shevchenko, 1987) and with the spike regime in the TOKAMAK (Parail and Pogutse, 1981). Such switchings of the instability indicate smooth (or sharp) changes in the direction of the whistler group velocity, which explain the frequently observed smooth (undulating) changes in the frequency drift of the stripes or sharper jumps in the form of saw-tooth stripes, if

the distribution function is deformed by a new impulse particle injection (Chernov, 1996).

Thus, smooth changes in the frequency drift of zebra stripes and the gradual conversion of ZP into FB and vice versa, shown in Figure 64a, it is possible to explain by the precisely quasi-linear effects of scattering of fast particles on whistlers. Changes in direction of v_{gr}^w to the opposite one during the switching of resonances it is confirmed by the observations of the positions of sources. In Figure 13 it is shown that the change of the sign of the frequency drift of stripes correlates with the change of the sign of the space drift of sources at the fixed frequency. Analogous correlation was shown in Figures 10 and 16 in two other events.

Figure 64c shows the qualitative scheme of the possible prolonged propagation of whistlers in the corona for the cases, when FB and ZP can appear alternatively during ~ 1 minute, and quasi-linear effects act in the shorter time intervals. Longitudinal whistlers excited in the base of the magnetic trap by particles accelerated in the region of magnetic reconnection at the normal resonance propagate upward along the trap and give fibers (F). The excitation on the anomalous Doppler resonance at large angle to the magnetic field can predominate at the apex of trap, and whistlers propagate downward (sometimes almost parallel to the level of constant f_p) to the possible mirror points (where $\omega_w \approx \omega_{LHR}$) (in ZP the positive frequency drift predominates).

3.7. EXPLANATION OF LF ABSORPTION

The dark stripes of the ZP indicate not the simple absence of the increased emission, but the real absorption of background continuous emission, which is modulated by the ZP. One of the very obvious cases of real absorption in the ZP is given in Figure 9 (Chernov *et al.*, 1994), where the absorption of the continuum exceeded 90% according to the data of NRH at the frequency 237 MHz.

The most reliable explanation of the absorption at the low-frequency edge from the stripe in the emission is obtained, if we take into account, that in the quasi-linear diffusion time the intensity of the plasma waves (critical for the continuous emission) is reduced in the volume of the whistler wave packet due to the electron diffusion on the whistlers.

So, with the whistler excitation on the normal resonance ($v_{\perp} > v_{\parallel}$) the maximum of the distribution function is displaced almost instantly to the high longitudinal velocities (to smaller pitch angles) due to the diffusion of fast particles on the whistlers, and the instability of the plasma waves on the double plasma resonance sharply weakens, that also is exhibited in the form of the dark stripe of the zebra-structure. But if the initial diffusion on the whistlers occurs on the anomalous resonance ($v_{\perp} < v_{\parallel}$), and the plasma Langmuir waves along the field are emitted, that in this case their level will be reduced because of the turn of the beam to the high transverse velocities.

Unusual fibers (without the noticeable absorption) in the type II bursts are sometimes observed. Such fibers structure can be naturally connected with the propagation of the whistlers through the clusters of the plasma waves before the shock wave front. But before the wave front there is no trap, particles and waves disperse in the space, and diffusion on the whistlers does not work. Therefore the instability of plasma waves is not reduced in the volume of whistler wave packets and the absorption is absent.

Thus, the natural and necessary consideration of the quasi-linear effects of the diffusion of fast electrons with the loss-cone anisotropy on the whistlers allows to explain a number of the important properties of fibers and ZP.

4. Discussion of the Selected Events

4.1. FEBRUARY 17, 1992 EVENT

Besides, we can naturally explain other phenomena in Figure 15 (in the event February 17, 1992), taking into account the possibility of the whistler generation at both Doppler resonances simultaneously. When a new beam of particles is injected (new v_{\parallel}), ω_w changes suddenly according to Equation (28), and the conservation laws break down locally, but are quickly restored at nearby plasma levels with a different value of ω_l . This will result in a sudden shift of the frequency ω_l , propagating from one zebra stripe to the next one at the speed of the beam. This corresponds precisely to the observed frequency shifts (Figure 16, top panel) at drift rates similar to type III bursts.

Another consequence of the injection of a new beam (at the moment marked by first arrow under the spectrum in Figure 16) is that the velocity distribution is suddenly filled up with high velocities parallel to the magnetic field, which tend to turn on the instability on the anomalous Doppler resonance. This offers a natural explanation for the split zebra stripes as due to simultaneous whistler instability at normal and at anomalous Doppler resonances at slightly different frequencies, $\omega_{w,s=1}$ and $\omega_{w,s=-1}$ (at slightly different plasma levels). For the observed frequency splitting $(\omega_{w,s=1} - \omega_{w,s=-1})/2\pi = 2$ MHz we need $v_{\parallel,s=1} \approx 16 \cdot 10^8$ cm s⁻¹ and $v_{\parallel,s=-1} \approx 26 \cdot 10^8$ cm s⁻¹, which are quite possible velocities in the source. Additional beams with a narrow velocity dispersion (high v_{\parallel}) do not change the conditions of instability for the normal Doppler effect (high v_{\perp}). Therefore, only the high frequency component of a split zebra stripe will be structured by these beams into a succession of emission dots, in synchronization with sudden reductions (see also Figure 17). The $l + w \rightarrow t$ model thus nicely accounts for the characteristic features of zebra stripe frequency shifts and splittings, and for their occurrence at times of enhanced sudden reductions, that is in the midst of repeated injections of electron beams with high v_{\parallel} .

Interpreting zebra patterns with the (loss-cone driven) electron cyclotron maser emission theory, operating at upper-hybrid frequency at the double plasma resonance, would give an average density of $n_e = 10^9 \text{ cm}^{-3}$ and a magnetic field of $B = 2.5 \text{ G}$. Oscillations of a large magnetic loop in the sausage mode with an amplitude of 1 or 2% are sufficient to produce the temporal frequency oscillations and the band splitting of zebra patterns. But this model requires too low a magnetic field (plasma beta $\beta \approx 1$), and does not readily explain the characteristics of split stripes: at most two components and a dot-like structure for the upper-frequency component only.

4.2. DISCUSSION OF THE OCTOBER 25, 1994 EVENT

In this short-term event, the ZP radio sources were located beyond the AR (see Figure 31). A detailed analysis of Yohkoh/SXT images in Manoharan *et al.* (1996) showed that an additional brightenings outside the main flare region was caused by the magnetic reconnection of the main flare loop with the upper loops that previously existed in the corona.

The frequency width of the ZP band is presumably determined by the distance between the X-point of magnetic reconnection above the flare loop and a point lying higher in the corona (in the shear region between the ascending flare loop and large transequatorial loops that are seen in Yohkoh/SXT images). An argument in favor of this assumption is that the low-frequency boundary of the ZP coincided with the frequency at which the drift of type III bursts terminated after 10:08:35 UT (see Figure 31). The ZP source at a frequency of 164 MHz drifted southward, i.e., in the direction opposite to the drift of the sources of type III bursts.

Taking into account the above assumption, this indicates that the fast electron beams accelerated in the lower lying current sheet (it is these beams that are responsible for periodic type III bursts) are reflected from the region with a magnetic shear. The loss-cone velocity distribution of the reflected particles leads to the generation of plasma waves and whistlers, whose interaction produces a ZP at corresponding frequencies. The fact that the direction of the spatial drift of the ZP source and the sign of the frequency drift change simultaneously indicates that the spatial drift at a fixed frequency is not an actual shift of the source, but rather a displacement of the energy maximum in the vertical direction within a finite-size plasma region that radiates at this frequency (due to the velocity spread of the fast particles) and also along a surface of equal density. Within the adopted whistler model, such a drift is quite realistic.

The excitation of whistlers by the reflected particles (which have a loss-cone velocity distribution) should occur at the anomalous Doppler resonance, at which the particles and waves propagate in the same direction. A positive frequency drift of the ZP stripes indicates that, in this case, whistlers propagate downward. Quasilinear scattering of whistlers by fast particles deforms the electron distribution function:

the longitudinal velocities decrease, whereas the transverse anisotropy increases. As a result, the excitation of whistlers switches to the normal Doppler resonance, at which the particles and waves propagate in different directions, and whistlers began to propagate upward. The switching occurs at the instants at which the ZP frequency drift changes its sign and the ZP source begins to drift in the opposite direction. Two such instants are marked in Figure 32 by light vertical lines.

Even greater shifts of the source center occur at the instants corresponding to the boundaries of the ZP absorption stripes. In this case, an angular shift of $\sim 4.8'$ over $1/3$ s (e.g., within the time interval 10:08:41.3–10:08:41.7 UT), which formally corresponds to velocities exceeding the speed of light, cannot be associated with the actual motion of particles. Such a fast angular shift is actually related to the switching of the source image to the maximum of the emission continuum, which indeed corresponds to an angular shift of more than $4'$ in the south-west direction above the maximum of the SXR burst (see Figure 31).

Thus, although the centers of the sources of the ZP and type III bursts almost coincide, the emission is produced by different particles moving in different directions: for type III bursts, these are particle beams propagating from the acceleration region, which is the highest part of the burst current sheet (the height of this region corresponds to $f_p \approx 450$ MHz), whereas for the ZP, these are the particles reflected from the region with a magnetic shear (at the height that corresponds to the minimal frequency of type III bursts and where $f_p \approx 125$ MHz). A new abrupt perturbation, which partially stops the frequency drift of type III bursts at 10:07:37–10:07:58 UT, indicates the position of a new X-point of magnetic reconnection (at the height where $f_p \approx 170$ MHz). At such heights, the particles generating type III bursts are partially captured in a new magnetic cloud (an island above the X-point). The size of this new magnetic cloud (between the new X-point and the sheared magnetic field) determines the initial ZP frequency range. Over 1 min (from 10:08 to 10:09 UT), whistlers gradually propagate downward to the region where $f_p \approx 210$ MHz.

The large transverse size of the source indicates that whistlers are excited throughout the entire layer with a given plasma density above the AR. However, the maximum of the radio emission intensity can be greatly shifted along this layer from the center of continuum. In the whistler model, each ZP stripe is related to an individual whistler packet. The ZP periodicity is mainly related to the periodicity of the quasilinear interaction of whistlers with fast particles (the periodic deformation of the electron distribution function). The ZP periodicity can also be caused by the periodicity in injection of fast particles and by the bounce motion of particles in a magnetic trap.

In the event under study, there were no explicit evidence of a trap, but an amazing coincidence was observed between the number of type III bursts (24 bursts) within the time interval 10:08–10:09 UT and the number of the ZP stripes along the time axis in the dynamic spectrum. Quasilinear effects lead to an additional modulation along the ZP stripes. These effects come into play only when the particles propagate together with waves (whistlers). A gradual shift of the ZP hump accompanied by

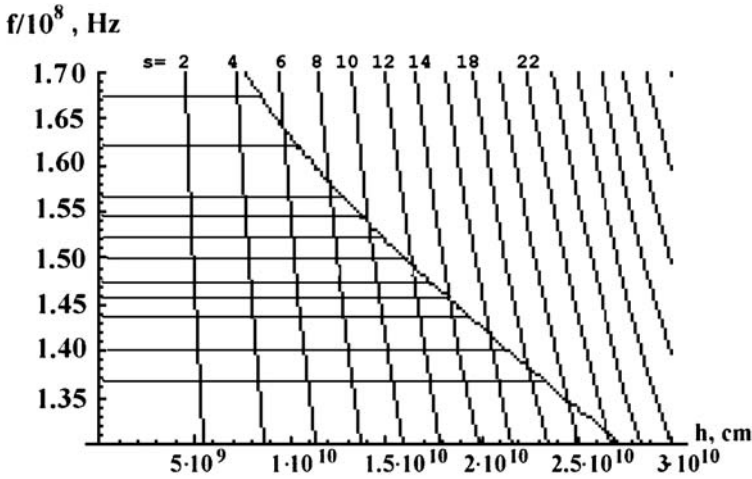


Figure 65. The graph of frequency (Hz) against of the height in the corona h (cm). A grid of gyroharmonics ($s = 2-26 \dots$) is plotted using the magnetic field model of Dulk and McLean (1978). The point like curve is the barometric plasma frequency dependence over height: $f_p = f_{p0} \exp(-h/10^4 T)$. The horizontal lines note the frequencies of zebra stripes at a fixed time moment (10:08:23 UT) (from Chernov *et al.*, 2005).

the change in the sign of the frequency drift (two such shifts are marked by dark curves in Figure 32) is caused by the diffusion of whistlers on fast particles under conditions such that the switching between resonances (see above) at different frequencies (heights) occurs with a small time delay equal to the diffusion time at a given height.

The double plasma resonance model proposed for this event in Zlotnik *et al.* (2003) does not explain the effects observed. First of all, it fails to predict the number of the ZP stripes in the frequency range of interest. If we consider realistic (rather than hypothetical) height profiles of the plasma density and the magnetic field above the AR, e.g., the double Newkirk model (formula (14)) and a dipole magnetic field whose height scale is much smaller than the height scale of the plasma density, then, instead of the observed eighteen stripes in the 135 to 170 MHz frequency range, we will obtain only ten stripes with harmonic numbers s varying from 10 to 20, as was shown in Figure 3 in Chernov (2005). Moreover, this model predicts a sharp increase in the frequency separation between the stripes (from 2.5 to 7 MHz), rather than an actually observed gradual increase from 1.7 to 2.2 MHz.

Concerning the result of Zlotnik *et al.* (2003), namely the finding of the barometric model for the plasma frequency from the observations of the ZP, that for the comparison it is possible to construct an analogous graph, utilizing no calculated magnetic force line (Figure 65). It is possible to take the known model of magnetic field in the corona, obtained on numerous radio data (Dulk and McLean, 1978),

$B = 0.5B_o(h/R_\odot)^{-1.5}$, and on the analogous graph to obtain even better agreement with the barometric dependence. Let us recall, that the horizontal lines note the frequencies of zebra stripes at a fixed time moment. On the edges of the frequency range the zebra stripes fall even better on the levels of the DPR (harmonic from 5 through 19), than at Figure 5a in Zlotnik *et al.* (2003). However, this does not mean at all that the barometric formula actually assigns dependence $f_p(h)$. For this agreement we have selected completely unreal values of $T = 0.9 \cdot 10^7$ K, although the initial frequency appears more adequate here, $f_{p0} \approx 1.05 \cdot 10^9$ Hz, than in Zlotnik *et al.* (2003).

All the other models (e.g., those with the plasma density profile described by the barometric formula and the dipole magnetic field profile) even greater disagree with observations. We note that the magnetic field model proposed in Dulk and McLean (1978) is quite appropriate because it is confirmed by numerous radio observations. On the other hand, the barometric formula certainly does not apply to magnetic loops with plasma $\beta \ll 1$, because this formula describes the density distribution in a gravitational field at a constant temperature without allowance for the magnetic field.

Thus, the ZP contains not only the emission stripes but also absorption stripes, which are sometimes dominant. In this context and also taking into account the simultaneous generation of the ZP, fiber bursts, and fast pulsations, the main properties of the ZP in the event under study can hardly be explained in terms of the new model proposed in LaBelle *et al.* (2003). It is not so obvious whether there are necessary conditions (first of all, the condition $T_e > T_i$ (Kaplan, Tsytovich, 1973)) for the generation of small-scale inhomogeneities (ion-acoustic solitons); in LaBelle *et al.* (2003), their presence was merely postulated. It is quite reasonable to assume that electrostatic plasma waves and whistlers are excited in new burst loops by the trapped fast particles.

In contrast to the double plasma resonance model, the model involving quasilinear interaction of whistlers with fast particles allows one to explain all the fine effects of the ZP dynamics (frequency band, connection with III type bursts, changes of the spatial drift of radio sources synchronized with the frequency drift of the stripes).

4.3. DISCUSSION OF MAY 2, 1998 EVENT

The rope of fibers shown in Figure 30 strongly resemble similar structures observed earlier at higher frequencies (200–250 MHz) and discussed in Mann *et al.* (1989), Chernov (1997) (Figure 26, 27). However, these latter structures were repeated multiple times over the entire decay phase of a flare (over more than an hour). They are associated with the whistler instability in a small magnetic trap that has formed between shock fronts moving away from a magnetic-reconnection X-point during the prolonged process of reestablishing the magnetic structure after a CME (Figure 27b).

In Figure 30 we can see ejections in various directions in five frames in the 195 Å line (SOHO/EIT), but two of these are most prominent: one toward the north from the main flare and the other toward the southeast (a slowly moving front). This is suggestive of a perturbation (shock front) moving toward the observer. According to the first EIT 195 Å image (13:42 UT), it is possible to assume, that the radio source of fine structure was located in a turbulent zone between two shock fronts. The different polarization signs of the main rope of fibers and surrounding its zebra structure (shown in Figure 30 at the top spectrum in circular polarization) testify to the presence within the source of different magnetic polarities, most likely in the form of the X-region of magnetic reconnection.

Thus, it is most probable that the source of the fiber rope is associated with the turbulent zone behind the fast shock fronts and is located in a narrow trap between the fast front and the slow front. The ropes are observed over only three minutes during the type II outburst, and the frequency drift of the main rope is determined by the motion of the shock front with a speed of 960 km s^{-1} , because the frequency drift of the main rope is almost equal to the drift of the fast front. Fast particles accelerated in the shock front were captured in this narrow trap. According to the dynamic spectra at the moment of the beginning of the second type II burst at 70 MHz the first burst through the crude estimate was located approximately at 20 MHz. Utilizing the density model of Leblanc *et al.* (1998), we estimate the distance between the shock fronts at this moment approximately of 300 000 km. Trapped fast particles with the typical velocity for the type III bursts of order $10^{10} \text{ cm s}^{-1}$ pass this distance for 3 s. Specifically, this is the average period between the separate fibers in composition of rope. As a result of the “bounce effect” – the motion of these particles between the two maxima of the magnetic field (between two shock fronts) – a loss-cone velocity distribution was formed, giving rise to a periodic whistler instability. The increasing distance between the two shock fronts can explain the smooth expansion of the main rope during the drift toward lower frequencies. In general, the shock front probably propagates at any angle to the magnetic field. In this case, the magnetic field and density of the shock front should have an oscillatory structure. This may be the origin of the presence of a number of other fragments of fiber ropes and zebra stripes at higher frequencies, whose sources are located further behind the fast shock front.

The whistlers propagate in the direction of propagation of the shock front. It is natural to assume, that whistlers are excited before the shock front (in parameters of the background plasma, with the ratio of cyclotron and plasma frequencies $f_B/f_p = 1/30$ and the relative whistler frequency $x = f_w/f_B = 0.01$). The magnetic field varies a little (according to the constant parameters of narrow fibers), but whistlers scatter on the background plasma, that results in sharp reduction of x (Chernov, 1989). Besides, the presence of broadband main rope means a density heterogeneity with increased plasma density (2–3 times). Therefore the group velocity of the whistlers $v_{gr} = 2c(f_B/f_p)[x(1-x)^3]^{1/2}$ (Kuijpers, 1975) should be noticeably less than 10^8 cm s^{-1} (e.g. for $f_B/f_p = 1/45$ and $x = 0.0033$, $v_{gr} = 760 \text{ km s}^{-1}$),

providing an explanation for the appreciably lower frequency drift of the fibers within the main rope in the comparison with the drift of the rope (whistlers lagged behind from the shock front). Thus, these unusual fiber ropes are most likely a manifestation of whistler wave packets propagation between two shock fronts in the corona. Short total duration of each fiber (gradually growing from approximately 2 s on 38 MHz to 7 s on 35 MHz), is determined by the not simply growing interval between the fronts, but most likely by cutting emission as a result of the cyclotron damping of whistlers with the decrease of the field strength and reaching $x = 0.5$. Evidently from Figure 30, that the shock fronts propagated at different angles, therefore it is possible to assume, that fibers and ZP were observed only in the time interval, thus far the fronts overlapped in space, that is below approximately 20 MHz (above $1.6R_{\odot}$). The type II bursts continued in IP space but only with the usual flocculent structure at frequencies of 14–8 MHz.

4.4. CENTIMETER WAVELENGTHS

4.4.1. *October 29, 2000 Event*

Since ZP and FB display similar spectral characteristics, we will consider both structures to be manifestations of the whistlers in the radio source, due to their interactions with the electrostatic plasma waves: $l + w \rightarrow t$, with both waves being excited by the same fast particles in hot flare loops, which have an anisotropic loss-cone distribution. The computations of Yasnov *et al.* (2000) show a growth in the whistler increment with the temperature of the background plasma in the flare region, with the growth in the cyclotron decay being compensated by the decrease in the whistler frequency with the maximum increment to $0.1\omega_{Be}$. The mean duration of a series of zebra structures and fiber bursts was about two seconds, and the propagation of whistlers without damping over this time places a constraint on the whistler increment of $<0.5 \text{ s}^{-1}$. This constraint can be used to estimate the magnetic field strength in the region in which the flare is generated. Electron temperatures in the range 2–20 MK yield magnetic fields of $B = 125\text{--}190 \text{ G}$ for regions in which the electron density is $(8\text{--}18) \times 10^{10} \text{ cm}^{-3}$.

These rough estimates coincide with estimates derived from the frequency-drift rate of the fiber bursts observed at the same time at these same frequencies, based on the formula $B = 15.43(\ln f - 3)^{-2} df/dt$ (Elgarøy, 1982), which was obtained for a 60-fold Newkirk model and a whistler frequency of $\omega_w = 0.1\omega_B$. In the model with the whistlers we can verify also the obtained values B using the frequency separation between the maximum in the emission and the adjacent minimum in the absorption (Δf_{ea}). This value must be equal to the frequency of whistlers, which is selected equal to 0.1 of the cyclotron frequency (on which the increment of whistlers is maximum). Thus, $B = \Delta f_{ea}/(0.1 \times 2.8G)$ and for the observed value $\Delta f_{ea} \approx 40 \text{ MHz}$ we can estimate $B \approx 140 \text{ G}$. This value is close to the values of field, obtained above by other two methods, which confirms the reliability of the determination of magnetic field in the model with whistlers.

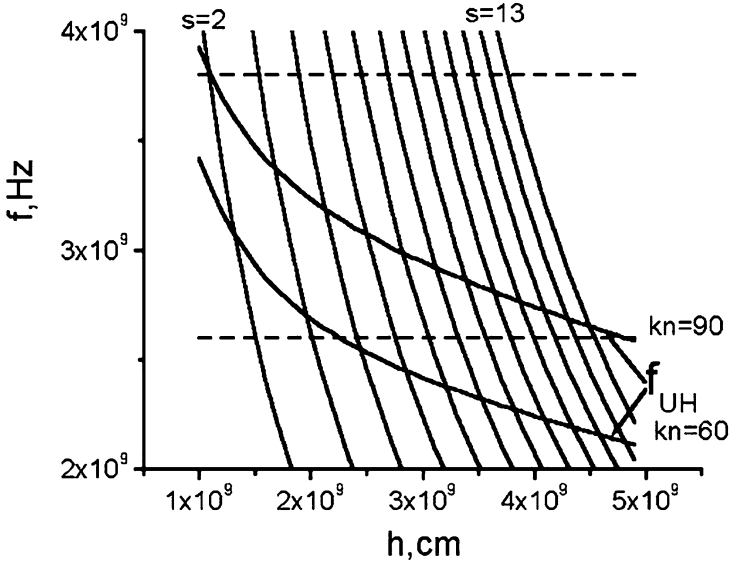


Figure 66. Dependences of upper hybrid and cyclotron frequencies on the height in the corona in the magnetic field model of Dulk and McLean (1978) and electron density model of Newkirk, multiplied by kn ($n = kn \cdot 8.26 \cdot 10^4 \cdot 10^{4.32/h} \text{ cm}^{-3}$) (from Chernov *et al.*, 2005).

If we estimate the magnitude of B in the new model of LaBelle *et al.* (2003), assuming that $\Delta f_s \approx 0.02 f_{Be}$, we obtain for $\Delta f_s = 80$ MHz implausibly high values $B \sim 1500$ G, close to photosphere values.

The alternative model based on the generation of plasma waves at the upper-hybrid frequency ω_{uh} under the conditions appropriate for the DPR was also considered. In the DPR model all estimations of field depend strongly (even in order of magnitude) on the unknown relationship between the scale heights in the corona for density and magnetic field, which was already noted above. We can see from Figure 66 that the main inadequacy of this model is associated with the increase in the frequency separation of the emission stripes Δf_s with increasing frequency: the model predicts an increase from 60 MHz at 2.7 GHz to ~ 450 MHz at 3.8 GHz, which is not generally observed. Usually, the frequency separation only slightly increases with frequency.

The conditions of the DPR realize probably rarely in the flare region with a set of thin magnetic loops. But if they nevertheless realize in the certain stable magnetic trap, that it follows to expect the stable emission of stripes, most likely, during entire event. Such stable stripes in emission were observed, for example, in the decimeter range in the event February 17, 1992 (Chernov *et al.*, 1998, (evolving emission lines, EEL)). The EEL with the slow wavy frequency drift of one or three harmonics during more than 2 hours satisfies actually to mechanism on DPR.

The frequency separation between harmonics in EEL (Figure 15) varies between ≈ 50 and 80 MHz, which corresponds to a maximum magnetic field strength in the

source $B \approx 17\text{--}28$ G, consistent with the 11 G deduced from the $l + w \rightarrow t$ model for ZP at a lower frequency (250 MHz) where we do expect a weaker field. The electromagnetic maser would require too high a magnetic field.

4.4.2. *April 21, 2002 Event*

The Figures 35 and 36 helps us to pay attention to the main flare moments to which appearance of a zebra can be connected. First, the interval of a zebra synchronizes precisely with HXR burst (44–67 keV, HXRS). Second, two most powerful series of ZP represented in Figures 37 and 38, coincide on time with appearance of two new HXR sources (RHESSI data in the lower left panel of Figure 36), which positions coincide with two maximum radio sources (Siberian Solar Radio Telescope (SSRT) data) in the polarized radiation. Thus, the formation of zebra was tightly connected with the presence of fast particles in the loop arcade, included two bright nodes in the form X-points of magnetic reconnection, visually seen on the difference picture in Figure 36. Certainly, the emission in line FeXII, 195 Å shows to us only bright loops with the temperature of $1.8 \cdot 10^6$ K, but radio sources at 5.7 GHz (SSRT) and 17 GHz (Nobeyama) in the polarized radiation were located exactly near two bright nodes, in which the bright being intersected loops had a configuration in the form of the singular X-points.

Dark material, falling out on top is probably overheated flare plasma (to 50–100 MK) ejected from the region of maximum energy release at the heights of decimeter range. Certainly, this prolonged flow of overheated plasma (from 01:34 through 02:15 UT) served as the source of heating of the entire arcade (but not only the mentioned nodes with the X-points), since the duration of its precipitation covered tightly the interval of the fine structure excitation.

It would be natural to connect radio sources exactly with these bright loops. Then the large number of loops with the bright apexes in the narrow height interval causes the specific doubt about the possibility of the realization of the condition of DPR in the wide interval of heights. In this connection, the example of the zebra structure shown in Figure 37, is noteworthy, since it shows that the DPR- model is not able to explain the presence of simultaneous emission in 34 zebra stripes with virtually identical intensities in the range 2.6–3.8 GHz.

At the same time, this situation is quite realistic in a whistler model, where strict periodicity of the stripes is specified by the whistler excitation mechanism itself (fluctuations in the instability under the action of quasi-linear effects, independent of the models for density and magnetic field in the corona). All the more, that frequently the zebra stripes are more similar to isolated fibers, as, for example, we see on the high-frequency edge of the spectrum in the Figure 38. Therefore we could consider both fine structures in a common model, as the whistler manifestation. The isolated packages of whistlers are excited more effectively below, near magnetic mirrors and they propagate upward along the magnetic loops. Approaching the singular points (X-points), whistlers gradually fill the entire radio source with almost standing

periodic wave packets, that also explains the presence of stripes barely drifting in the frequency at the low-frequency edge of the spectrum in Figure 38.

The new model of LaBelle *et al.* (2003) can theoretically explain any parameters of zebra structure and mainly – the large number of zebra-pattern stripes from a point radio source. But the stable appearance of series of zebra structures in a pulsating regime cannot be understood, since this model predicts a strong dependence for the frequency separation and the number of zebra stripes on the parameters of the inhomogeneities, while we observe only a very small growth in the frequency separation with increasing frequency. The parameters of inhomogeneities such as propagating ion-sound waves cannot remain so similar over a wide range of frequencies (interval of heights) over extended periods of time. Furthermore, large problem remains to explain the large intensity of all zebra stripes from numerous point radio sources, exciting the total (incoherent) emission i.e., the spectrum of the stripes would be expected to blend into the continuum.

The frequency profiles in Figure 37 and 38 demonstrate rapid pulsations in the bright ZP stripes with a well defined period of 30 ms. Thus, these new observations support the conclusions of Chernov *et al.* (2003), that the ZP at centimeter wavelengths has always fine spike-like structure, which can be explained in a natural way in whistler models for zebra structure.

Figure 39 shows, that in the cloud of spikes zebra stripes are gradually formed. Therefore it is possible to assume, that the emission of spikes is a primary process. In dm-range the analogous conversion was observed by Kuijpers *et al.* (1981). They assumed even, that spikes and zebra can be excited by the same mechanism. On the basis of our previous results (Chernov *et al.*, 2003), we can assume, that near the flare region spikes can be excited by the nonlinear mechanism of interaction of plasma Langmuir waves with ion-sound waves. The ionic sound can be always present in shock wave fronts, departing from regions of magnetic reconnection (Chernov *et al.*, 2001a). But zebra appears with the excitation of whistlers by fast particles with the loss-cone distribution, forming only after the reflection of particles from the magnetic mirrors. So that a certain delay is always permissible.

If we determine the magnetic field strength on the frequency separation between the maximums in emission and absorption in one stripe (Δf_{ea}), that for the moment 01:48:34 UT we will obtain the small value $B \approx 90$ G.

After 02:00 UT we do not have a possibility to estimate B thus, since the zebra stripes did not detect noticeable absorptions even in the single stripes at HF edge. A decrease in the intensity of plasma waves due to scattering of fast particles on the whistlers in the periodic wave packets is the basic reason for absorptions. Therefore we are right to assume, that in this case the particles and waves diverged in the space, which completely is allowed with a fast particle injection and the emission of whistlers on the normal Doppler effect (in a regime of weak diffusion). It is not excluded also, that the large number of stripes with the narrow frequency separation is the result of the imposition of emission from the different loops with the observation in the projection of radio sources at the solar limb.

In this case the polarization will be most likely determined by propagation conditions of radio emission perpendicularly to the magnetic field.

Thus, new data on zebra structure and fiber bursts at centimeter wavelengths testifies that they have similar structures to those observed at meter wavelengths. ZP was not observed at frequencies higher than ~ 6 GHz. The radiation of electrostatic plasma waves at higher frequencies is probably suppressed in the dense flare plasma. A unified model for zebra structure and fiber bursts involving whistlers can yield realistic values for the magnetic field strength $B \sim 140\text{--}160$ G at a plasma level of about 3 GHz. Using realistic dependences for the electron density and magnetic field, the DPR-model for zebra structure predicts a frequency dependence for the frequency separation between stripes that is much stronger than is observed.

Altyntsev *et al.* (2005) and then Kuznetsov (2005) (in more detail) assume, that properties of ZP in the January 5, 2003 event are more inherent to the point-like radio source, and the authors conclude that the most probable generation mechanism of this zebra pattern is nonlinear coupling of Bernstein waves. In this case the value of the magnetic field in the burst source, determined by the frequency separation between the adjacent stripes, is 60–80 G, too low values at the level of plasma frequency about 5.7 GHz. Altyntsev *et al.* (2005) and then Kuznetsov (2005) do not discuss in their model the superfine structure of ZP (as millisecond spikes), observed in this event.

4.5. DISCUSSION OF THE SUPERFINE STRUCTURE OF ZP

The superfine structure of ZP allows the possibility to compare different models. Let us be turned to parameters of ZP with the superfine structure.

In the bottom panel of Figure 40, in left polarization with a well pronounced ZP one sees about 6 zebra stripes between 3.5 and 3.8 GHz, so the separation is $\Delta f_e = 60$ MHz. If one interprets the zebra bands as harmonics of the gyrofrequency, $f_{uh} = s \times f_{Be}$ one would get a gyrofrequency of $f_{Be} = 60$ MHz, which corresponds to $B \approx 20$ G, and a harmonic of $s = 3600/60 = 60$. If we believe the model at the double plasma resonance of Zheleznyakov and Zlotnik (1975) or Winglee and Dulk (1986), $s > 20$ are unlikely at the fundamental frequency f_{uh} . We cannot believe the emission at the second harmonic of f_{uh} , because in most cases the zebra pattern is strongly polarized. But at the frequency near 3.5 GHz a density of $n_e = 1.5 \times 10^{11}$ cm⁻³ and a magnetic field of $B = 20$ G is not unreasonable near a reconnection site in a flare loop. At the same time an interpretation in terms of the sum of the local upper hybrid frequency and low harmonics of the electron cyclotron frequency $f = f_{uh} + s f_{Be}$ is less likely, because it requires multi-step processes of wave coupling from a compact radio source.

In two recent papers (Karlicky *et al.*, 2001 and Barta and Karlicky, 2001) it is supposed that the radio emission at double plasma resonance is generated in plasma with rapidly changing plasma parameters in turbulent magnetic loops. A

possible source of the turbulence can be the plasma outflows from the magnetic field reconnection. It is supposed that scales of heights of density and the magnetic field in a loop vary chaotically along the loop, and the condition of double plasma resonance can be realized only at certain points along a loop. It is supposed that the area around each such point can be a source of spike emission accompanying ZP. However, the authors do not discuss processes that could result in such a loop structure with strongly turbulent plasma. Thus spikes can form chaotic chains, however the occasional realization of a double plasma resonance (both in one loop and in neighboring ones) excludes formation of parallel drifting zebra stripes.

Recent SOHO and TRACE data suggest narrow pre-flare loops, along which the density and magnetic field change very slowly (Aschwanden *et al.*, 1999, 2002), when density and magnetic field scale heights are about the same, $\sim 55 \pm 10$ Mm, comparable with the length of the loop. This proves that double plasma resonance surfaces cannot exist in such loops.

In Karlicky *et al.* (2001) and Barta and Karlicky (2001) the nonlinear process that causes saturation of the instability is not studied in detail, nor are the wave transformation processes. Notice that in our case spikes as superfine structure of zebra stripes have much smaller duration (8 ms). For an explanation of the discussed structure we will consider alternative models of whistlers and ion-sound waves, in which the radio emission is formed as a result of the more effective interactions: $l + s \rightarrow t$ and $l + w \rightarrow t$.

Microwave spikes as a part of ZP have millisecond durations, and for such spikes a new model was proposed in Chernov *et al.* (2001a), namely the coupling of plasma and ion-sound waves: $l + s \rightarrow t$ in a radio source, related to fast shock fronts in the flare region. The behavior of ion-sound waves and whistlers in coronal magnetic traps was considered in Chernov (1989), where it was shown that a dynamic energy transfer between s -waves and whistlers can operate in a pulsating regime with the processes $s + s' \rightarrow w$. The efficiency of these processes becomes maximal when the whistler frequency is about equal to the ion plasma frequency: $\omega_w \sim \omega_{pi}$. In the meter and decimeter ranges such a coincidence takes place when $\omega_w \sim (0.1 - 0.25)\omega_B$ (see Figure 57). In our case the generation of whistlers occurs in the flare region, where the plasma temperature is higher than in the corona. According Yohkoh/SXT data it may be $\geq 10^7$ K (Yasnov *et al.*, 2002), and the maximum of whistler instability displaces to $\omega_w \leq 0.1\omega_B$ (Figure 52). In such a case the condition $\omega_w \sim \omega_{pi}$ should be realized in the microwave range around 3 GHz.

Thus, the radio emission of zebra stripes in the process of the coupling $l + w \rightarrow t$ could be modulated due to the oscillating whistler spectrum due to the interaction $s + s' \rightarrow w$.

Ion-sound waves can be excited in the whole radio source connected with magnetic reconnection in the flare region, but whistlers only near magnetic plugs or in the upstream of fast shock fronts. This explains, why sometimes spikes cover entire burst continuum and not only zebra stripes (see Figures 39, 40).

The process $s + s' \rightarrow w$ has a limitation with regard to the angles of whistler wave vectors to the magnetic force line (Chernov, 1989) (they must be $>70^\circ$), that explains why the spiky structure is almost not present in FB: because in this case whistlers propagate along magnetic loops. This process works effectively for inclined whistlers generated at anomalous Doppler resonance and responsible for ZP.

However, in the metric range we did not practically observed similar superfine structure in ZP (see time profiles in Figures 5, 7, 8, 26, obtained with 0.01 s time resolution. Therefore it is possible to expect, that this structure will be discovered by observations with the higher millisecond resolution.

The dot-like structure with the period ≈ 0.25 s in event February 17, 1992 in the splitted stripes of ZP synchronously with the same structure in EEL (Figures 16 and 17) has other nature. They appeared only during fast broadband pulsations of type sudden reductions with the same period, and dot-like structure was connected with new injections of fast particles with the period 0.25 s. The emission/absorption character of dot-like structure in the EEL is simply explained in frames of the sudden reduction mechanism proposed by Zaitsev and Stepanov (1976) and Benz and Kuijpers (1976). The EEL is emitted at double plasma resonance and the dots in absorption correspond to a quenching of the upper hybrid wave instability at moments of new fast particle injections. In the ZP we do not see dots in absorption (Figure 16), the usual absorption stripes in ZP do not distorted, since the absorption is defined there by whistlers. So, on this example we are once again convinced of different generation mechanisms of ZP and EEL in this event.

4.6. INTERPRETATION OF ROPE-LIKE FIBERS

Comparing the rope-like fibers in Figures 26–29, it is possible unambiguously to conclude, that these are the kindred phenomena and they require special consideration.

One published theory (Mann *et al.*, 1989) was based on a threshold switch-on process of whistler loss-cone instability in a localized wave packet of the fast magneto-acoustic mode. The critical loss-cone angle is exceeded due to additional perturbation of the magnetic trap by the fast magneto-acoustic mode. However this model is applicable only in the case of injection of a large relative number of energetic particles $n_h/n_c \sim 10^{-2}$ into a magnetic trap with a large plug ratio. A whistler excitation threshold in terms of the loss-cone angle that is realized only when we take into account the contribution of thermal ions in the dispersion relation is of general importance for sources of type II–IV radio emission; however we must stretch the theory to explain the more rapid repetition of the fibers in ropes, the deep modulation of the continuum and certain other properties accompanying the ropes – the slowly drifting absorption fibers and the millisecond pulsations (see Figure 27a).

We will, therefore, consider another probable source of rope-like fibers, which directly related to the reconnection model of Anzer and Pneuman (1982) (for CME

during two ribbon flare) and which is located in a vertical current sheet with magnetic X-points (Chernov, 1990a; 1997). Similar scheme of the radio source was used by Aurass *et al.* (1987), which first have presented the chains of these fibers. The multiple formation of magnetic islands along a vertical current sheet with X-points high in the corona was calculated by Forbes and Priest (1983). A reconnection between the magnetic island and lower closed loop begins from a stationary phase (Figure 27b).

With the onset of nonstationary reconnection two pairs of slow shock waves (S^-) and two fast shock fronts (S^+) move outward from the reconnection region (Sidneva and Semenov, 1985, Xu and Forbes, 1992). The fast shock fronts form here, because streams of plasma flowing upward and downward from the rarified region (surrounded by the slow fronts) with the Alfvén velocity are encountered with the transverse magnetic field. The fast shock front appearance was predicted and confirmed in the calculations by Podgornii and Syrovatskii (1981). The numerical calculations of Sakai and Ohsava (1987) indicate that during the explosive reconnection the magnetic field triples in the fast fronts and ions and electrons undergo quasi-periodic acceleration by the induced electric field.

The accelerated fast particles could be reflected off the fast fronts and became captured in a small trap between the upper and lower fast fronts (S^+). The reflected particles form the loss-cone distribution and a sharp increase of whistler loss-cone instability develops near the fast fronts. The whistlers propagate toward the slow fronts (S^-) until the instantaneous cyclotron damping in the minimum of the magnetic field strength in the slow front. The whistler trajectories are shown by dashed line in Figure 27b.

The most obvious and necessary effect from this picture is a decrease of the continuum emission from the rarified regions due to the screening by the shock fronts. Because of this screening, the slowly moving rarified region between shock fronts should give rise to slowly drifting absorption fibers, which are in fact the most characteristic features accompanying ropes. Their bandwidth of ~ 2 MHz corresponds to the size of the rarified region along ∇f_p in the corona $\sim 2 \cdot 10^8$ cm. Using this estimation we can roughly estimate the time for whistler propagation between the fast and the inclined slow fronts with the group velocity $\sim 5 \cdot 10^8$ cm s^{-1} (for $\omega_p/\omega_B \sim 15$ and $x = 0.03$, determined for this event by Mann *et al.* (1989)). The result is ~ 0.4 s, which corresponds to the observed duration of separate fibers in a rope.

The whistlers propagate toward decreasing density, which explains the observed negative frequency drift of individual fibers in a rope. The periodicity of the fibers is associated with the bounce motions of particles in the small trap between the fast fronts. This leads to the higher periodicity of the fibers in a rope $\sim 5-6$ s^{-1} in comparison with the periodicity of usual fibers bursts $\sim 1-2$ s^{-1} .

In this model, the plasma in the reconnection region should not be isothermal ($T_e \gg T_i$), primarily due to the predominant heating of electrons in the shock fronts. Therefore, a mechanism in which the millisecond pulsations are the result

of a pulsating regime of the coupling whistlers and ion-sound waves should work (Chernov, 1989). The ion-sound waves should encompass a large height interval in the reconnection region, so that the millisecond pulsations appear at a wide range of frequencies.

Thus, this model should work in the direct association with reconnection region during big flares (with CME), it does not require any additional disturbances, and it can explain not only all main properties of the rope-like fibers but also a number of accompanying features of the radio fine structure.

5. Conclusions

We have considered several of the most recent events with the radio fine structure of type ZP and FB using a multi-faceted approach to study the flare processes based on all available new data from the Yohkoh, SOHO, TRACE and RHESSI satellites.

The complex study of flare processes has allowed in some cases to find a connection of occurrence of the fine structure with shock waves and CME.

Fine structure was observed simultaneously with the ascent into the corona of new, hot magnetic loops, and the frequency range occupied by the fine structure in the dynamical spectrum is determined by the extent of these new loops in the corona.

In the April 21, 2002 event the zebra structure was developed in the area of the magnetic reconnection at the apexes of loops, in base of which the new hard X-ray sources appeared, and entire interval of structure was accompanied by precipitation from above the overheated plasma.

In each new event the new special features of the fine structure are revealed, however, they are usually connected with the varied conditions in the source. Therefore one ought not to find the special mechanism of emission for each event, which was repeatedly done before.

In recent years the new page is opened of similar experiments in connection with detection ZP and FB in the microwave range due to the observations on the Chinese spectrometers with the high resolution (10–20 MHz and 5 ms). New data on zebra structure and fiber bursts at centimeter wavelengths show that they are similar to the corresponding structures at meter wavelengths. The discovery of the superfine structure, in the form of millisecond spikes is the most significant new effect in cm range.

Zebra structure and fiber bursts are observed at frequencies from 20 to 6000 MHz. The radiation of electrostatic plasma waves at higher frequencies is probably suppressed in the dense flare plasma. The main relative spectral parameters and degree of circular polarization of zebra structure and fiber bursts are nearly identical. The continuous transition from fiber bursts to zebra structure and vice versa testifies to a single nature for these two structures.

Important new results are obtained by simultaneous studies of the positions of radio sources, using Nançay Radio Heliograph at 164 and 236 MHz, and SSRT at 5.7 GHz. In particular, correlation between the direction (sign) of the frequency drift of stripes on the spectrum and the direction of the drift of source in the space is discovered. In the most of events the polarization correspond to the O-radio mode. In some events with X-emission mode a polarization conversion in the course of the propagation across to the magnetic field is supposed.

All new properties are considered in light both known earlier, and new theoretical models. All the main properties of the emission and absorption stripes can be explained in a model involving interactions between electrostatic plasma waves and whistlers, taking into account the quasi-linear diffusion of fast particles with the loss-cone distribution on whistlers. Within the framework of only this mechanism not simply the stripes in the emission and the absorption are explained, but also entire dynamics of the stripes on the spectrum and of their radio sources (splitting of stripes, movements of the sources, superfine spiky structure).

In this model it is possible to obtain realistic values for the magnetic field strength of $B \approx 5$ G at the plasma level in the corona about 250 MHz, $B \approx 160$ G at the plasma level of about 3 GHz and $B = 250$ G at the level of 5.2 GHz and consequently the plasma $\beta \ll 1$.

The double-plasma-resonance model for the zebra pattern based on the known realistic dependences for the electron density and magnetic field yields a frequency dependence for the frequency separation between stripes that does not agree with the observations.

The mechanism at double plasma resonance can be invoked to account for the large-scale stripes in the emission whose duration is comparable to that of the entire event, as was shown, for example, for the fibers (EEL), oscillating during two hours in the event February 17, 1992. The relative significance of several possible mechanisms remains uncertain.

The future observations should see better definition of the some ZP and FB features, for example, through simultaneous observations of spectra and source positions at microwaves and millisecond resolution in the metric range. Such experiments could confirm or disprove many theoretical models.

Acknowledgements

The author thanks Dr. K.L. Klein for the preparation and discussion of the Nançay radioheliograph data, M. Poquerusse for the ARTEMIS spectrograph data (Meudon), and P. Zlobec for the data from the Trieste Astronomical Observatory polarimeter. The author is grateful also for the support of the Chinese Academy of Sciences and NSF of China that enabled him to work with colleagues at NAOC. The SOHO, TRACE and RHESSI data were obtained from the SOHO, TRACE

and RHESSI databases and the X-ray data – from the Yokoh/SXT database (ISAS, Japan). The author is grateful to SOHO, TRACE and RHESSI teams for operating the instruments and performing the basic data reduction, and especially, for the open data policy. This review was supported by the Russian Foundation of Basic Research, grants No. 05-02-16271.

References

- Altyntsev, A. T., Kuznetsov, A. A., Meshalkina, N. S., Rudenko, G. V., and Yan Yihua: 2005, *Astron. Astrophys.* **431**, 1037.
- Anzer, U., and Pneuman, G. W.: 1982, *Solar Phys.* **79**, 129.
- Aschwanden, M. J.: 2002, *Particle Acceleration and Kinematics in Solar Flares*, Kluwer Academic Publisher, Dordrecht.
- Aschwanden, M. J.: 2004, *Astrophys. J.* **515**, 842.
- Aschwanden, M. J., Newmark, J. L., Delabouiniere, J.-P., Neupert, W. M., Klimchuk, J. A., Gary, G. A., *et al.*: 1999, *Astrophys. J.* **515**, 842.
- Aurass, H., and Chernov, G. P.: 1983, *Solar Phys.* **84**, 339.
- Aurass, H., Chernov, G. P., Karlicky, M., Kurths, J., and Mann, G.: 1987, *Solar Phys.* **112**, 347.
- Aurass, H., Vršnak, B., Hofmann, A., Ruždjak, V.: 1999, *Solar Phys.* **190**, 267.
- Aurass, H., Klein, K.-L., Zlotnik, E. Ya., and Zaitsev, V. V.: 2003, *Astron. Astrophys.* **410**, 1001.
- Aurass, H., Rausche, G., Mann, G., and Hofmann, A.: 2005, *Astron. Astrophys.* **435**, 1137.
- Bakunin, L. M., Ledenev, V. G., Nefedyev, V. P., and 10 co-authors: 1991, *Solar Phys.* **135**, 107.
- Barta, M., and Karlicky, M.: 2001, *Astron. Astrophys.* **379**, 1045.
- Barta, M., and Karlicky, M.: 2006, *Astron. Astrophys.* **450**, 359.
- Benz, A. O.: 1993, *Plasma Astrophysics*, Kluwer Academic Publisher, Dordrecht, The Netherland.
- Benz, A. O., and Kuijpers, J.: 1976, *Solar Phys.* **46**, 275.
- Benz, A. O., and Mann, G.: 1998, *Astron. Astrophys.* **333**, 1034.
- Berney, M., and Benz, A. O.: 1978, *Astron. Astrophys.* **65**, 369.
- Bernold, T. E. X.: 1983, *Fibre Fine Structure in Solar Flare Radio Emission Observations and Theoretical Interpretation*, Diss. ETH No 7409, Zurich.
- Bernold, T. E. X., and Treumann, R. A.: 1983, *Astrophys. J.* **264**, 677.
- Bespalov, P. A., and Trakhtenherz, V. Iu.: 1974, *Geom. Aeron.* **14**, 321.
- Bespalov, P. A., and Traxtenherz, V. Iu.: 1986, *Alvenic Mazers*, IPFAN, Gorkii (in Russian). *Rev. Plasma Phys.* **10**, 155.
- Boischot, A.: 1957, *Ann. d'Astrophys.* **21**, 273.
- Boischot, A., Haddock, F. T., and Maxwell, A.: 1960, *Ann. d'Astrophys.* **23**, 478.
- Breizman, B. N.: 1987, in B. B. Kadomtsev (ed.), *Problems in Plasma Theory*, Energoatomizdat, Moscow, no. 15, 55.
- Caroubalos, C., Maroulis, D., Patavalis, N., and 9 co-authors: 2001, *Exp. Astron.* **11**, 23.
- Chernov, G. P.: 1974, *Solnechnye Damye* **N12**, 75 (in Russian).
- Chernov, G. P.: 1976a, *Sov. Astron.* **20**, 449.
- Chernov, G. P.: 1976b, *Sov. Astron.* **20**, 582.
- Chernov, G. P.: 1989, *Sov. Astron.* **33**, 649.
- Chernov, G. P.: 1990a, *Solar Phys.* **130**, 75.
- Chernov, G. P.: 1990b, *Soviet Astron.* **34**, 66.
- Chernov, G. P.: 1996, *Astron. Rep.* **40**, 561.
- Chernov, G. P.: 1997, *Astron. Lett.* **23**, 827.



- Chernov, G. P.: 2005, *Plasma Phys. Rep.* **31**, 314.
- Chernov, G. P., Chertok, I. M., Fomichev, V. V., Gnezdilov, A. A., Gorgutsa, R. V., and Markeev, A. K.: 1984, *Report UAG-96*, World Data Center, Boulder, p. 88.
- Chernov, G. P., and Fomichev, V. V.: 1989, *Soviet Astron. Lett.* **15**(5), 410.
- Chernov, G. P., Klein, K.-L., Zlobec, P., and Aurass, H.: 1994, *Solar Phys.* **155**, 373.
- Chernov, G. P., Markeev, A. K., Poquerusse, M., Bougeret, J.-L., Klein, K.-L., Mann, G., *et al.*: 1998, *Astron. Astrophys.* **334**, 314.
- Chernov, G. P., Poquerusse, M., Bougeret, J.-L., and Zlobec, P.: 1999, *Proceeding of the 9th European Meeting on Solar Physics, Magnetic Fields and Solar Processes*, Florenc, Italy, 12–18 September 1999 (ESA SP-448 p. 765).
- Chernov, G. P., Fu, Q., Lao, D. B., and Hanaoka, J.: 2001a, *Solar Phys.* **201**, 153.
- Chernov, G. P., Yasnov, L. V., Yan, Y., and Fu Q.: 2001b, *China Astron. Astrophys.* **1**, 525.
- Chernov, G. P., Poquerusse, M., Bougeret, J.-L., and Zlobec, P.: 2001c, *Radio Sci.* **36**, 1745.
- Chernov, G. P., Yan, Y., and Fu Q. J.: 2003, *Astron. Astrophys.* **406**, 1071.
- Chernov, G. P., Yan, Y. H., Fu Q. J., and Tan, Ch. M.: 2005, *Astron. Astrophys.* **437**, 1047.
- Dory, R. A., Guest, G. E., and Harris, E. G.: 1965, *Phys. Rev. Lett.* **14**, 131.
- Dulk, G. A., and McLean, D. J.: 1978, *Solar Phys.* **57**, 279.
- Edgar, B. C.: 1972, *The Structure of the Magnetosphere as Deduced from Magnetospherically Reflected Whistlers*, Stanford University.
- Elgarøy, Ø.: 1959, *Nature* **184**, 887.
- Elgarøy, Ø.: 1961, *Astrophys. Norv.* **7**, 123.
- Elgarøy, Ø.: 1982, *Intermediate Drift Bursts*, Report N 53, ITA, University of Oslo.
- Fedorenko, V. N.: 1975, *Sov. Astron.* **52**, 978.
- Fleishman, G. D.: 2001, *Astron. Lett.* **27**, 254.
- Fleishman, G. D., Fu, Q. J., Huang, G. L., Melnikov, V. F., and Wang, M.: 2002, *Astron. Astrophys.* **385**, 671.
- Fomichev, V. V., and Chertock, I. M.: 1977, *Izvest. Vuzov, Radiofizika* **20**, 1255.
- Fomichev, V. V., and Fainshtein, S. M.: 1981, *Solar Phys.* **71**, 385.
- Fomichev, V. V., and Fainshtein, S. M.: 1988, *Sov. Astron.* **32**, 552.
- Forbes, T. G., and Priest, E. R.: 1983, *Solar Phys.* **84**, 169.
- Gallagher, P. T., Dennis, B. R., Krucker, S., Schwartz, R. A., and Tolbert, A. K.: 2002, *Solar Phys.* **210**, 341.
- Gendrin, R.: 1981, *Geophys. Space Phys.* **19**, 171.
- Gershman, B. N., and Ugarov, V. A.: 1960, *Uspekhi Fiz. Nauk, (Sovjet Uspekhi* **72**, 235).
- Ginzburg, V. L., and Tsytoovich, V. N.: 1984, *Transition Radiation and Transition Scattering*, Nauka, Moscow, 1990, Bristol: Adam Hilger.
- Haselgrove, J.: 1955, *Ray Theory and a New Method for Ray Tracing, Physics of the Ionosphere, Report of the Conference held at the Cavendish Laboratory*, Cambridge, September, 1954. London: The Physical Society, 1955, p. 355.
- Hashimoto, K., and Kimura, J.: 1977, *J. Plasma Phys.* **18**, 1.
- Hayes, L. M.: 1985, *Aust. J. Phys.* **38**, 705.
- Islaker, H., and Benz, A. O.: 1994, *Astron. Astrophys.* **104**, 145.
- Jamin, E., Parkinson, D., Rogister, A., and Bernatici, M.: 1974, *Phys. Fluids* **17**, 419.
- Jiricka, K., Karlický, M., Meszarosova, H., and Snizek, V.: 2001, *Astron. Astrophys.* **375**, 243.
- Kaplan, S. A., and Tsytoovich, V. N.: 1973, *Plasma Astrophysics*, Pergamon Press, New York.
- Karlický, M., Bárta, M., Jiříčka, K., Meszárosová, H., Sawant, H. S., Fernandes, F. C. R., *et al.*: 2001, *Astron. Astrophys.* **375**, 638.
- Karlický, M., Bárta, M., Klassen, A., Aurass, H., and Mann, G.: 2002, *Proceedings of the 10th European SPM, Solar Variability: From Core to Outer Frontiers*, Prague, (ESA SP-506), p. 303.
- Kennel, C. F.: 1966, *Phys. Fluids* **9**, 2190.

- Kennel, C. F., and Thorne, R. M.: 1967, *J. Geophys. Res.* **72**, 871.
- Kimura, I.: 1966, *Radio Sci.* **1**, 269.
- Klassen, A., Aurass, H., and Mann, G.: 2001, *Astron Astrophys.* **370**, L41.
- Krüger, A.: 1979, *Introduction to Solar Radio Astronomy and Radio Physics*, D. Reidel Publ. Comp., p. 128.
- Kuijpers, J.: 1975a, *Collective Wave-Particle Interactions in Solar Type IV Radio Sources*, Utrecht University.
- Kuijpers, J.: 1975b, *Astron. Astrophys.* **40**, 405.
- Kuijpers, J.: 1975c, *Solar Phys.* **44**, 173.
- Kuijpers, J.: 1980, in M. R. Kundu and T. E. Gergely (eds.), *Theory of Type IV dm Bursts*, Radio Physics of the Sun, p. 341.
- Kuijpers, J., Van der Post, P., and Slottje, C.: 1981, *Astron. Astrophys.* **102**, 331.
- Kundu, M.: 1965, *Solar Radio Astronomy*, Interscience, New York.
- Kuznetsov, A. A.: 2005, *Astron. Astrophys.* **438**, 341.
- LaBelle, J., Treumann, R. A., Yoon, P. H., and Karlicky, M.: 2003, *Astrophys. J.* **593**, 1195.
- Lapuhov, A. I., and Chernov, G. P.: 2006, *Plasma Phys. Rep.* **32**, 866.
- Leblanc, Y., Dulk, G. A., and Bougeret, J.-L.: 1998, *Solar Phys.* **183**, 165.
- Leblanc, Y., Dulk, G. A., Cairns, I. H., and Bougeret J.-L.: 2000, *J.G.R.* **105**(A8), 18215.
- Ledenev, V. G., Karlicky, M., Yan, Y., and Fu, Q.: 2001, *Solar Phys.* **202**, 71.
- Ledenev, V. G., Yan, Y., and Fu, Q.: 2006, *Solar Phys.* **233**, 129.
- Livshits, V. A., and Tsytoich, V. N.: 1972, *Sov. Phys. JETP* **35**, 321.
- Mal'tseva, O. A., and Chernov, G. P.: 1989a, *Kinemat. Fiz. Neb. Tel* **5**, 32.
- Mal'tseva, O. A., and Chernov, G. P.: 1989b, *Kinemat. Fiz. Neb. Tel* **5**, 44.
- Mann, G., Baumgaertel, K., Chernov, G. P., and Karlický, M.: 1989, *Solar Phys.* **120**, 383.
- Manoharan, P. K., van Driel-Gesztelyi, L., Pick, M., and Demoulin, P.: 1996, *Astrophys. J.* **468**, L73.
- Markeev, A. K., and Chernov, G. P.: 1970, *Astron. zhurnal* **47**, 1044 (*Soviet Astron.* **14**, 835).
- Melrose, D. B.: 1983, *Solar Phys.* **87**, 359.
- Messmer, P., Benz, A. O., and Monstein, C.: 1999, *Solar Phys.* **187**, 335.
- Messmer, P., Chernov, G. P., Zlobec, P., and Gorgutsa, R. V.: 2002, *Proc. 10th European SPM, Solar Variability: From Core to Outer Frontiers*, Prague, (ESA SP-506), p. 701.
- Mishin, E. V., Rouzhin, Yu. Ya., and Telegin, V. A.: 1989, *Interaction of Electron Fluxes with the Ionospheric Plasma*, Gidrometeoizdat, Leningrad, 264 p.
- Molchanov, O. A., Trahtendertz, V. Ju., and Chmyrev, V. M.: 1974, *Izv. VUZov Radiofizika* **17**, 325.
- Mollwo, L.: 1983, *Solar Phys.* **83**, 305.
- Mollwo, L.: 1988, *Solar Phys.* **116**, 323.
- Mollwo, L., and Sauer, K.: 1977, *Solar Phys.* **51**, 435.
- Newkirk, G.: 1961, *Astrophys. J.* **133**, 983.
- Ning, Z., Fu, Q., and Lu, Q.: 2000, *Astron. Astrophys.* **364**, 793.
- Omura, Y., and Matsumoto, M.: 1987, *J.G.R.* **92**(A8), 8649.
- Ossakov, S. L., Ott, E., and Haber, I.: 1972, *J.G.R.* **15**, 2314.
- Parail, V. V., and Pogutse, O. P.: 1981, in B. B. Kadomtsev (eds.), *Problems in Plasma Theory*, Atomizdat, Moscow, no. 11 p. 5.
- Pisareva, V. V.: 1958, *Sov. Astron.* **35**, 112.
- Podgornii A. I., and Syrovatskii, S. I.: 1981, *Phys. Plat.* **7**, 1055.
- Priest, E. R.: 1982, *Solar Magnehydrodynamics*, D. Reidel Publishing Company, Dordrecht.
- Sakai, J.-L., and Ohsava, Y.: 1987, *Space Sci. Rev.* **46**, 113.
- Sawant, H. S., Karlický, M., Fernandes, F. C. R., and Checatto, J. R.: 2002, *Astron. Astrophys.* **396**, 1015.
- Sazhin, S. S.: 1987, *Planet. Space Sci.* **35**, 753.

- Shapiro, V. D., and Shevchenko, V. I.: 1987, *Plasma Turbulence in Space*, Itogi Nauki i Tekh., Ser. Astronomiya, Moscow, VINITI, p. 235.
- Sharma, R. R., and Vlahos, L.: 1984, *Astrophys. J.* **280**, 405.
- Slottje, C.: 1972, *Solar Phys.* **25**, 210.
- Slottje, C.: 1981, *Atlas of Fine Structures of Dynamic Spectra of Solar Type IV -dm and Some Type II Bursts*, Utrecht Observatory.
- Stepanov, A. V., Kliem, B., Krüger, A., Hilderbrandt, J., and Garaimov, V. I.: 1999, *Astrophys. J.* **524**, 961.
- Stepanov, A. V., and Tsap, Y. T.: 2002, *Solar Phys.* **211**, 135.
- Storey, L. R.: 1953, *Philos. Trans.* **A246**, 113.
- Tarnstrom, G. L., and Philip K. W.: 1971, *Solar Radio Spike Bursts*, University of Alaska, College, 186 p.
- Thompson, A. R., and Maxwell, A.: 1962, *Astrophys. J.* **136**, 546.
- Tsyтович, V. N.: 1970, *Nonlinear Effects in Plasma*, Plenum Press, New York.
- Tsyтович, V. N.: 1977, *Theory of Turbulent Plasma*, Plenum Press, New York.
- Walter, F.: 1969, Nonducted VLF Propagation in the Magnetosphere: Techn. Report N 3418-1, Stanford: Stanford University, 145 p.
- Wild, J. P., and Smerd, S. F.: 1972, *Ann. Rev. Astron. Astrophys.* **10**, 159.
- Wild, J. P., Smerd, S. F., and Weiss, A. A.: 1963, *Ann. Rev. Astron. Astrophys.* **1**, 291.
- Willes, A. J.: 1999, *Solar Phys.* **186**, 319.
- Winglee, R. M., and Dulk G. A.: 1986, *Astrophys. J.* **307**, 808.
- Xu, P., and Forbes, T. G.: 1992, *Solar Phys.* **139**, 315.
- Yasnov, L. V., Chernov, G. P., Yan, Y., and Fu, Q.: 2002, *Proceedings of the 10th European SPM, Solar Variability: From Core to Outer Frontiers*, Prague, (ESA SP-506), p. 791.
- Yasnov, L. V., and Karlický M.: 2004, *Solar Phys.* **219**, 289.
- Yip, W. K.: 1970, *Aust. J. Phys.* **23**, 161.
- Zaitsev, V. V.: 1975, *Soviet Astron. Lett.* **1**, 28.
- Zaitsev, V. V., and Stepanov, A. V.: 1976, *Astron. Astrophys.* **40**, 135.
- Zheleznyakov, V. V.: 1964, *Radio Emission of the Sun and Planets (in Russ)*, Izdat. Nauka, Moscow (engl. transl. Pergamon Press, Oxford, 1970).
- Zheleznyakov, V. V.: 1995, *Radiation in Astrophysical Plasmas*, engl. transl. Kluwer Academic Publisher, Dordrecht (in Russ., Izdat. Nauka, Moscow, 1977).
- Zheleznyakov, V. V., and Zlotnik, E. Ya.: 1975a, *Solar Phys.* **43**, 431.
- Zheleznyakov, V. V., and Zlotnik, E. Ya.: 1975b, *Solar Phys.* **44**, 447.
- Zheleznyakov, V. V., and Zlotnik, E. Ya.: 1975c, *Solar Phys.* **44**, 461.
- Zlobec, P., Li, H. W., Messerottii, M., Comari, M., and Barry, M. B.: 1987, *Solar Phys.* **114**, 375.
- Zlotnik, E. Ya.: 1976, *Izv. VUZov Radiofizika* **19**, 481.
- Zlotnik, E. Ya.: 1979, *Issled. po geomagnetizmu, aeronomii i fizike Solntsa*, SibIZMIR, Irkutsk, **48**, 132 (in Russian).
- Zlotnik, E. Ya., and Zaitsev, V. V.: 2002, *Proceedings of the Conference: Active Processes on the Sun and Stars*, NIIRF, Spb. University, p. 257 (in Russian).
- Zlotnik, E. Ya., Zaitsev, V. V., Aurass, H., and Hofmann, A.: 2003, *Astron. Astrophys.* **410**, 1011.